University of Southampton

Faculty of Engineering and Physical Sciences

School of Chemistry

Studies of Cocrystal-Excipient Interaction by a Combination of Experimental and Computational Approaches

by

Joseph Cadden

Thesis for the degree of Doctor of Philosophy

July 2022

University of Southampton

Abstract

Faculty of Engineering and Physical Sciences

Chemistry

Doctor of Philosophy

Studies of Cocrystal-Excipient Interaction by a Combination of Experimental and

Computational Approaches

by

Joseph Cadden

Herein is presented a report on the study of a low-solubility active pharmaceutical ingredient (API), Leflunomide (LEF). Novel multi-component systems, both pharmaceutically and non-pharmaceutically acceptable, of LEF have been synthesised. Their multi-component nature was confirmed, and each system has been comprehensively characterised using X-ray Powder Diffraction (XRPD), Single-Crystal X-ray Diffraction (SCXRD) and detailed structural analysis.

A cocrystal design approach, using judicious selection of coformers based upon crystal-engineering principles was taken for the cocrystal screening process. This resulted in five new cocrystal systems, four of which are pharmaceutically acceptable. All pharmaceutically acceptable cocrystals were subjected to a comprehensive evaluation of their physicochemical properties, such as thermal properties, stability, dissolution rate and solubility. These were performed alongside that of LEF, in order to compare the physicochemical behaviour of the cocrystals with their parent API. This been performed using a variety of techniques, including DSC, TGA, DVS, XRPD, HPLC, and FTIR.

The two most promisingly performing cocrystals were then selected for further experimental formulation studies alongside complementary molecular dynamics simulations; providing a combined approach to probe the relationship between cocrystal-excipient interactions in water and the associated factors determining the dissolution properties of cocrystal formulations. These formulations, with the excipients lactose (LAC) or dibasic calcium phosphate (DCP), were experimentally evaluated for their dissolution rates and solubilities; properties which appeared to be influenced by their formulation. The parameters deduced from MD simulations, such as solvent accessible surface area (SASA), intermolecular hydrogen bonds among formulation ingredients and water, and interaction energy between the API (or cocrystal) and water were found to be essential indicators of cocrystal formulation dissolution performance.

In order to strengthen the understanding of the impact of intermolecular and interparticular interactions on their physicochemical behaviour, the cocrystals subjected to formulation studies were also analysed through quantum crystallographic studies. Their related intermolecular interaction energies provide experimental insight into the role cocrystallisation plays in influencing solid-state stability, and therefore physicochemical performance.

This was performed via theoretical computational calculations, using PIXEL and Crystal Explorer, of intermolecular interaction energies and their individual energetic contributions to relate these properties to structural assembly and physicochemical properties.

Table of Contents

Table of Tables

Table of Figures

Research Thesis: Declaration of Authorship

Print name: Joseph Cadden

Title of thesis: Studies of Cocrystal-Excipient Interaction by a Combination of Experimental and
Computational Approaches

I declare that this thesis and the work presented in it are my own and has been generated by me as the result of my own original research.

I confirm that:

1. This work was done wholly or mainly while in candidature for a research degree at this University;
2. Where any part of this thesis has previously been submitted for a degree or any other qualification at this University or any other institution, this has been clearly stated;
3. Where I have consulted the published work of others, this is always clearly attributed;
4. Where I have quoted from the work of others, the source is always given. With the exception of such quotations, this thesis is entirely my own work;
5. I have acknowledged all main sources of help;
6. Where the thesis is based on work done by myself jointly with others, I have made clear exactly what was done by others and what I have contributed myself;
7. Parts of this work have been published as:-

    a) Cocrystals of Leflunomide: Design, Structural, and Physicochemical Evaluation Cadden, J.; Klooster, W. T.; Coles, S. J.; Aitipamula, S. *Cryst. Growth Des.* **2019**, 19, 3923-3933.
    b) Cocrystal Formulations: Evaluation of the Impact of Excipients on Dissolution by Molecular Simulation and Experimental Approaches Cadden, J.; Gupta, K. M.; Kanaujia, P.; Coles, S. J.; Aitipamula, S. *Cryst. Growth Des.* **2021**, 21, 2, 1006-1018.

Signature: .... Date:...........................

Acknowledgements

COVID-19 Impact Statement

Due to the unexpected and unprecedented nature of the COVID-19 pandemic, this thesis and the work presented herein was greatly impacted. A number of key experiments and research aims were consequently unable to be performed, altering the outcomes and context of the overall project. Where these are still relevant to the thesis, and the holistic view of the research project, these points have been included as part of Conclusions and Further Work chapters.

Examples of the impact of the COVID-19 pandemic and the subsequent University-wide shutdown are as follows:

- Unable to perform necessary high-resolution data collection refinements that would provide data for a large part of the latter chapters of this thesis. Some data collection was performed in the week prior to, and in anticipation of, the shutdown, however the slow restart and the restrictions on time and occupancies within the department greatly impacted the ability to collect, process, and refine the data – ultimately meaning that this entire project objective was essentially on hold

- Prevented from initiating an interdepartmental collaboration to undertake experimental work accounting for the final stretching chapter of this thesis. A number of alternative avenues were explored, aiming to extract more meaning from calculations on data already acquired, as well as exploring new aspects that could be worked on from home were considered and attempted. However, these yielded only partial success in terms of developing content that would form a solid thesis chapter

Ultimately, despite the above detailed action taken in attempt to mitigate impact, there remained a significant impact of the COVID-19 pandemic on this research project and thesis. It is the hope that consideration of this is taken when reading and assessing this work.

Definitions and Abbreviations

Terms

API: Active Pharmaceutical Ingredient

BCS: Biopharmaceutics Classification System

CSD: Cambridge Structure Database

CIF: Crystallographic Information Framework

Instruments and Analytical Tools

DSC: Differential Scanning Calorimetry

DTA: Differential Thermal Analysis

DVS: Dynamic Vapour Sorption

FTIR: Fourier Transform Infrared (Spectroscopy)

HPLC: High Performance Liquid Chromatography

XRPD: X-Ray Powder Diffraction

SCXRD: Single-Crystal X-Ray Diffraction

TGA: Thermogravimetric Analysis

Materials

2APYM: 2-aminopyrimidine

2PIC: 2-picolinic acid

3HBA: 3-hydroxybenzoic acid

LAC: Lactose (monohydrate)

LEF: Leflunomide

PG: Pyrogallol

DCP: Dibasic calcium phosphate

Chapter 1   Introduction

The work herein presented in this thesis is focused on the design, synthesis, and structural and physicochemical evaluation of cocrystals and their pharmaceutical formulations, using a combination of both experimental and computational approaches. This incorporates knowledge-based design of a series of pharmaceutical cocrystals, using crystal engineering principles, of a low-solubility active pharmaceutical ingredient, extensive evaluation of their physicochemical properties, including thermal, solution, and stability properties, thorough analysis of their crystal structures, down to the subatomic level, and the effects therein on its pharmaceutical profile. The comprehensive assessment described was also extended to the consideration of "real world" formulation situations, whereby the experimental and computational study of structural and physicochemical properties was repeated to include suitable excipients and understand their effect and how they are themselves affected.

This thesis is composed of six parts, breaking down into chapters comprising the aforementioned focuses of the work. **Chapter 1** will introduce the concept of crystal engineering, types and natures of multi-component crystals, their scientific significance, and routes to their synthesis, particularly pertaining to the pharmaceutical space, following up with the notion of cocrystal-excipient interactions and both the experimental and computational methods of their study. These will be contextualised with relevant literature examples of their study and application.

Outlining the overall aims of the project, as stated in the above abstract and extended abstract, **Chapter 2** will contextualise these aims within the current knowledge sphere, e.g. pharmaceutical cocrystallisation, cocrystal/API–excipient interactions and their effects, and the combination of experimental and theoretical approaches to understanding these.

An introduction to, presentation, discussion, and analysis of results for the initial design, synthesis, and structural and physicochemical characterisation of a number of chosen cocrystal systems will follow in **Chapter 3**. The foundation for this chapter will be based upon the work published by Cadden, J.; Klooster, W. T.; Coles, S. J.; Aitipamula, S. *Cryst. Growth Des.* 2019, **19**, 3923-3933.

Chapter 4 will present the computational approach to studying the cocrystal systems. This will begin with a molecular level method of viewing cocrystal-excipient complex interactions and complex–water interactions through molecular dynamics simulations, enabling the prediction of dissolution and solubility hierarchies, which will be compared to those seen in experimental formulation work. Formulation aspects of these will then also be considered, as an experimental

observation of the effect of cocrystal-excipient combinations on its properties. Physicochemical characterisation of solubilities and dissolution rates of various formulations will be presented and investigated. In line with the aforementioned aims of the project, this chapter will compare and contrast the preliminary results obtained from theoretical molecular dynamics simulations with those obtained from experimental investigations into the physicochemical properties of cocrystal formulations. This work will focus on the nature of particles within a system, i.e. cocrystals and excipient, with respect to their size, morphologies, and interactions. The purpose here will be to use insights from the previous two chapters and build upon these towards a quantum crystallographic approach, specifically molecular pair interaction energies of cocrystals. The work discussed in this chapter, and the molecular simulations performed, will draw heavily from the work published by Cadden, J.; Gupta, K. M.; Kanaujia, P.; Coles, S. J.; Aitipamula, S. *Cryst. Growth Des.* 2021, **21**, 2, 1006-1018.

Succeeding this, **Chapter 5** will discuss the quantum crystallographic investigation of a selected series of these systems, detailing theoretical approaches focusing on molecular pair interactions, which further highlights the relationship between the observed physicochemical properties and the nature of the various intermolecular interactions in these cocrystals, influenced by electronic density distributions. This will also serve as a final discussion of computational approaches, to which some of the experimental work will inform and compare, e.g. intermolecular interaction natures and strengths influencing cocrystal formation, assembly, and measured physicochemical properties.

Finally, concluding the work and summarising the results obtained, **Chapter 6** will contextualise this with and address the initial aims outlined in **Chapter 2**. Proposals for future work, based upon promising results or methods to further develop this work and how this could be performed, will be provided, and outlined.

1.1   Cocrystals, Salts and Solvates

Multi-component crystal systems are defined as those with two or more different residues in the crystal lattice, with a residue considered as a complete set of covalently bonded elements.[1,2] Such systems include, but not limited to, cocrystals, hydrates, salts, and solvates,[3] with co-amorphous, eutectics,[4] and solid solutions also falling under this definition. Cocrystals are generally comprised of two or more neutral components (coformers) that are solid under ambient conditions.[5] Multi-component systems defined as either hydrates or solvates consist of a crystal lattice containing a solid component, with a guest water or solvent molecule.[6] As with cocrystals, the components of hydrates and solvates exist in their neutral form,[7] while the opposite is true to define salts. A proton transfer between components must occur, leaving one positive and one negative component in the complex.

1.1.1   Distinguishing Cocrystals and Salts

Predicting and distinguishing multi-component system formation and its nature, e.g. between cocrystal, salts, solvates, and intermediate structures, based on the pKa values of its components generally adheres to the rule of three, whereby the ΔpKa of a system (pKa (protonated base) – pKa (acid)) dictates the type of multi-component system formed.[8] If the ΔpKa is less than 0, no proton transfer is expected to occur and the resultant multi-component solid is a cocrystal, and if the ΔpKa is greater than 3, proton transfer occurs to afford a molecular salt. For ΔpKa values between 0 and 3, prediction of proton transfer is less accurate and thus a cocrystal, salt, or a hybrid structure with partial proton transfer could potentially form.[9,10] It must however be noted that despite the general acceptance and use of the rule of three, the basis of it being pKa values derived from and used to describe solution equilibrium properties, means it is not entirely applicable when used with respect to the solid-state.[11,12]

1.1.2   Cocrystals, Salts or Solvates

At present, the majority of studies into the optimisation of physicochemical properties involving APIs through polymorphic control and multi-component synthesis, is focused on that of cocrystals rather than salts and solvates. This is due to a number of factors: the large array of available coformers with which to crystallise the API, the ability to form cocrystals of non-ionisable APIs, and the increased stability of cocrystals – as desolvation at high temperature/humidity or during storage causes recrystallisation, affecting the physicochemical properties of solvates.[13] Despite this, salt and solvate formation have proved useful tools in certain cases, such as the improved

dissolution rate displayed in the solvated form of spironolactone,[14] and the noticeable stability and enhancement of properties shown in this study through salt formation.

1.2   Pharmaceutical Cocrystals

The use of single-component crystalline API compounds in solid oral dosage forms in a clinical application is becoming scarcer.[15] This is due to modern methods of drug discovery enabling the selection of typically more potent drug molecules. However, this results in the majority of these potential drug candidates belonging to class II, III, and IV of the Biopharmaceutical Classification System (BCS), where bioavailability is limited by low solubility or membrane permeability.[16,17] Up to 40% of newly discovered pharmaceutical compounds are hydrophobic, and thus have their pharmacological activities limited by poor solubility,[18] a problem that is likely to worsen: with potentially between 70 and 90% of current drug candidates predicted to possess low solubility.[19]

There are a variety of commonly employed formulation techniques to counter this problem, such as particle size reduction,[20] complexation, solid dispersion, and co-solvency.[21] The use of multi-component systems is a viable tool for modulating the physicochemical profile of crystalline active pharmaceutical ingredients (APIs). Conventional design of crystalline forms of APIs within a multi-component system generally involves the use of salts, polymorphs, solvates and hydrates.[22]

Over the past two decades, cocrystallisation has emerged as a viable tool for the fine-tuning of materials' properties without the need for chemical modification.[1] Control over solid-state molecular packing, through application of crystal engineering strategies and wise selection of partner molecules (coformers), produces a solid form that shows desirable physiognomic and chemical characteristics including, but not limited to, morphology, stability, solubility, dissolution rate, mechanical strength, and bioavailability.[2-8] This technique has showcased far-reaching impact, particularly in the pharmaceutical industry through development of novel solid-forms of new and existing active pharmaceutical ingredients (APIs), which has paved the way for many current marketed cocrystal-based drugs.[9-14] Ergo, optimisation of the physicochemical properties of suitable cocrystals, and subsequent development of appropriate formulations are crucial for the progress of this research interest.

Marketable pharmaceutical cocrystals are generally comprised of an active pharmaceutical ingredient (API) and an inactive cocrystal former (coformer) ingredient that is solid under ambient conditions.[23] The considerable recent interest in this area is due to the ability to use careful selection of coformers with which to crystallise the API. Incorporation of these coformers into the crystal lattice has the potential to modify the physiochemical properties of the API such as solubility, stability and bioavailability without making or breaking covalent bonds, or affecting its

pharmacological activity.[24,25] However, this approach is a complicated case of supramolecular chemistry, and the understanding of the structure-property relationship is currently limited.

1.2.1   Design of Pharmaceutical Cocrystals

Traditionally, the search for and discovery of viable new pharmaceutical cocrystals are performed via high-throughput or random screening by solid-state grinding and crystallisation, whereby only a handful of "hits" may be generated from an initial selection of many candidates.[26] This low hit rate in the HT screening process arises partly due to the rules of crystal engineering being built on relatively low-resolution geometry arguments with little fundamental understanding of the nature of interactions occurring between components, whether complementary or competitive. Current literature shows efforts to improve and streamline the cocrystal screening process. By using *a priori* design and selection of coformers, employing the principles of crystal engineering alongside a library of crystal structures and intermolecular interactions, a variety of methods for logical coformer selection can be employed.[27] These include hydrogen-bond propensity calculations (HBPCs),[9] and similar two-stage rational selection of coformers based on structural diversity,[28] and the use of known structurally similar compounds to enable the identification of appropriate coformers for cocrystal screening.[12,29]

The design of pharmaceutical cocrystals using crystal engineering approaches – defined as "the understanding of intermolecular interactions in the context of crystal packing and in the utilisation of such understanding in the design of new solids with desired physical and chemical properties"[30] – means that suitable coformers can be selected from libraries of thousands.[3] This is typically achieved using the abundance of structures found in the Cambridge Structural Database (CSD) to analyse how common functional groups interact with each other and select coformers that are most likely to form cocrystals, most notably by the creation of supramolecular synthons from hydrogen bonding moieties (**Figure 1.1**).

Galek *et al.* introduced a knowledge-based approach to the analysis and prediction of crystal properties of the drug lamotrigine and applied this to predict the potential for cocrystal formulation and optimal selection of coformers.[31] The same hydrogen bond propensity

Figure 1.1 Examples of (a) a supramolecular heterosynthon displaying O–H···N hydrogen bonding and (b) a supramolecular homosynthon displaying O–H···O hydrogen bonding

calculations (HBPCs) have been demonstrated by Delori *et al.* to be useful in the screening of potential coformers to target those that are more likely to form strong interactions with the API pyrimethamine.[9,32]

Zhou *et al.* proposed a similar two-stage rational selection of coformers for cocrystal screening of an early development Novartis drug candidate.[28] By firstly identifying coformers with potentially strong intermolecular hydrogen bonding with the API, the number of feasible coformers from the initial selection was narrowed from 20 to 2. The second stage involved the incorporation of structural diversity within these two coformers to find 19 closely related structures, of which 5 produced hits and resulted in a 4-aminobenzoic acid cocrystal of the API possessing a 12-fold exposure increase when compared to the free API *in vivo*. Present supramolecular synthon design strategies have been shown to fail when applied to molecules that lack these accessible hydrogen-bonding functionalities, such as artemisinin,[33] spironolactone,[34] and griseofulvin.[35]

This problem has recently been tackled; Lucy Mapp's studies with A*STAR into the design of cocrystals for pharmaceutical use have involved using a knowledge-based strategy, using known structurally similar compounds, enabling the identification of appropriate coformers for the analgesic drug propyphenazone (PROPY), an API with limited hydrogen bonding functionality, and the cancer treatment drug lonidamine (LON). Comparisons with free PROPY revealed a hydroquinone cocrystal with a significantly higher initial dissolution rate along with a 1.16:1 solubility ratio,[29] while a number of LON cocrystals displayed improved physicochemical properties.[12]

The enormous amount of current literature on cocrystals has established the evolution of reliable cocrystal design strategies, characterisation, scale up, and application of such cocrystals in the improvement of drug properties. However, the successful development of a drug formulation mostly depends on a selection of the right combination of excipients, and to do so, in-depth knowledge of interactions between excipient and active ingredient is important. In the case of cocrystal formulations, understanding the behaviour of a cocrystal in the presence of excipients would provide vital knowledge on the performance attributes of cocrystals.

1.2.2   Cocrystal-Excipient Interactions

The majority of research in the field of pharmaceutical cocrystals has been focused on the improvement of their solubility profiles through judicious selection of coformers. As such, formulation aspects of cocrystals have not been investigated fully.[36] In the case of cocrystal formulations, gaining an understanding of the behaviour of a cocrystal in the presence of excipients, such as solubility and dissolution, would provide vital knowledge of the performance

attributes. Therefore, studying impact of different excipients of the cocrystal performance, for the purpose of identifying suitable excipients to demonstrate the true potential of cocrystals in the development of drugs would prove valuable and encouraging.

Excipients are an integral part of any drug formulation and although generally characterised as a pharmacologically inert ingredient, can interact with drug molecules in the formulation. They are largely used as carriers for delivery of the API, most drug-excipient complexes dissociate at the absorption site *in vivo*, releasing the free drug into the plasma. The formation of a cocrystal-excipient complex can alter the drug's physiochemical and pharmaceutical properties, as the complexed system becomes the predominant molecular entity in the dosage form, meaning that appropriate selection is important.[37] This method has been employed in the increase in drug dissolution and solubility profiles of the previously poorly soluble APIs artemisinin,[38] spironolactone,[39] and griseofulvin[40] by complexation with the excipient cyclodextrin. Formulation of drugs with excipients can also cause a decrease in dissolution rate and solubility through formation of poorly soluble complexes, or formation of a drug-excipient complex that does not dissociate.

While it is clear that the physiochemical and pharmacological properties of a cocrystal API are affected by cocrystal-excipient interactions, a mechanistic understanding of the interactions and their effects is not yet fully understood, particularly at a molecular level. Currently, selection of appropriate formulations is built upon the knowledge gained from previous experimental results,[41] and the properties of an API are often largely ignored during this process with the formulations tested in a somewhat technology-agnostic fashion, e.g. selection for an API with a background of formulation with cyclodextrins will likely be investigated with similar excipients first.[42]

There have been a few experimental attempts reporting the impact of certain excipients on the performance and developability of cocrystals.[22] For example, the earliest study that shed light on the importance of exploring formulation concepts for cocrystals has been performed by Remenar *et al*.[43] The authors found that using a combination of 2 % sodium lauryl sulfate (SLS) and polyvinylpyrrolidone (PVP) together with a celecoxib-nicotinamide cocrystal led to *in vitro* formation of incipient amorphous materials, metastable polymorphs, and submicron particles of the API which are associated with good oral bioavailability.

Li *et al*. have studied the impact of hydroxypropylmethylcellulose (HPMC) on the phase transformation and dissolution of a carbamazepine (CBZ)-nicotinamide cocrystal.[44] It was found that, at a lower percentage of HPMC in tablets, the release of CBZ from the cocrystal was nonlinear and declined overtime, which was attributed to conversion of the cocrystal into CBZ

dihydrate. However, higher concentrations of HPMC helped to improve CBZ release from the cocrystal formulation, which was rationalized through dissolution of only the outer surface of the matrix when HPMC undergoes a process of disentanglement.

Concerning a cocrystal of danazol and vanillin, studied by Childs *et al*., the synergistic use of a solubiliser (vitamin E-TPGS) and a precipitation inhibitor (hydroxypropylcellulose) resulted in a dramatic increase in the apparent solubility levels in *in vitro* powder dissolution experiments which were very well reflected in high danazol plasma levels in *in vivo* animal studies.[45]

The impact of polymer and surfactant concentration on the dissolution of a cocrystal has been investigated by Alhalaweh *et al*.[46] Using an indomethacin-saccharin cocrystal as a model system, the authors observed different solubilisation effects of SLS and PVP on indomethacin and saccharin, respectively, which was suggested to maintain drug supersaturation levels sufficiently long enough for absorption.

In a recent study, Koranne *et al*. revealed that the nature of the excipient (whether neutral or ionic) has a significant impact on the stability of the cocrystal.[47] Using the theophylline-glutaric acid cocrystal as a model system, the authors demonstrated that the use of ionisable and hygroscopic excipients, such as magnesium stearate, led to dissociation of the cocrystal, whereas neutral and non-hygroscopic crystalline excipients, e.g. lactose monohydrate prevented cocrystal dissociation.

In another study dealing with three cocrystals of a hypothetical drug, Lipert *et al*. noted that, even though the neat cocrystals are more soluble than the drug, not all cocrystals have a solubility higher than the drug in the presence of a solubilising agent, emphasizing the importance of greater care in choosing the right formulation ingredients.[48]

Furthermore, in a 2017 study by Duggirala *et al*. it was found that caffeine-oxalic acid cocrystals, widely reported to be stable at diverse temperature and humidity conditions, dissociate in the presence of numerous pharmaceutical excipients.[49] A mechanism for cocrystal dissociation proposed by the authors suggested cocrystal dissociation, in the presence of excipients, was a consequence of the water sorption followed by dissolution of the cocrystal and excipient, respectively, in the sorbed water. Regarding ionisable excipients, the authors found the driving force for dissociation involved a proton transfer from oxalic acid to the excipient, forming metal salts and caffeine hydrate.

In an attempt to demonstrate potential applications of freeze-drying for the synthesis of cocrystals, Ogienko *et al*. prepared a solid dispersion of the cocrystal meloxicam-succinic acid in a solubilising agent, polyethylene glycol, by freeze-drying and found the dissolution rate of the solid

dispersion to be significantly higher than the cocrystal prepared by liquid-assisted grinding and conventional freeze-drying.[50]

Most recently, in an extensive study on the impact of physical properties of excipients on the physical stability of the cocrystal, Duggirala *et al*. conducted binary cocrystal-excipient compatibility studies on a cocrystal of ertugliflozin and L-pyroglutamic acid.[3] The study revealed that, among the various properties studied, pH and hygroscopic nature of the excipients play a greater role in the dissociation of the cocrystal in formulation. Using this knowledge of cocrystal dissociation in the presence of excipients and its propagating factors, the authors responded by coating the cocrystal particles with a pH modifier and hydrophobic silica. This strategy proved effective in mitigating cocrystal dissociation and the tablet formulations, thus prepared, were found to be stable at accelerated stability condition (40 °C/75 % RH), even after 4 weeks.

There have been a few studies reported which aim to develop the models using mathematical/numerical modelling techniques that predict melting properties, ideal mole fraction solubility and aqueous solubility product of pure cocrystals.[51,52] However, these studies have mainly focused on mathematical model development for prediction of pure cocrystal properties and the impact of molecular-level interactions between cocrystal and excipients in formulations has not been considered.[53] In this respect, a fundamental understanding of the types and nature of molecular interactions between cocrystal and excipients is essential in order to discern their effect on physicochemical properties such as solubility, dissolution rate, and stability. With the rapid growth of computational resources in the last 10-20 years, molecular simulation techniques have evolved as reliable tools for effective understanding of complex phenomena at a molecular level, as well as computational *a priori* design of novel materials preceding synthesis.[54,55]

For example, in order to understand dissolution of APIs, Jha *et al*. performed a series of MD simulations, highlighting the molecular interactions between polymeric excipients and a poorly soluble API (phenytoin) in an aqueous medium.[56]

Again, with an objective to understand dissolution and precipitation of a drug in the presence of excipients, Li *et al*. employed a combination of docking calculations and molecular dynamics simulations to analyse and evaluate a variety of API-excipient combinations of the non-steroidal antiandrogen agent bicalutamide (BIC).[57] The study revealed an underlying relationship between the structure and energy of a drug-excipient complex and its dissolution performance, as well as excipient-water hydrogen-bonding and solvent accessible surface area (SASA) – defined as the surface area of the molecule or complex that is accessible to a solvent or dissolution media. A complex of BIC with lactose (BIC/LAC) was computationally determined to have the best solubility and dissolution profile, possessing the largest hydrophilic surface area, most excipient-water

hydrogen bonds, and strongest BIC-excipient interaction – a prediction that was experimentally verified.

A novel method for the *in silico* design of new pharmaceutical formulations using a latent variable regression model (LVRM) has been proposed by Tomba *et al*. to select the best excipient types and amounts for the formulation of a proprietary API.[58] This approach was partnered with experimental investigation into the preparation and characterisation of the formulation and comparison of the properties, which validated the model predictions.

Huynh *et al*. have shown the use of a computational model as a reliable tool for the ranking of a selection of suitable excipients for the solubilisation of the lipophilic anticancer agent docetaxel (DTX) through computational prediction of its solubility in a variety of excipients, using of Cerius2 software and COMPASS force-field.[59] Results predicted tributyrin to be the most effective excipient choice for DTX solubility with a simulated solubility of 114.4 mg/ml, which was in agreement with the experimental value of 108 ± 1.8 mg/ml. The preferable solubility in this excipient was proposed to be related to the drug's ability to engage in hydrogen-bonding interactions with the excipient, something that was supported by the higher number of moles of excipient carbonyl functional groups available to hydrogen bond with DTX. This is consistent with the results of Li *et al*. whereby BIC solubility in LAC is aided by stronger drug-excipient interactions.[57]

Full atomistic MD simulations using the COMPASS force-field have also been employed by Gupta *et al*. to successfully compute the miscibility of the nonsteroidal anti-inflammatory drug (NSAID) indomethacin (IND) in three different excipients: polyethylene oxide (PEO), glucose (GLU) and sucrose (SUC).[78] The simulations PEO to be the most effective excipient for formulation with IND as they possessed the smallest difference in solubility parameter ($\Delta\delta$), which was experimentally verified using thermoanalytical techniques. The nature and strength of the various intermolecular interactions contributing to this miscibility was also examined.

The results of these *ab initio* calculations show promise for a fundamental understanding of the relationship between cocrystal-excipient interaction at a molecular level and the physiochemical properties and could assist the selection of excipients, increasing the efficiency of the cocrystal screening process. These microscale interactions have been shown to control the macroscopic behaviour of the particle formulation; an aspect of pharmaceutical processing that has been well studied using discrete element methods.[60] With the rise in computing potential to inform such predictive methods, and in aiming to lead interdisciplinary research into pharmaceutical formulation on both the micro and macroscopic scale, attention has now also turned to the use of

discrete particle simulation techniques to develop a more comprehensive theory and study and quantify the interaction forces between formulation particles.[61]

Chapter 2   Aims

2.1   Aims

The context and importance of cocrystals and, specifically pharmaceutical cocrystals, has been shown in **Chapter 1.2** while typical and reported methods of design, synthesis, and utilisation of these are presented in **Chapters 1.2.1 and 1.2.2**.

With the knowledge of the appeal of pharmaceutical cocrystals, this study initially aims to use judicious coformer selection to synthesise a number of these cocrystal systems with a view to improving, but ultimately assessing, their pharmaceutical profiles and the effects of cocrystallisation therein. Through successful cocrystallisation and analysis, with a variety of different coformers, rationalisation of their formation and composition with respect to the informed, systematic coformer selection process – based upon robust crystal engineering principles – will follow as its assessment and justification via thorough investigation into their crystal structures and packing obtained via both powder and single crystal X-ray diffraction.

In line with the aforementioned goal of cocrystallisation, in a pharmaceutical, industrial, and commercial aspect, the requisite physicochemical properties analysis will be performed. Namely, solution properties – solubility and dissolution rate – of the synthesised cocrystals will be the focus as a comparison to their parent, single-component API in order to evaluate whether they are improved as a result. This will utilise the methods and such as dissolution rate apparatus, and the shake-flask method feeding into HPLC elucidation of API concentrations. Additionally, thermal properties such as melting point and thermal stability accompany those of solution as a complement to the pharmaceutical applicability and potential of the cocrystal systems. Finally, similar to their thermal stabilities, each cocrystal will be subjected to accelerated storage and solution stability (for the possibility of coformer dissociation) studies as a rehearsal for "real world" applications.

2.2   Further Project Aims

These techniques and assessment routes follow a well-trodden path in this scientific space and have been duly adopted by academic researchers and pharmaceutical drug companies alike, with increasing numbers of cocrystal-based drug products now entering the market. Surprisingly, however, studies into the formulation aspects of cocrystal-based drugs are relatively few and far between compared to the vast literature on their design, synthesis, and characterisation.

In order to fully understand the nature of their cocrystal-excipient interactions and the effect of these upon the physiochemical properties, the project aims to use this initial study as a platform to expand upon. Further work will focus on the formulations of select cocrystals of these APIs, with the aim of understanding the effect of excipients on cocrystal properties as well the effect of cocrystallisation on API properties. With the aim of identification of suitable drug formulation excipients, the experimental approach will be supplemented by a computational approach to viewing these systems.

The further objectives of this study are therefore to integrate MD simulations as a complement to experimental methods and gain a molecular-level understanding of the interactions between an API or cocrystal and selected excipients and water. Such studies would be expected to streamline excipient screening and help in the selection of suitable excipients for the development of cocrystal formulations. The knowledge gained from MD simulations was subsequently used to prepare prototype oral dosage formulations, such as tablets, and evaluate their resulting performance in comparison to those of "neat" samples as described above. Toward this goal, the current work indicates a detailed underlying mechanism in molecular interactions among the active (API or cocrystals), excipients, and water, and identifies governing factors to explain a hierarchy of the aqueous dissolution of formulations obtained experimentally.

To tie in with the title and theme of this thesis, the final aim is to combine and compare two prominent and contrasting approaches: theoretical and experimental. To this end, the best performing, and pharmaceutically acceptable, cocrystals were to be subjected to quantum crystallographic analysis as a method of discerning their electronic distribution differences, molecular-pair interaction energies from theoretical calculations using the PIXEL and Crystal Explorer programs, and resulting intermolecular interactions and strengths, aiming to highlight the reasons and means by which the API structure and properties are altered by the addition and difference of coformers. This approach provides a molecular- and electronic-level understanding of cocrystal properties whose purpose is also to extrapolate to a higher, particle-level view of interactions.

2.3   Objectives

There are ultimately 6 main objectives to the work undertaken in this project and outlined in this thesis. They can be summarised by the following statements:

1. Apply the principles of crystal engineering to successfully inform a knowledge-based design approach to cocrystallisation.
2. Assess the subsequent impact of cocrystallisation upon the structural and physicochemical properties of a low-solubility API.
3. Elucidate the effect of different coformers on the electronic distributions and how this can be related to both physicochemical properties and API/cocrystal-excipient interactions.
4. Combine and complement both qualitative and quantitative approaches towards a quantum crystallographic understanding of these cocrystals.
5. Employ theoretical molecular dynamics simulations to shed light on certain indicative properties of an API/cocrystal that impact its solution behaviour and assess its success relative to experimental observations.
6. Acquire a particle-level perspective on cocrystal-excipient interactions from atomic- and electronic-level data and compare to experimentally derived parameters.

Chapter 3 Cocrystals of Leflunomide

The discussion in this chapter centres around the design, structural, and physicochemical evaluation of a series of leflunomide cocrystal systems and is be based upon the work published by Cadden, J.; Klooster, W. T.; Coles, S. J.; Aitipamula, S. *Cryst. Growth Des.* 2019, **19**, 3923-3933.

3.1 Objectives

Chapter 3 herein describes the use of cocrystallisation as a tool to improve the pharmaceutical profile of the low-solubility drug leflunomide, fulfilling two of the six key objectives outlined in **Chapter 2.3**:

1. Apply the principles of crystal engineering to successfully inform a knowledge-based design approach to cocrystallisation.

This study aimed to use judicious selection of coformers, based upon knowledge-based strategy and crystal engineering principles, for the synthesis of cocrystals of LEF with a view to evaluate their pharmaceutical profile. Experiments have yielded four pharmaceutically acceptable cocrystals

2. Assess the subsequent impact of cocrystallisation upon the structural and physicochemical properties of a low-solubility API.

Crystal structure analysis revealed that the hydrogen bonding in the crystal structures corroborate well with the knowledge-based prediction tool. Physicochemical properties such as thermal behaviour, stability, solubility, and dissolution rate of the pharmaceutically acceptable cocrystals were evaluated to assess their impact on the pharmaceutical profile of leflunomide. When compared with their parent compound leflunomide and the physical mixtures, cocrystals were found to exhibit improved physicochemical properties, showing their potential for development of new solid dosage forms.

3.2   Leflunomide

Many known APIs suffer from poor aqueous solubility and dissolution rate, which leads to a reduced bioavailability. Leflunomide is no exception, its high lipophilicity and low solubility in water (reported to be less than 40 mgL-1) firmly place it in BCS class II.[62]

Leflunomide (5-methyl-N-[4-(trifluoromethyl) phenyl]-isoxazole-4-carboxamide) (LEF, **Figure 3.1**) is an immunosuppressive disease-modifying antirheumatic drug (DMARD) that is used to slow down the progression of the rheumatoid arthritis disease through pyrimidine synthesis inhibition.[63] It is formulated as Arava and is converted into its active water-soluble metabolite *in vivo*. The notable clinical efficacy of LEF, coupled with its solubility limited (< 40mg/L) bioavailability, makes cocrystallisation an attractive prospect for improving its drug formulation and delivery properties through increased solubility.

3.2.1   Leflunomide Crystal Structure

There are two reported polymorphic forms of LEF, reported by Vega *et al*., (Form I and Form II) both of which crystallise in the monoclinic space group *P2₁/c* with Z' values of 2 and 1 respectively, with Form I being the thermodynamically stable form at room temperature.[64] The presence of amide and isoxazole functional groups in LEF enables formation of a number of possible supramolecular synthons with complementary functional groups for the synthesis of multicomponent systems. The crystal structure of Form I shows the O2 carbonyl and amide N2 atoms forming N–H···O amide interactions (**Figure 3.2**).
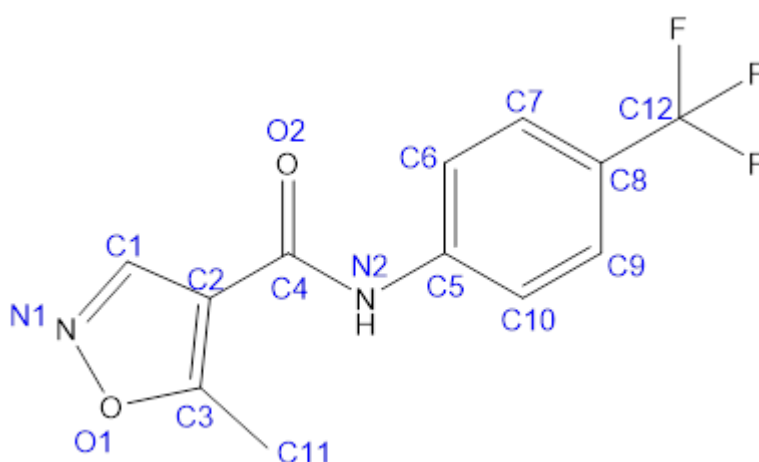
Figure 3.1 Chemical diagram of LEF with atomic numbering scheme
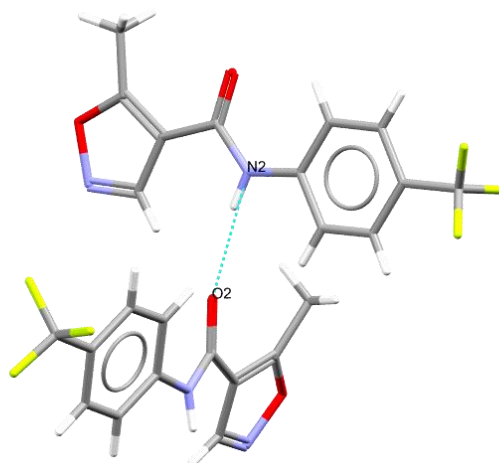
Figure 3.2 Crystal packing motif of LEF Form I showing the primary N–H···O amide intermolecular interaction

3.3 Interaction Searching

Propensity of the functional groups present in LEF to interact with other complementary functional groups can be understood through statistical analysis of the crystal structures deposited in CSD. Selecting "ligands", representative of the functional groups in LEF, and possible contact groups from a pre-set list available in Isostar v2.2.5[65] enabled the determination of the most preferential contacts for each functional group. LEF contains a number of functional groups with potential for intermolecular interactions, mainly an amide group (bonded either side to aromatic rings), an isoxazole ring (methyl substituted), and a trifluoromethyl group. These were initially modelled using selected ligands available in the Isostar library: aromatic-aromatic amide, isoxazole, aromatic O, aromatic N in 5-membered rings, trifluoromethyl, and were labelled the central groups (**Figure 3.3**).

aromatic-aromatic amide   isoxazole   aromatic O   trifluoromethyl
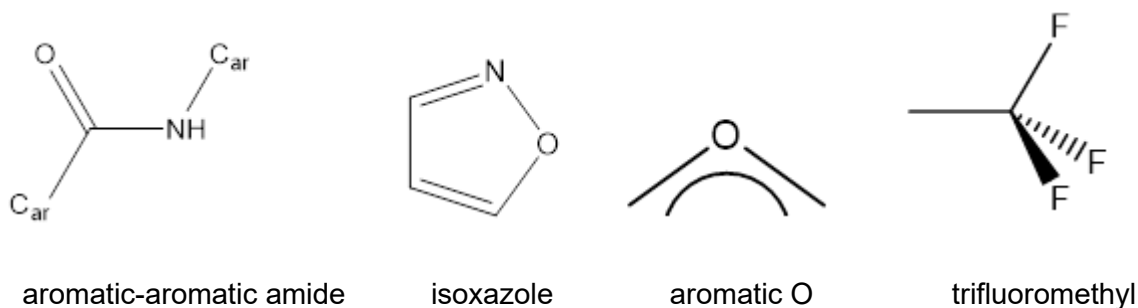
Figure 3.3 Chemical diagrams of the predefined ligands used to represent LEF functional groups in contact searching

Isostar searching based on these central groups, with respect to a variety of common functional groups (contact groups), gave statistical information on the number of crystal structures containing both the central and contact groups, and the number of these structures in which the central and contact groups form a contact with distance (R) less than the sum of the van der Waals' radii (V). Detailed results of these searches can be found in **Appendix B.2.1**.

Statistical analysis of intermolecular contacts in the Isostar allowed for a primary evaluation of the preferred interactions between the functional groups of LEF and potential coformers. All five aforementioned contact groups showed a general high affinity to form contacts with groups containing an aromatic component, such as C(ar)-NH_2, aromatic C–H, and phenol OH groups. In addition to these, polar X–H groups (X=N, O or S) were amongst the highest occurring contacts for all the central groups, with specifically OH groups showing a high affinity for contact with the aromatic-aromatic amide, isoxazole and aromatic N central groups, and N–H groups likewise for the aromatic N and trifluoromethyl central groups. This leads to three initial preferences in coformer structure and functional groups for the design of LEF cocrystals: OH groups, and either amide or amine NH groups.

With Isostar interaction search providing an initial insight into the nature and preference of interactions in the various functional groups of LEF, specific contact searching was then conducted using the motif search tool integrated in Mercury. Rather than investigating contacts between predefined ligands and groups, each functional group could be tailored to more accurately represent those involved in LEF and its possible contacts (**Appendix B.2.2**). In addition to this, the nature of interactions could be defined, such as separation into donor and acceptor atoms. Similar to the Isostar interaction search, the dominant hydrogen bonding motifs from the various LEF functional groups involved amide, various aliphatic and aromatic hydroxyl (including COOH) and amine contact groups. The results of these specific contact searches are described in detail in **Appendix B.2.2**.

3.4   Molecular Complementarity and Selection of Coformers

Based on the most frequently occurring intermolecular interactions, involving central groups representative of those in LEF and a variety of contact groups, a library of favourable functional groups for cocrystal design was formed. These functional groups include primary amine, amide, and hydroxyl groups, with an additional preference for aromaticity when C–H groups are considered. Interestingly, these functional groups represent the possibility for formation of a number of well-known supramolecular synthons, such as O–H$\cdots$N(ar) and O–H$\cdots$$CONH_2$. In addition to this, the potential for COOH/hydroxyl–N(ar) heterosynthon formation involving the

isoxazole moiety of LEF provides an argument for carboxylic acid functional groups to be considered.

Using the knowledge of these preferred functional groups, a number of coformers were chosen from a list of those commonly used in cocrystal screening experiments, ensuring a wide range of structures to encompass the varying types of motifs shown to be favourable. These were checked against a library of coformers from the CCDC which are provided within the molecular complementarity search tool implemented in Mercury.[66] Any coformers that were not already present within this library, but used in the cocrystal screening, were manually added. The molecular complementarity search uses analysis of properties such as coformer shape, size, and polarity, amongst other factors, to generate a list of potential hits for a particular molecule. Results of these predictions in turn allowed selection of coformers for the solid form screening of LEF. Consistent with those from the interaction searches, these results predicted a high complementarity of LEF with aromatic O–H, N–H and heteroatom containing coformers, as well as a number of dicarboxylic acids. Details of the coformers searched and those that predicted cocrystal formation can be found in **Appendix B.2.3**.

3.5   Solid Form Screening

Judicious selection of coformers based on the in-depth CSD analysis of LEF interactions and application of prediction tools followed by solid-form screening using solvent drop grinding methods yielded a total of five new cocrystals. Three of these coformers, 2-picolinic acid (2PIC), 2-aminopyrimidine (2APYM), and 3-hydroxybenzoic acid (3HBA), were identified as hits from the molecular complementarity search, with pyrogallol (PG) falling into the fail list. The chemical structures of these coformers are shown in **Figure 3.4**.

pyrogallol
PG

3-hydroxybenzoic acid
3HBA

2-aminopyrimidine
2APYM

2-picolinic acid
2PIC
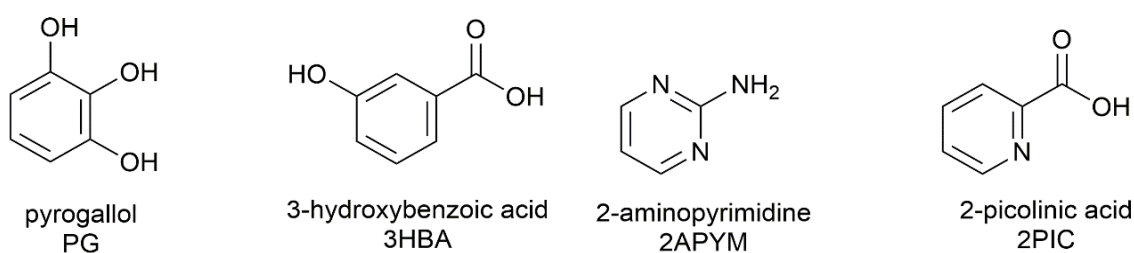
Figure 3.4 Chemical diagram of the coformers that formed new multi-component systems with LEF

3.6   Experimental

3.6.1   Solid-State Screening

Cocrystal screening by grinding was performed via solvent drop grinding using a Retsch Mixer Mill model MM301. In each experiment, 270.2 mg (0.1 mmol) of LEF, a stoichiometric amount of the coformer and 2 drops of methanol were added to stainless steel grinding jars (10 mL) with one 7 mm stainless steel grinding ball and ground at a rate of 20 Hz for 20 min. The resultant products were characterised by X-ray powder diffraction (XRPD) and compared with the reference starting materials for identification of a promising new solid form.

3.6.2   Solvent-Based Cocrystallisation

Solution crystallisation by solvent evaporation was used to prepare single crystals of the new solid forms identified as promising from the grinding experiments. These were used in single crystal X-ray diffraction experiments.

3.6.2.1   LEF-PG Cocrystal

LEF (270.2 mg, 0.1 mmol) and PG (126.1 mg, 0.1 mmol) were dissolved in chloroform (10 mL) at 50 °C and the solution left for evaporation at ambient conditions. After 1-2 days large needle-like crystals were formed.

3.6.2.2   LEF-3HBA Cocrystal

LEF (270.2 mg, 0.1 mmol) and 3HBA (138.1 mg, 0.1 mmol) were dissolved in acetic acid (10 mL) at 90 °C and the solution left for evaporation at ambient conditions. After 2 weeks small needle-like crystals were formed.

3.6.2.3   LEF-2PIC Cocrystal

LEF (270.2 mg, 0.1 mmol) and PIC (123.1 mg, 0.1 mmol) were dissolved in methanol (5 mL) at 50 °C and the solution left for evaporation at ambient conditions. Large block-shaped crystals were obtained after 2-3 days.

3.6.2.4   LEF-2PIC 1:2 Cocrystal

LEF (270.2 mg, 0.1 mmol) and PIC (246.2 mg, 0.2 mmol) were dissolved in methanol (10 mL) at 50 °C and the solution left for evaporation at ambient conditions. After 5-6 days small whitish needle-like crystals were formed.

3.6.2.5 LEF-2APYM Cocrystal

LEF (270.2 mg, 0.1 mmol) and 2APYM (95.1 mg, 0.1 mmol) were dissolved in methanol (5 mL) at 50 °C and the solution left for evaporation at ambient conditions. After 2-3 days large block-shaped crystals were formed.

3.6.3 X-ray Powder Diffraction

XRPD data for samples generated through solid-state grinding, stability, and slurry experiments were collected using a Bruker D8 Advance powder X-ray diffractometer with Cu-Kα radiation (λ = 1.54060 Å), with 35 kV and 40 mA voltage and current applied. The sample was scanned within the range 2θ = 5° to 50° with continuous scanning mode, and a scan rate of 5° min^{-1}.

3.6.4 Single-Crystal X-Ray Diffraction

3.6.4.1 Standard Resolution Data

Standard resolution data (<0.7 Å) for all cocrystals were collected on an Agilent Technologies Dual Source Supernova, four-circle diffractometer fitted with CCD detector, with graphite monochromated Mo-Kα radiation (λ = 0.71073 Å) for the LEF-PG, LEF-2PIC and LEF-2APYM cocrystals, and Cu-Kα radiation (λ = 1.54184 Å) for the LEF-3HBA and LEF-2PIC 1:2 cocrystals. CrysAlisPro software[26] was used for data collection, reduction, and absorption correction using face indexing and Gaussian corrections. Structure solution and refinement were carried out using Intrinsic Phasing in SHELXT-2015[27] and refined by full-matrix least squares on F^2 using SHELXL-2015,[28] both implemented in the Olex2 software.[29] Non-hydrogen atoms in all structures were refined with anisotropic displacement parameters. Hydrogen atoms for heteroatom (N and O) were located from the difference Fourier map and refined freely, maintaining isotropic displacement parameters (U$_{iso}$) whilst the remaining hydrogen atoms were fixed in idealized positions with their displacement parameters riding on the values of their parent atoms. Bond lengths to hydrogen were neutron normalised (for O−H, N−H and C−H at 0.983 Å, 1.009 Å and 1.008 Å respectively) using PLATON[67] for the calculation of bond lengths and bond angles. Crystallographic data, crystal structure information, and hydrogen bond parameters for all structures presented can be found in Appendix B.5 B.6.

3.7 Cocrystal Structure Analysis

Each of these cocrystals were first analysed using XRPD to initially confirm their cocrystal nature. Once this was visually verified through comparison of their experimental patterns with those of their respective components, single crystals of each cocrystal were grown via slow, room-temperature evaporation of an appropriate solvent. Full experimental details of each cocrystallisation can be found in **Chapter 3.6.2**, full crystallographic information is available **Appendix B.5**, along with hydrogen-bond parameters for all structures presented in **Appendix B.6**.

3.7.1 LEF-PG Cocrystal

The crystal structure of the LEF-PG cocrystal belongs to the tetragonal *I-4* space group with the asymmetric unit containing two molecules each of LEF and PG. The crystal structure features hydrogen bonded chains of PG molecules via O–H⋯O (D⋯A 2.852 Å, D–H⋯A 166.7°) hydrogen bonds. These hydrogen bonded chains are interconnected to each other by LEF molecules, stacked along the crystallographic c-axis via π⋯π interactions, involving O_{PG}-H⋯O_{LEF} (2.749 Å, 136.6°) and N_{LEF}-H⋯O_{PG} (2.980 Å, 138.4°) hydrogen bonds. These LEF molecules are stacked in an alternating orientation forming an ABAB type of arrangement. Within this alternating framework of LEF molecules, the 'A' molecules form O–H⋯O and N–H⋯O hydrogen bonds with PG molecules above and below the plane, respectively, and vice versa for the 'B' molecules of LEF (**Figure 3.5**).
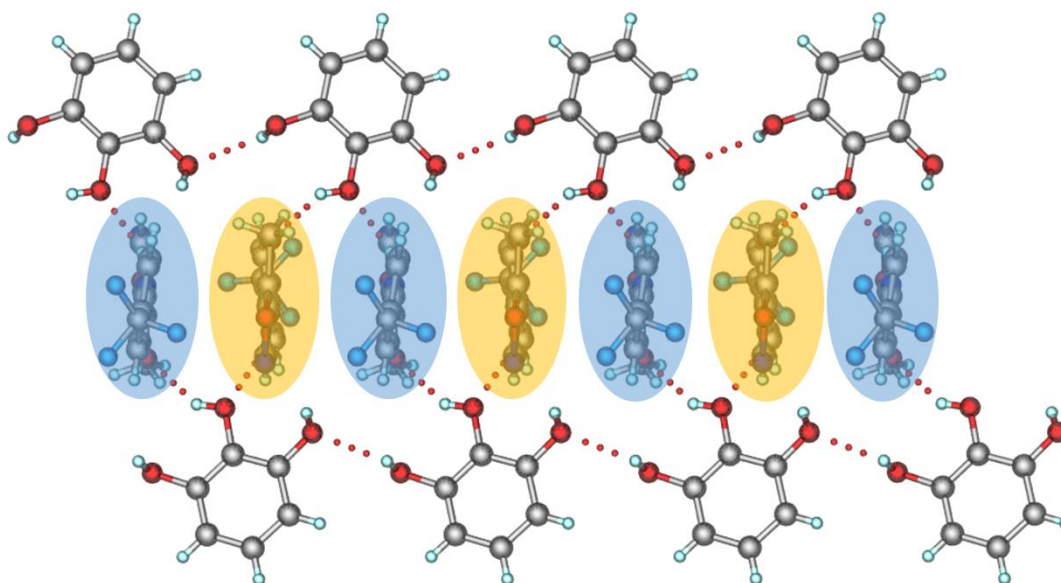
Figure 3.5 Crystal structure of the LEF-PG cocrystal viewed along the (*a+b*)/2 axis
The primary hydrogen-bonding interactions are shown, along with the alternating ABAB type orientation of LEF molecules. 'A' molecules are shown in blue with 'B' molecules in orange

3.7.2 LEF-3HBA Cocrystal

The LEF-3HBA cocrystal crystallises in the monoclinic *P21/n* space group and contains one molecule each of LEF and 3HBA in the asymmetric unit and features a mixture of hydroxyl-acid, acid-isoxazole and amide-amide interactions. Self-assembly of LEF molecules via amide-amide N–H···O (2.976 Å, 156.8°) hydrogen bond along the crystallographic b-axis generate hydrogen bonded chains. 3HBA molecules also self-assemble to form hydrogen bonded chains via O–H···O (2.735 Å, 168.7°) hydrogen bonds involving hydroxyl and carbonyl groups. These chains consist of 3HBA molecules in alternating orientations connected either side by acid-isoxazole O–H···N (2.784 Å, 174.2°) hydrogen bonding to LEF chains that extend parallel along the *b*-axis through amide-amide N–H···O (2.976 Å, 156.8°) hydrogen bonds (**Figure 3.6**).

3.7.3 LEF-2PIC Cocrystal

The first LEF-2PIC cocrystal (monoclinic *P21/c*) obtained was a 1:1 stoichiometric cocrystal, with an intramolecular proton transfer occurring within 2PIC from O3 to N3. This proton transfer enables formation of coformer carboxylate-pyridinium dimers through charge-assisted N+–H···O– (2.666 Å, 150.7°) hydrogen bonds. These dimers connect inversion related LEF molecules through amide-carboxylate N–H···O– (2.893 Å, 159.7°) hydrogen bond that results in discrete four-membered LEF-2PIC-2PIC-LEF units that self-assemble next to each other in mirrored arrangements along the *c*-axis (**Figure 3.7**).
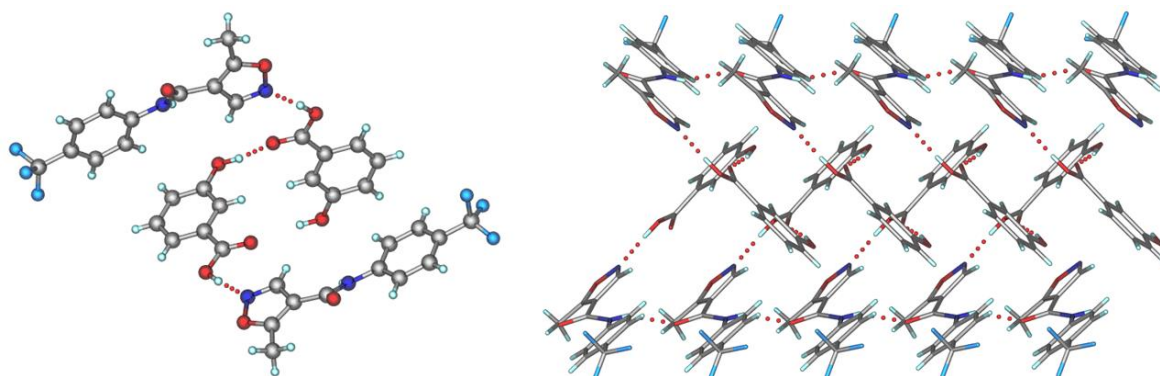
Figure 3.6 Left, LEF-3HBA viewed down the b-axis (left) showing the hydrogen bonding between components, and the (*a*+*c*)/2 axis (right) showing the alternating orientation of 3HBA molecules
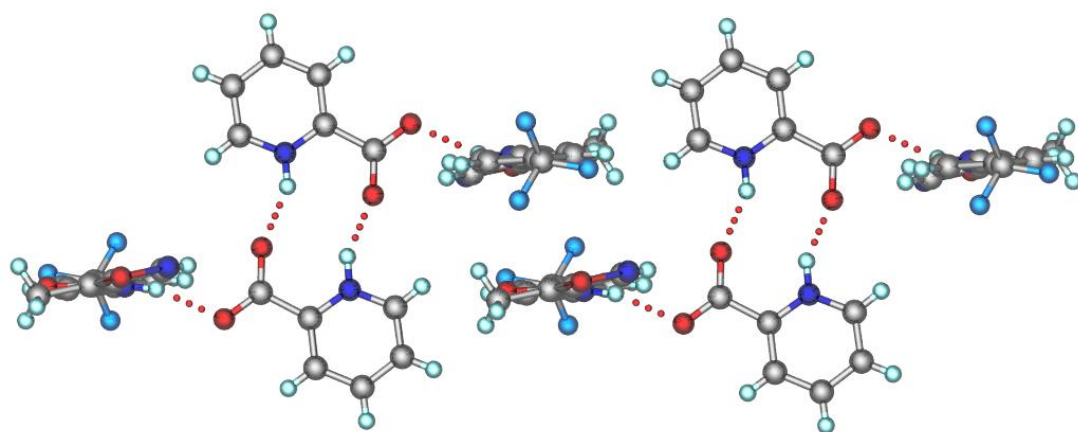
Figure 3.7 Crystal structure of the LEF-2PIC cocrystal viewed down the (*a+b*)/2 axis

The 2PIC dimers, four-membered supramolecular units, and the arrangement of neighbouring units are all shown

3.7.4   LEF-2PIC 1:2 Cocrystal

LEF also forms a 1:2 cocrystal with 2PIC (monoclinic *P21/c*), again with the 2PIC molecule exhibiting intramolecular proton transfer from the carboxylic acid group to the pyridine nitrogen that leaves the complex overall neutral and therefore a cocrystal rather than a salt. This affords two charge-assisted N+–H···O– (2.649 Å, 159.3°; 2.703 Å, 157.9°) hydrogen bonds between 2PIC molecules possessing alternating orientations orthogonal to each other. These hydrogen bonds result in a ladder network of 2PIC molecules along the c-axis, which are linked to the bordering LEF molecules via amide-carboxylate N–H···O– (2.848 Å, 168.9°) hydrogen bonds (**Figure 3.8**).
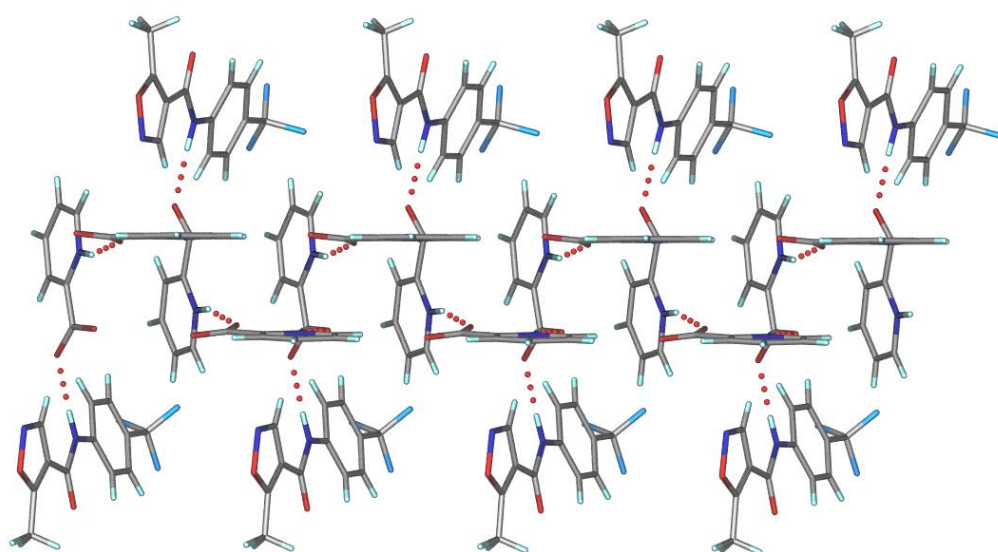
Figure 3.8 Crystal structure of the LEF-2PIC 1:2 cocrystal

The 2PIC central ladder rungs with peripheral LEF molecules are shown

3.7.5   LEF-2APYM Cocrystal

LEF and 2APYM form a 1:1 cocrystal, in the monoclinic *P21/n* space group, featuring a primary hydrogen bonding of amine-pyrimidine dimer between N4⋯N5 of 2APYM molecules (2.943 Å, 176.0°). Each 2APYM molecule also interacts separately with two LEF molecules through amide N–H⋯pyrimidine (3.072 Å, 166.6°) and amine N–H⋯amide O=C (2.941 Å, 127.7°) hydrogen bonds. These result in a crystal packing similar to that of the LEF-2PIC 1:1 cocrystal, whereby 2APYM-2APYM dimers connect LEF molecules that stack above each other in inverted orientations. However, unlike the LEF-2PIC 1:1 cocrystal, four-membered supramolecular unit is not formed in LEF-2APYM cocrystal due to the fact that the amide C=O of LEF molecule helps to form an extended hydrogen-bonded network along the crystallographic *b*-axis (**Figure 3.9**).

3.8   Thermal Analysis

Thermal properties of the pharmaceutically acceptable solids (LEF-PG, LEF-3HBA, LEF-2PIC and LEF-2PIC 1:2 cocrystals) were analysed using DSC (**Figure 3.10**). All four solid forms exhibit melting endotherms lower than the melting point of LEF (165-166 °C), with modification of the melting point of an API a characteristic trait observed in pharmaceutical cocrystals and commonly attributed to the effect of coformer melting point.[68] The coformers PG, 3HBA, 2PIC and 2APYM possess melting points of 131-134, 201-202, 136-138 and 122-126 °C, respectively.

Therefore, the two pharmaceutically acceptable cocrystals LEF-PG and LEF-2PIC and the non-pharmaceutically acceptable cocrystal LEF-2APYM were found to display melting points falling between that of API and coformer. With LEF-3HBA and LEF-2PIC 1:2 both possessing a lower melting point than their individual components, these results are consistent with the literature on the cocrystal melting point with respect to its individual components. Studies suggest that an intermediate cocrystal melting is true for more than 50% of cases, while a lower cocrystal melting point is seen in fewer than 40%.[69]
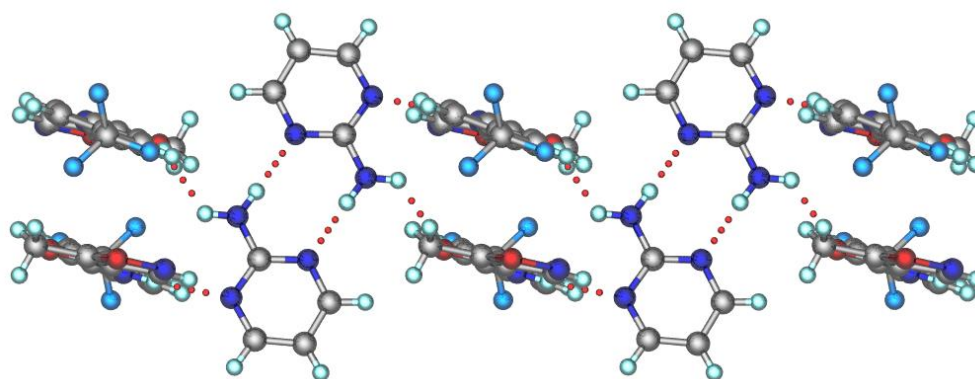
Figure 3.9 Crystal structure of the LEF-2APYM cocrystal viewed down the (*a*+*c*)/2-axis
The formation of 2APYM dimers and the continuous hydrogen-bonded sequence are shown
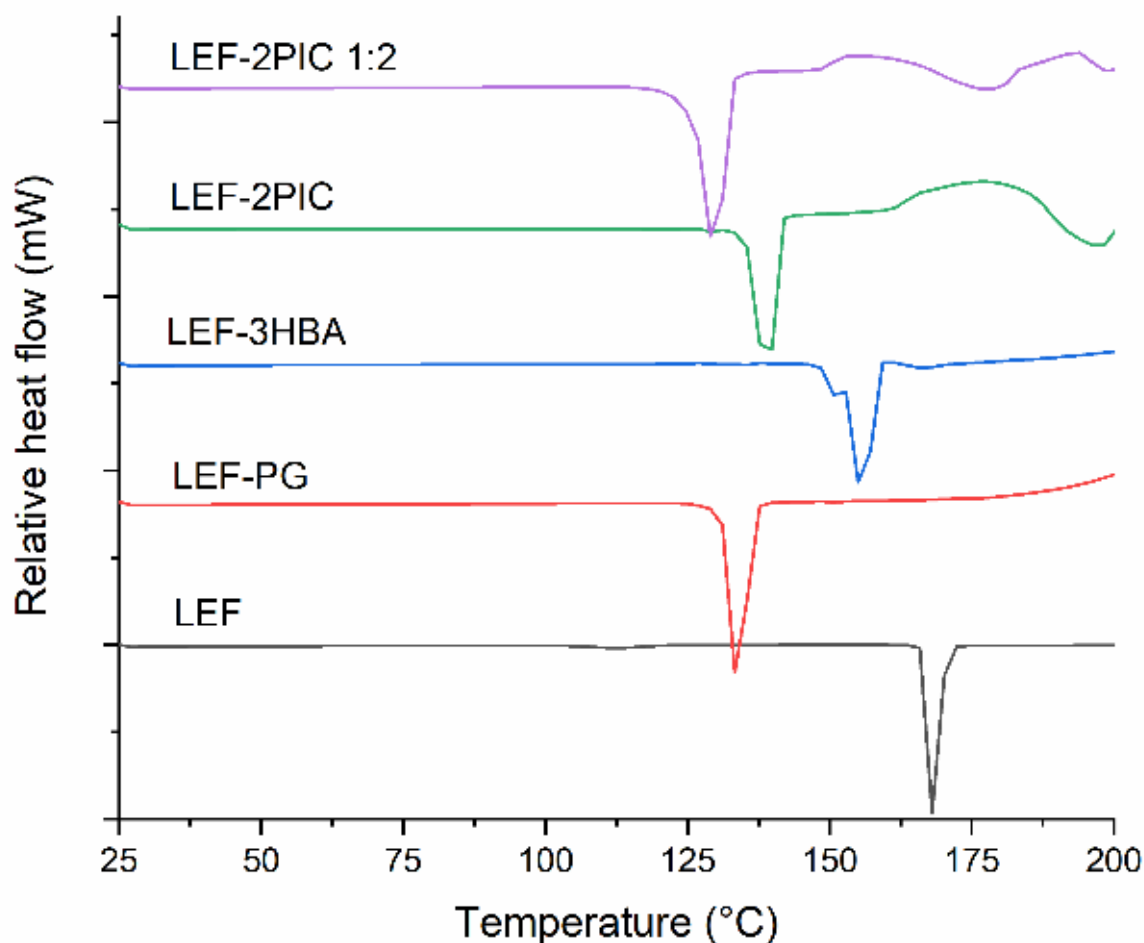
Figure 3.10 DSC thermograms of LEF and cocrystals

3.9   Stability Analysis

Stability of the cocrystals LEF-PG, LEF-3HBA, LEF-2PIC and LEF-2PIC 1:2 was evaluated, with respect to the parent API, under accelerated storage conditions (40 °C, 75% RH) over a period of 13 weeks, and also measured under slurry conditions.

3.9.1   Accelerated Storage Stability

XRPD data showed that all samples remained stable over the course of the testing period. Peaks associated with LEF were not observed in the XRPD patterns of the cocrystals throughout the testing period, indicating that there was no sign of cocrystal dissociation. The only minor stability issue was a slight loss of crystallinity in the LEF-2PIC cocrystal after 13 weeks. There was broadening in characteristic peaks at 2θ values of 8.9, 14.8 and 15.0 but the peak positions remained consistent (**Appendix B.8**)

3.9.2   Slurry Stability

Excess powder samples were suspended in vials of ultrapure water and stirred for 24 hours at 37 °C, then filtered and dried for XRPD analysis. The results for the LEF-PG, LEF-2PIC and LEF-2PIC 1:2 cocrystals show crystalline peaks corresponding to LEF in their respective post-slurry XRPD patterns, which suggest that these cocrystals dissociate and the more soluble PG and 2PIC coformers dissolve in solution to leave behind the parent LEF in solid form. On the other hand, LEF-3HBA remained stable in slurry as seen from the near perfect match of XRPD patterns before and after slurry test. The sample of LEF showed consistency in the XRPD patterns taken before and after slurry with no indication of polymorphic transformation (**Appendix B.8**).

Overall stability results show that cocrystallisation of LEF with the coformers did not impact upon stability under accelerated storage. While the cocrystals with PG and 2PIC showed dissociation under slurry conditions, LEF-3HBA remained stable. As mentioned previously, CSD interaction searching did not demonstrate the propensity of LEF to form carboxylic acid···N(ar) heterosynthons, however COOH functional groups were considered due to the reported abundance, strength, and preference for synthon formation over other possible motifs such as acid-acid dimers.[70,71] This could explain the greater stability of the LEF-3HBA under slurry conditions, as the formation of stronger acid···N(isoxazole) hydrogen bonds serves to maintain the crystal lattice, with such hydrogen bonds absent in the other cocrystals.

3.10   Solution Properties

The impact of cocrystallisation on the solution behaviour, namely the solubility and dissolution rate of LEF was evaluated.

3.10.1   Solubility

Many known APIs suffer from poor aqueous solubility and dissolution rate, which leads to a reduced bioavailability. Leflunomide is no exception, its high lipophilicity and low solubility in water (reported to be less than 40 mgL-1) firmly place it in BCS class II. Optimisation of the pharmacological profile, through increasing both solubility and dissolution rate, therefore, maintains a goal for cocrystallisation of LEF.

The effect of cocrystallisation on these properties was evaluated. The solubilities of the samples LEF and the stable cocrystal, LEF-3HBA, were measured using the shake-flask method.[72] Prior stability results showed that cocrystals LEF-PG, LEF-2PIC and LEF-2PIC 1:2 were unstable under slurry conditions therefore their true solubility is not reflected in these calculations. Apparent

solubility of these samples was calculated by extracting the gradient of the linear portion of their respective dissolution rate plots.[73] **Table 3.1** shows the solubility values of the cocrystals, and their improvement with respect to that of LEF. The greatest improvements in solubility are seen in the LEF-PG and LEF-2PIC cocrystals, both of which have been shown to dissociate in solution. This improvement is partially expected as dissociable cocrystals are reported to possess higher solubility than their stable counterparts.

A mechanism proposed by Babu *et al*. attributes the initial improved apparent solubility of cocrystals to "spring effect" whereby the dissociation of a cocrystal leaves amorphous dissociated API molecules in solution, which lack the strong intermolecular interactions present in the crystalline form and thus showing a sudden spike in the observed solubility.[74] The stable, non-dissociating LEF-3HBA cocrystal also shows a slight increase in solubility compared to LEF. Again, this is something which is expected, as 3HBA possesses a much higher aqueous solubility of $7.57gL^{-1}$,[75] and cocrystal solubility is reported to be directly proportional to its constituents.[76]

3.10.2 Dissolution Rate

The dissolution rates of the cocrystals with respect to LEF also show a marked improvement (**Figure 3.11**). An increase in the initial dissolution rate is expected for the dissociable cocrystals LEF-PG, LEF-2PIC and LEF-2PIC 1:2 due to the aforementioned "spring effect". LEF-3HBA also shows a higher dissolution rate than LEF, with all three cocrystals reaching plateau in their dissolution profiles within 360 minutes. Comparatively, only 81% of LEF was dissolved during the same time frame.

Table 3.1 Solubility of LEF and cocrystals and the improvement in cocrystal solubility compared to LEF, calculated as a ratio of cocrystal solubility:LEF solubility

Sample	Solubility/mgL^{-1}	Solubility Improvement
LEF	31.65	1
LEF-PG	44.63[a]	1.41
LEF-3HBA	36.58	1.16
LEF-2PIC	40.11[a]	1.27
LEF-2PIC 1:2	34.45[a]	1.09

[a]Apparent solubility
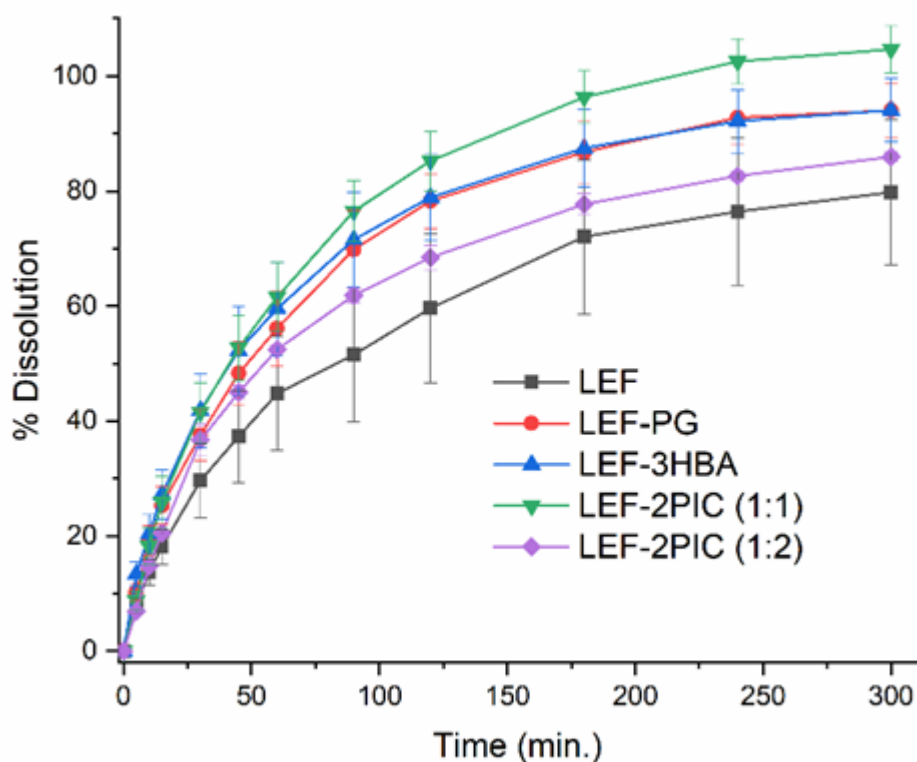
Figure 3.11 Dissolution rate profile for LEF and cocrystals in ultrapure water

All four cocrystals show an improvement in dissolution rate of LEF in accordance with their increased solubility, however, the dissolution rates do not follow the same trend as that of their solubility. LEF-2PIC cocrystal showed the fastest dissolution rate among all the samples, whereas LEF-PG is the most soluble cocrystal.

However, it must be noted that these are apparent solubility values, which are calculated from the initial linear portion of the dissolution curves at which kinetics dominate the dissolution rate and are thus not wholly representative of the thermodynamically dependent equilibrium solubility and therefore may not reflect the true solubility. LEF-3HBA shows both the lowest improvement in solubility and dissolution rate of all cocrystals but is nonetheless enhanced compared to the parent API.

3.11 Conclusions

Leflunomide, a BCS Class II immunosuppressive disease-modifying antirheumatic drug, has its bioavailability limited by poor aqueous solubility and dissolution rate. Through detailed analysis of its structure and intermolecular interaction capabilities, using Isostar and Mercury, a range of favourable functional groups for its cocrystallisation, and a selection of coformers possessing these, have been identified. This rational selection of coformers has resulted in five new cocrystals of LEF. Crystal structure of the cocrystals has been determined and described in detail,

with their intermolecular interactions highlighted with respect to the CSD interaction analysis. Their observed interactions display a number of supramolecular synthons previously recognised through prediction methods as promising interactions for LEF, such as amine···amide, COOH···amide and COOH···isoxazole.

Physicochemical properties, such as thermal behaviour, stability, solubility, and dissolution rate have been evaluated for the four pharmaceutically acceptable cocrystals: LEF-PG, LEF-3HBA, LEF-2PIC, and LEF-2PIC 1:2. Cocrystallisation was found to notably modify these properties. All four cocrystals possess different melting points compared to LEF, with LEF-PG and LEF-2PIC cocrystals falling in between and LEF-3HBA cocrystal displaying a higher melting point than their respective components. LEF-3HBA cocrystal was the only cocrystal found to be stable under both accelerated and slurry conditions, as LEF-PG and both LEF-2PIC cocrystals showed signs of dissociation when slurried for 24 hours. This dissociation most likely allowed for the LEF-PG and LEF-2PIC cocrystals to exhibit the highest apparent aqueous solubility of all samples, while LEF-3HBA cocrystal also improved the solubility of LEF. Dissolution profiles of all the samples showed that cocrystallisation improved the rates at which LEF was dissolved in solution, in line with their enhanced solubility. Collation of all the results for the four pharmaceutically acceptable cocrystals indicates LEF-3HBA cocrystal as a viable solid form for development of novel drug formulations due to its ability to improve the weakest aspects of the LEF pharmaceutical profile – solubility and dissolution rate – whilst maintaining stability under a variety of conditions.

Attention now turns to garnering a greater understanding of the structure-property relationships of these cocrystal systems, through electronic-resolution and formulation aspects. Currently not a great deal is understood about the effects of excipients, and their interactions with drug molecules (whether single or multi-component), on the physicochemical properties.

Further direction for the work begins with the development of pharmaceutically applicable formulations of the multi-component systems identified thus far – based on current marketed ingredients. The physicochemical properties, i.e. solubility and dissolution rate of these will be assessed and compared to that of the systems sans formulation. This will serve as a reference point for proposed computational investigation of selected cocrystals with respect to cocrystal-excipient interactions.

Looking to further work, subjecting these chosen systems to high-resolution charge-density studies would not only provide a unique view of the electronic behaviour within the systems, but will also serve as a complementary study to planned *ab initio* calculations of formulation properties via molecular dynamics simulations. Refinement of high-resolution data of these systems would elucidate various properties of these cocrystals, such as electronic distribution and

number, type, and strength of intermolecular interactions. Results of these investigations, used at the particle-level to both computationally and experimentally inform characteristics including morphology and potential interfacial interactions, would serve to further the understanding of the effects of crystal structure on physicochemical properties.

Chapter 4   Formulation Studies of LEF Cocrystals

The objectives of this chapter are to integrate MD simulations as a complement to conventional experimental methods and gain a molecular-level understanding of the interactions between drug, selected excipients, and water. Such studies would be expected to streamline excipient screening and help in the selection of suitable excipients for the development of cocrystal formulations. The knowledge gained from MD simulations was subsequently used to prepare prototype oral dosage formulations, such as tablets, and evaluate their performance. Toward this goal, the current work indicates a detailed underlying mechanism in molecular interactions among LEF and its cocrystals, excipients, and water, and identifies governing factors to explain a hierarchy of the aqueous dissolution of formulations obtained experimentally.

This work herein described therefore addresses the main objective outlined in **Chapter 2**:

5. Employ theoretical molecular dynamics simulations to shed light on certain indicative properties of an API/cocrystal that impact its solution behaviour and assess its success relative to experimental observations.

The results discussed in this chapter is taken from the work published by Cadden, J.; Gupta, K. M.; Kanaujia, P.; Coles, S. J.; Aitipamula, S. *Cryst. Growth Des.* 2021, **21**, 2, 1006-1018. MD simulations were performed by Krishna M. Gupta as part of a collaborative effort towards the publication. All other experimental work referred to herein was performed by Joseph Cadden.

4.1   Background

Cocrystallisation has matured into an established technique for fine-tuning the physicochemical properties of active pharmaceutical ingredients.[2] This technique has been adopted by pharmaceutical drug companies, with increasing numbers of cocrystal-based drug products now entering the market. Surprisingly, however, studies into the formulation aspects of cocrystal-based drugs are relatively few and far between compared to the vast literature on their design, synthesis, and characterisation.

This leaves scope to introduce a more informed process of decision making whereby favourable formulation strategies are developed based on molecular structure and interactions between drug and excipient. In order to fully understand the nature of cocrystal-excipient interactions and the effect of these upon the physiochemical properties, the combination of computational methods with experimental approaches has shown to be an effective tool. Of these computational methods, molecular dynamics (MD) simulations have most notably been the

subject of significant recent interest in the field of science and engineering.[77] The MD method is a deterministic technique that integrates Newton's equation of motion, by taking small time increments to predict new positions and velocities of atoms in a dynamic process. MD simulations have been extensively used to understand the solubility and miscibility phenomena of APIs in the presence of excipients,[78,79] and have also gained attention in elucidating excipient-assisted solubilisation of water insoluble drugs.[80,81,82]

This chapter herein reports results of our investigations into cocrystal-excipient interactions in water that determine the dissolution properties of cocrystals in formulation by a combination of molecular dynamics (MD) simulation and experimental approaches.

Two cocrystals of an antirheumatic drug, leflunomide (LEF) with 3-hydroxybenzoic acid (3HBA) and 2-picolinic acid (2PIC) were assessed in formulation with the frequently used excipients, lactose and dicalcium phosphate (DCP). For comparison, the dissolution of neat LEF formulations with these excipients was also evaluated. The parameters deduced from MD simulations, such as solvent accessible surface area, intermolecular hydrogen bonds among formulation ingredients and water, and interaction energy between an API or cocrystal and water were found to be essential indicators in the prediction of cocrystal formulation dissolution trends. It was found that the presence of lactose as an excipient improved dissolution of cocrystal formulation compared to the neat cocrystals, most notably for the LEF-2PIC cocrystal. In contrast, DCP was seen to have a detrimental effect on the dissolution of cocrystal formulations, all exhibiting lower dissolution than their neat cocrystal counterparts and LEF. Careful analysis of these results revealed that the nature of excipient plays a significant role in the dissolution properties. While the improved dissolution of the lactose formulations was attributed to its hydrophilic nature, the ionic and hydrophobic nature of DCP was likely responsible for its detrimental effect. The results of the MD simulations were found to be in excellent agreement with the experimentally observed dissolution hierarchy.

4.2   Selection of Cocrystals and Excipients

Evaluation of the physicochemical properties of the formulations revealed that three of these cocrystals showed improved behaviour compared to the analogous physical mixtures, as well as the parent API. As described in previously, there was a degree of commensurate modulation found in the crystal structure of LEF-PG therefore, this cocrystal, and the nonpharmaceutical cocrystal with 2-aminopyridine, were not considered for the current study. Specifically, MD simulations were conducted with the parent API, and the three best physicochemically

performing cocrystals: LEF, LEF-3HBA, and LEF-2PIC in the presence of two frequently used pharmaceutical excipients, lactose, and dibasic calcium phosphate ($CaHPO_4$, DCP).

4.2.1   Lactose

Lactose is a disaccharide consisting of the sugars D-galactose and D-glucose. Pharmaceutical applications of lactose as a tablet and capsule diluent, filler, binder, dry powder inhaler carrier, and lyophilisation aid have been well documented.[83] Its high water solubility, low hygroscopicity, cost effectiveness, bland taste, and compatibility with several active ingredients and excipients make it a widely used excipient in pharmaceutical formulations.[84] Lactose has also been used as an effective excipient in direct compression tableting applications and is a key component of the LEF oral tablet formulations.[83]

4.2.2   Dibasic Calcium Phosphate

DCP is a water-insoluble inorganic substance that has been used in pharmaceutical tablets and capsules as a filler and diluent, as well as a source of calcium in nutritional supplements.[84] Its non-hygroscopicity, associated with excellent compaction and flow properties, makes it an ideal excipient for direct compression processes.[85] DCP has also been used as an alternative to lactose in the development of lactose-free formulations. The choice of DCP as an excipient in the current study was made to understand (a) the impact of an ionic and water-insoluble excipient on the dissolution of the cocrystal and (b) whether DCP has a similar or different effect on cocrystals, so it may be used as an alternative to lactose in cocrystal-based formulations.

4.3   MD Simulation Results

4.3.1   Lactose as an Excipient

The stability of the LEF/cocrystal-excipient system was gauged by root-mean-square deviation (RMSD) with respect to the initial structure. **Figure 4.1** shows the RMSD of LEF, LEF-3HBA, and LEF-2PIC with lactose as an excipient, without water. For each combination, the RMSD remains almost constant throughout the simulation. This reveals that lactose is strongly bonded to the molecular components and that, in the absence of water, each complex is at a stable state. In contrast, in the presence of water, the RMSDs are fluctuating throughout the simulation (**Figure 4.1 (b)**), particularly in the case of the LEF-2PIC cocrystal. This is an indication of a comparatively higher dissolution of the LEF-2PIC cocrystal-lactose complex. With a higher dissolution in water, the complex would dissociate to a larger extent, and thus the RMSD would be expected to fluctuate more. Note that, even though the RMSD could be used to understand the dissolution behaviour to a certain extent, it will not be possible to predict the dissolution hierarchy, as the RMSDs are calculated based on the deviation of the atoms in a molecule with respect to its initial structure. To further elucidate the dissolution phenomena, the SASA of LEF and the cocrystals and their combinations with lactose in water were calculated with a probe of diameter 0.28 nm. Herein, the SASA represents the available surface area of the LEF/cocrystal and their complex with the excipient to interact with water. **Table 4.1** lists the hydrophilic, hydrophobic, and total SASAs of LEF/cocrystals and complexes. Since the volume of each component (API or cocrystal) is different, the SASA is calculated per volume of components. Without lactose, the LEF-3HBA cocrystal possesses the highest SASA compared to pure LEF and LEF-2PIC cocrystal, indicating the higher water accessibility.
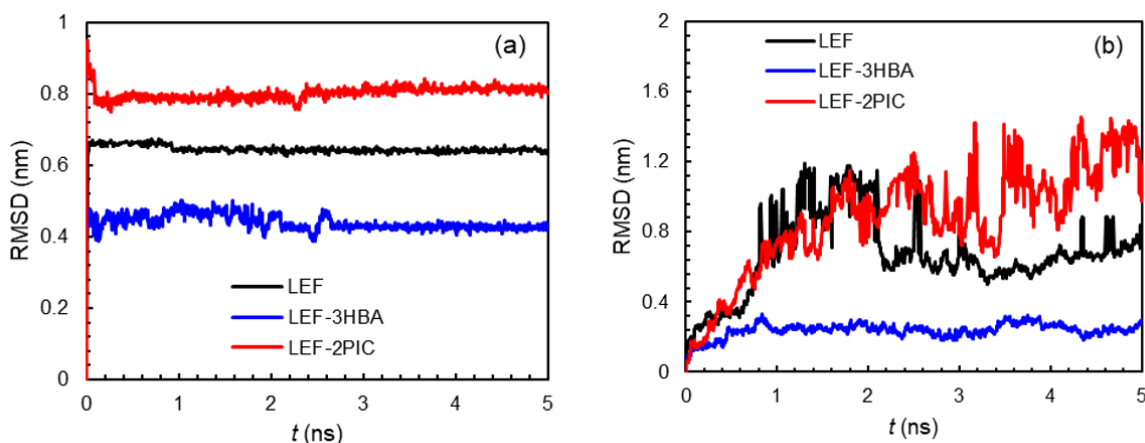
Figure 4.1 Root mean-squared deviations (RMSDs) of complexes in the (a) absence of water and (b) presence of water

Table 4.1 Solvent accessible surface areas (SASAs) of LEF/cocrystals and complexes with lactose
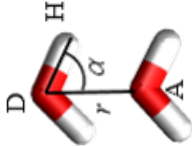
System	Hydrophilic (nm^2)	Hydrophobic (nm^2)	Total (nm^2)
	without lactose		
LEF	2.06	6.18	8.24
LEF-3HBA	2.69	7.23	9.93
LEF-2PIC	2.06	6.23	8.29
	with lactose		
LEF	6.04	7.66	13.70
LEF-3HBA	6.40	8.85	15.25
LEF-2PIC	7.57	9.28	16.85

However, in the presence of lactose, the highest SASA is observed for the LEF-2PIC cocrystal-lactose complex. Interestingly, as lactose is introduced, each complex shows significant increase in total SASA, which is mainly contributed by the hydrophilic component. Owing to the hydrophilic nature of lactose, this contribution dominates when compared to the hydrophobic component. This indicates that the hydrophilic nature of each system is enhanced considerably in the presence of lactose, hence leading to a higher dissolution of the complex in water. Among the three systems studied, the LEF-2PIC cocrystal-lactose complex exhibits the highest total, as well as hydrophilic, SASAs and therefore suggests greater dissolution for the LEF-2PIC cocrystal in the presence of lactose in water.

Hydrogen bonds play an important role in the solubility and dissolution of a solute in water.[86] MD simulations have proved effective in the prediction of hydrogen bonds between a solute and bulk solvent, such as water, and hence aid in the prediction of the solubility/dissolution of a solid.

The number of hydrogen bonds between molecular components of drug crystals and water have been calculated, with and without lactose. Two geometrical criteria were implemented to calculate the hydrogen bonds (1) the distance (r) between a donor and an acceptor ≤ 3.5 Å and (2) the angle of hydrogen-donor-acceptor, $\alpha \leq 30°$.[87] Two water molecules representing r and α, are shown in **Table 4.2**. Similar to SASA, the number of hydrogen bonds are estimated based on per volume of the components.

Table 4.2 The number of hydrogen bonds between LEF/cocrystal and water with and without lactose

System	LEF	LEF-3HBA	LEF-2PIC	Geometrical description
without lactose				
LEF/cocrystal-water	8.27	13.63	15.55	
with lactose				
LEF/cocrystal-water	32.56	38.53	44.59	
LEF/cocrystal-lactose	0.15	3.28	2.29	

As tabulated in **Table 4.2**, in the presence or absence of lactose, the number of hydrogen bonds between LEF/cocrystals or complexes and water follows the trend LEF < LEF-3HBA < LEF-2PIC, thereby representing the dissolution trend of pure LEF/cocrystals and complexes in water.

It is worthwhile to note that the number of hydrogen bonds between any system and water in the presence of lactose (i.e. between complexes and water) is much higher compared to without lactose (i.e. between LEF/cocrystals and water), which is consistent with SASA. Besides, the number of hydrogen bonds between neat LEF and lactose is fewer than the number of hydrogen bonds between the cocrystal and lactose. Among this, the LEF-3HBA cocrystal has the highest number of hydrogen bonds followed by the LEF-2PIC cocrystal. This can be attributed to the fact that the –OH and –COOH groups of HBA act as both hydrogen bond donors and acceptors. In contrast, the –N⁺H and –COO⁻ groups of 2PIC in the LEF-2PIC cocrystal only act as hydrogen bond donor and acceptor, respectively, hence forming fewer hydrogen bonds with lactose.

We further evaluate the interaction sites of water in the pure drug crystal and complex by radial distribution function g(r) as:

$$g_{ij}(r) = \frac{N_{ij}(r, r+\Delta r)V}{4\pi r^2 \Delta r\, N_i N_j} \qquad (5)$$

where r is the distance between atoms i and j, N_i and i are the numbers of atoms *i* and *j*, $N_{ij}(r, r+\Delta r)$ is the number of atoms *j* around *i* within a shell from *r* to *r + Δr*, respectively.

Figure 4.2 (a) shows the *g(r)* of the hydrogen (H) atom of water around the O1, O2, N1, N2 and F atoms of LEF without lactose. Two prominent peaks are observed at r ~ 2.1 Å corresponding to the O2 and N1 atoms, indicating the most favourable sites for water. These peaks also indicate
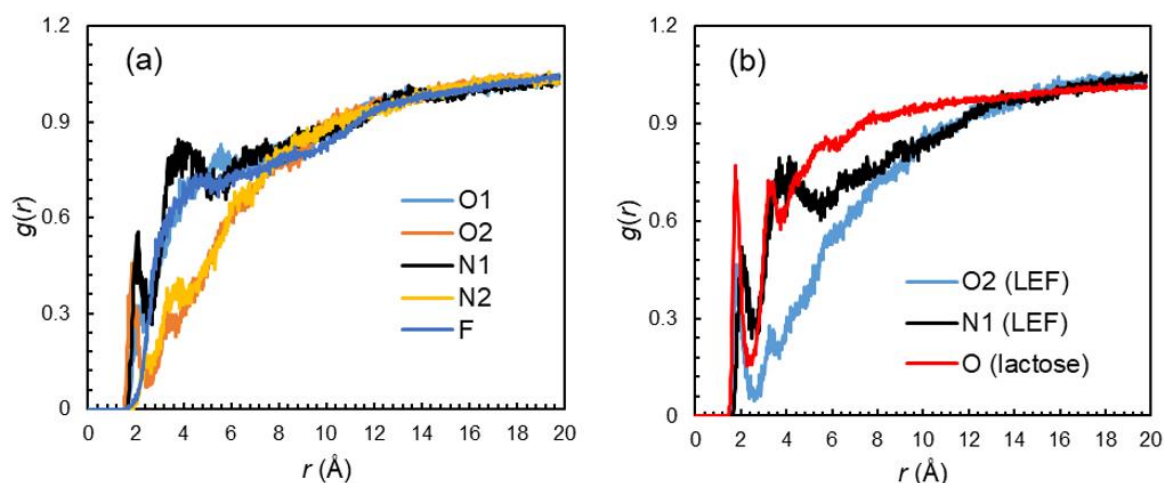
Figure 4.2 The $g(r)$ of the H atom of water around (a) the atoms of LEF and (b) the O2 and N1 atoms of LEF, and the O atom of lactose

that LEF is able to form hydrogen bonds with water around these atoms. In the case of the LEF-lactose complex, the $g(r)$ of the H atom of water around the most favourable atoms (O2 and N1) and all oxygen (O) atoms of lactose are plotted in **Figure 4.2 (b)**. Along with two earlier peaks, a third peak is observed at a shorter distance ($r \sim 1.8$ Å) corresponding to the O atom of lactose. The peak height here is the highest, reflecting the most dominating interaction site for water. A similar phenomenon is also observed for the cocrystal-lactose complexes (**Appendix C**). All oxygen atoms of the 3HBA in the LEF-3HBA cocrystal and 2PIC in the LEF-2PIC cocrystal are involved in hydrogen bond formation with water. The analysis identified the possible atoms which could form hydrogen bonds and suggests that the addition of lactose to pure drug/cocrystals enhances the dissolution of the complex by providing additional interaction sites for water.

To quantify the strength of interactions between molecules, their energies in terms of electrostatic (E_{coul}), Lennard-Jones (E_{LJ}), and total (E_{total}) are calculated for each molecule. Usually, attractive, or favourable interaction is indicated by a negative value of the energy.

A higher absolute value of energy is an indicator of stronger interaction among interacting molecules. Moreover, a positive value denotes repulsive or unfavourable interaction. The calculated interaction energy terms for LEF and cocrystal systems are negative, thus indicative of favourable interactions (**Table 4.3**). Both in pure LEF/cocrystals and complexes, the interaction energies with water are found to increase in the order of LEF < LEF-3HBA cocrystal < LEF-2PIC cocrystal. Compared to pure LEF/cocrystals, complexes with lactose possess much higher interaction energy. The observed trend is consistent with hydrogen bond analysis.

The interaction energy terms E_{coul}, E_{LJ}, and E_{total} for the LEF-2PIC-lactose complex are -713.7, -97.8 and -811.5 kJ mol^{-1}, respectively.

Table 4.3 LEF/cocrystals-water and complex-water interaction energies (kJ mol^{-1})

System	E$_{coul}$	E$_{IJ}$	E$_{Total}$
without lactose			
LEF	-64.04	-63.01	-127.05
LEF-3HBA	-188.50	-97.82	-286.32
LEF-2PIC	-338.64	-69.59	-408.23
with lactose			
LEF	-527.13	658	-607.18
LEF-3HBA	-543.22	96	-647.31
LEF-2PIC	-713.70	132	-811.54

The contribution from electrostatic interaction is dominated over Lennard-Jones in the total energy term due to the polar moiety of water strongly interacting with the hydrophilic lactose and ionic moieties of 2PIC in the LEF-2PIC cocrystal. By attributing the highest interaction energy to water, the LEF-2PIC cocrystal-lactose combination is predicted to have higher solubility/dissolution in water.

Consistent with our prediction, it is reported that the interaction energy between drug and water plays an important role in elucidating the dissolution phenomena; specifically, a stronger interaction between drug and water is considered to positively favour dissolution. The predicted dissolution trend in water by MD simulations is in direct agreement with the experimental observations (*vide supra*).

While providing useful molecular-level insights, the above examined parameters (SASA, hydrogen bonds, and interaction energy) govern the dissolution hierarchy of the complexes in water. Nevertheless, to directly capture the dissolution event by MD simulations, additional simulations were conducted without applying position restraints on LEF/cocrystals. The dissolution event of the complexes in water were gauged by intermolecular contacts. Physically, a complex is considered to be dissolved completely in water if there are no, or almost no, intermolecular contacts remaining. **Figure 4.3** depicts the time evolution of intermolecular contacts during MD simulations. For the LEF-lactose complex, as time lapses, the number of contacts between LEF and lactose decreases; finally reaching ~ 0 after 1000 ps. However, the number of LEF-LEF contacts remains almost constant throughout the simulation, which in turn reflects insignificant dissolution of LEF. Therefore, this complex is deemed to be in an undissolved state. For the LEF-3HBA
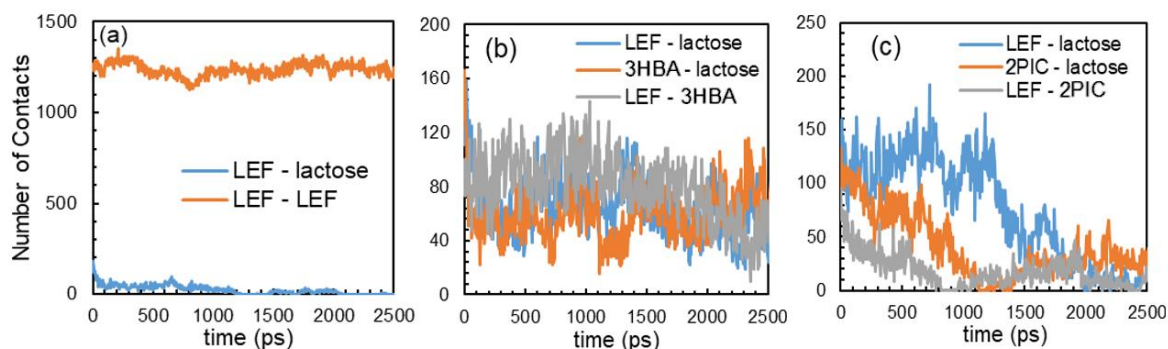
Figure 4.3 Time evolution intermolecular contacts in complexes in water (a) LEF–lactose, (b) LEF-3HBA–lactose, and (c) LEF-2PIC–lactose.

cocrystal-lactose complex, there is a slow decreasing trend in the number of intermolecular contacts with time despite a fluctuation in the plots. Notably, the intermolecular contacts between cocrystal and lactose (LEF-lactose and HBA-lactose), as well as those between LEF and HBA does not reach ~0, which indicates that this complex holds slow or reduced dissolution characteristics in water. On the other hand, in the LEF-2PIC cocrystal-lactose complex, all intermolecular contacts decrease in number with simulation time and reach almost zero after 2000 ps. This complex shows fast and complete dissolution in water, thereby suggesting best dissolving complex in water.

4.3.2 Dibasic Calcium Phosphate as an Excipient

MD simulations were performed to gauge the impact of DCP on the hierarchy of dissolution, as well as to gain atomic-level insights into trends in dissolution.

Table 4.4 lists the hydrophilic, hydrophobic, and total SASAs of LEF/cocrystals and complexes. Similar to lactose as an excipient, addition of DCP to LEF or cocrystal significantly increased SASA. The LEF-3HBA cocrystal-DCP complex possesses the largest SASA, whereas in the case of lactose the LEF-2PIC cocrystal-lactose complex showed the highest SASA.

Table 4.4 SASA of LEF/cocrystals and complexes with DCP

System	Hydrophilic (nm²)	Hydrophobic (nm²)	Total (nm²)
LEF	5.58	6.12	11.70
LEF-3HBA	7.76	7.42	15.18
LEF-2PIC	4.89	5.62	10.50

The hierarchy of both the number of hydrogen bonds and interaction energies between complexes and water follows the trend: LEF < LEF-2PIC < LEF-3HBA (**Table 4.5** and **Table 4.6**).

A fewer number of hydrogen bonds and lower interaction energy for the LEF-2PIC cocrystal-DCP complex in water as compared to the LEF-3HBA cocrystal-DCP complex could be attributed to the ionic nature of 2PIC and DCP. The total interaction energy between the LEF-2PIC cocrystal and DCP is the highest and the contribution from ionic interaction dominates (**Table 4.6**).

The fact that the potential interaction sites of 2PIC are partially blocked by the Ca^{2+} and HPO_4^{2-} ions of DCP means a fewer number of interactions between 2PIC and water, which would suggest lower dissolution of the LEF-2PIC cocrystal-DCP complex than the LEF-3HBA cocrystal-DCP complex. Analysis of the number of hydrogen bonds and interaction energy terms in greater detail further revealed that 8.11 out of the 24.20 hydrogen bonds and -127.20 kJ mol^{-1} of the -1239.84 kJ mol^{-1} interaction energy in the LEF-DCP complex were contributed by LEF.

Table 4.5 The number of hydrogen bonds between LEF/cocrystals and complex with DCP

System	LEF	LEF-3HBA	LEF-2PIC
LEF/cocrystal-DCP	00.00	00.00	01.97
Complex-water	24.20	34.71	29.77

Table 4.6 LEF/cocrystals–water and complex-water interaction energies (kJ mol^{-1})

System	E_{coul}	E_{IJ}	E_{Total}
	without DCP		
LEF	-1290.68	50.84	-1239.84
LEF-3HBA	-1467.37	16.77	-1450.60

In comparison, the presence of 2PIC as an integral part of the cocrystal

LEF-2PIC	-1289.66	32.57	-1257.09
with DCP			
LEF	-0.02	-0.02	-0.04
LEF-3HBA	-0.03	-0.06	-0.09
LEF-2PIC	-71.46	2.25	-69.21
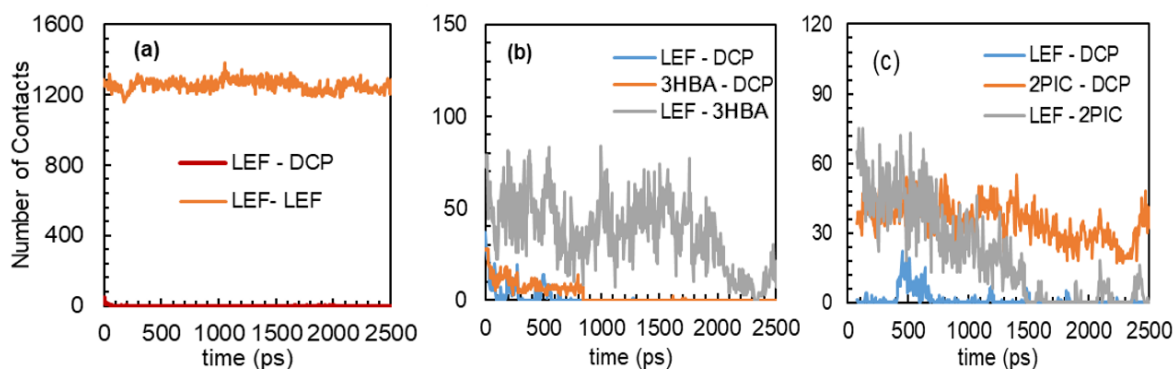
Figure 4.4 Time evolution inter-molecular contacts in complexes (a) LEF, (b) LEF-3HBA, and (c) LEF-2PIC with DCP in water

increases the number of hydrogen bonds by 29 % and interaction energy by 60 % in the LEF-2PIC cocrystal-DCP complex. The greater number of hydrogen bonds and interaction energy in the LEF-2PIC cocrystal-DCP complex than the LEF-DCP complex suggest higher dissolution of LEF-2PIC cocrystal-DCP complex. Therefore, the dissolution trend in the presence of DCP follows the trend LEF < LEF-2PIC cocrystal < LEF-3HBA cocrystal, which is in good agreement with the experimentally observed dissolution trend (*vide supra*).

On the other hand, in the LEF-3HBA cocrystal-DCP complex, all intermolecular interactions decrease with time and finally reach zero, suggesting that the LEF molecules are free to form hydrogen bonds with water molecules thus making it the best dissolving solid. Comparatively, in the LEF-2PIC cocrystal-DCP complex, there is a slower decrease in the number of intermolecular contacts between 2PIC and DCP over time that make this complex a slightly less or slower dissolving solid in water.

4.4 Experimental Observations

Dissolution is an important parameter that directly determines the bioavailability of a pharmaceutical active and therefore is a subject of great significance for pharmaceutical industry. In general, dissolution proceeds through a process of detachment of molecules from the solid (or crystal), which primarily depends on the breaking of solute-solute interactions and formation of

new solute-solvent interactions. Addition of certain excipients or solubilising agents help to improve the dissolution of solutes by way of increasing the number and strength of solute-solvent interactions. As described above, MD simulations provide a vital information on the molecular interactions (solute-solvent, solute-excipient, and excipient-solvent) and estimate dissolution trends in a family of solids. The MD simulations' results presented above suggest that the use of lactose and DCP as excipients could potentially have differing impacts on the dissolution rate of all the solids studied herein. It was noted that while lactose would be expected to improve dissolution rate, a detrimental effect on the dissolution rate would be predicted from DCP.

Prior to the dissolution experiments, bulk samples of LEF and cocrystals were ground and sieved to achieve a uniform particle size of 53-90 μm. Microscopic analysis of the powdered samples using SEM revealed that all the samples adopt a broadly similar shape (**Appendix D.3**). These attributes negate the impact of particle size and shape on bulk dissolution. It has been reported that the choice of excipient and their compressional behaviour may have a profound impact on the release of the API from the formulations.[88] In the current study, the impact of differing compressional behaviour of excipients was mitigated by the use of tablets of the same hardness. This was achieved through assessing the hardness of test tablets of each formulation pressed at varying loads followed by choosing a pressing load that gave each tablet ~30 N hardness (**Appendix D.1**) Furthermore, during dissolution experiments all tablets were observed to completely disintegrate within 5-10s – showing that the compressional behaviour of the excipients had little to no impact on the dissociation and thus release of LEF/cocrystals.

Figure 4.5 shows the dissolution profiles of LEF and cocrystals in the presence of the chosen excipients and their comparison with dissolution profiles of LEF and cocrystals in neat form. It is evident that both the cocrystals show improved dissolution rate compared to dissolution rate of LEF in the absence of excipients. In addition, both cocrystals exhibited a similar dissolution rate for the first 60 min, with the LEF-2PIC cocrystal showing a higher supersaturation level compared to both LEF and LEF-3HBA cocrystal after 5 h. The addition of lactose as an excipient, which is soluble in water, improves the dissolution rate of all the three samples. However, it should be noted that while the initial dissolution of the formulations is greater than the neat samples, upon reaching plateau the cocrystal formulations exhibit a lower supersaturation level than the neat cocrystals. Therefore, the observed supersaturation level of LEF and cocrystal formulations with lactose at 5 h is in the order of LEF < LEF-3HBA cocrystal < LEF-2PIC cocrystal, which corroborates the dissolution trend that was predicted by the MD simulations.

The dissolution profile of the formulations with DCP are shown in. Comparison of the dissolution profiles of the formulations with those of the neat samples reveals that the presence of water-
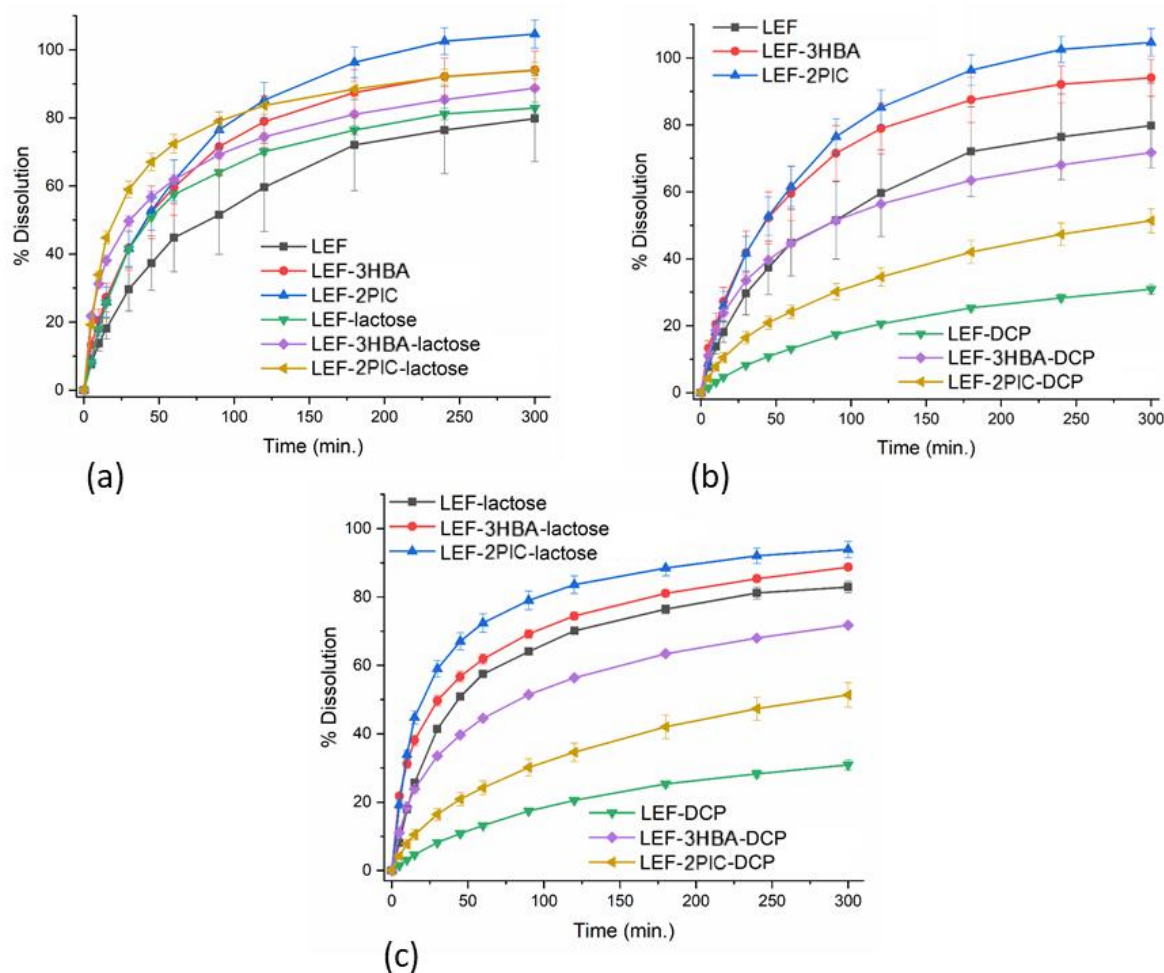
Figure 4.5 Comparison of the dissolution profiles (a) lactose formulations vs. neat samples of cocrystals and LEF, (b) DCP formulations vs. neat samples of cocrystals and LEF, and (c) lactose and DCP formulations

insoluble DCP has a detrimental effect on the dissolution rate. All three formulations displayed a lower dissolution rate than that of their respective neat samples. However, as with the neat samples, the cocrystal formulations show a higher dissolution rate than the LEF formulation. The supersaturation level observed at the end of the dissolution experiment (5 h) follows the trend LEF < LEF-2PIC < LEF-3HBA, which is once again in good agreement with the predicted hierarchy of dissolution from MD simulation results.

A comparative analysis of the dissolution trends of the formulations, neat cocrystals and LEF reveals that the solubility and the nature of the excipient, whether it is neutral or ionic, have a significant impact on the dissolution rate. While the water-soluble lactose improves the dissolution rate, the ionic and water-insoluble DCP has the reverse effect. In the case of lactose as an excipient, the hydrophilic nature and greater aqueous solubility of lactose facilitate the attraction of a greater number of water molecules towards the solute and contribute to the enhanced dissolution rate. On the other hand, the lower dissolution of formulations that contained DCP could be attributed to its hydrophobic nature. Furthermore, the ionic components of DCP potentially interact with the ionic components of the PIC coformer, blocking the hydration

sites of the solute leading to an additional decrease in the dissolution of the LEF-2PIC cocrystal in the formulation. It is worth noting that the computationally derived parameters, such as RMSDs, SASA and intermolecular interaction energies, point to the higher dissolution of the LEF-2PIC and LEF-3HBA cocrystal formulations, compared to LEF formulations, when formulated with lactose and DCP, respectively. This is in excellent agreement with the experimentally observed trends, thus emphasizing the significance of MD simulations in understanding the dissolution behaviour of cocrystal formulations.

FT-IR has been extensively used for analysis of drug-excipient interactions. It has been established that the shifts in the vibrational frequencies determine the extent of interaction between drug and excipient, and an inference of a chemical reaction can be made from the disappearance of characteristic vibrational bands.[89] In the present study, LEF, neat cocrystals and their formulations were analysed by FT-IR and their characteristic peaks were compared (**Appendix C.2.3**). It was found that there is no discernible difference, in either frequency or intensity, in the characteristic peaks of LEF when compared with pure LEF and cocrystals and their formulations with lactose, thus indicating that there is no chemical interaction between LEF and lactose. However, the FT-IR spectra of all formulations with DCP show an absence, or greatly reduced intensity, of the peak characterizing the N–H stretching vibration seen in LEF (strong broad peak at ~3350 cm^{-1}). Previous studies on physical characterisation of DCP have asserted to its Lewis acidity,[90,91] while LEF is basic in nature (pKa value of 10.8 at 23 °C).[92] Therefore, there is a high likelihood of a strong interaction between DCP and LEF potentially weakening the amide N–H bond and hence reducing the intensity of, or removing, the N–H stretching vibration in the IR spectra of the DCP formulations. The interaction between LEF and DCP, particularly between the H atom of N–H in LEF and the O atoms of DCP in all the three formulations was also evidenced by MD simulations. Strong interactions between LEF and water insoluble DCP could contribute to the lower observed dissolution of the DCP formulations.

It has been reported that lactose intolerance affects 70 % of the world's population, which is known to occur due to a deficiency of the enzyme lactase.[93] In some pharmaceutical formulations DCP has been suggested as a potential alternative to lactose for development of lactose-free drug formulations. The results of the current study emphasize the distinct dissolution behaviour of lactose and DCP formulations, which has been computationally predicted and experimentally validated. Therefore, it is essential to gain prior knowledge of the impact of different kinds of excipients on the performance of cocrystals. In this respect, MD simulations can be considered a reliable tool for gaining a molecular-level understanding of the interactions between components of the cocrystal/API and dissolution medium and aid in the prediction of dissolution hierarchies.

4.5   Conclusions

Pharmaceutical cocrystallisation has evolved as a much sought-after technique for addressing the solid-state issues of active pharmaceutical ingredients. It has been established that the choice of a coformer plays a critical role in determining the properties of neat cocrystals. As cocrystals are being developed and increasingly marketed as novel drug products there is a heightened interest in studies concerning cocrystal-excipient interactions. A review of the current literature revealed varied effects of excipients on the stability, solubility, dissolution, and bioavailability of cocrystals.

This chapter has shown that MD simulations provide vital information for understanding the nature, number, and strength of cocrystal-excipient interactions and resultant prediction of dissolution trends in a family of cocrystal-excipient combinations. Calculated parameters such as SASA, hydrogen bonds between an API or cocrystal in formulations with water, interaction energy between an API or cocrystal in formulation and water are found to be essential to elucidate experimentally observed dissolution trends of pure LEF/cocrystals and formulations in water. For LEF/cocrystals or complexes, dissolution in water would be expected to increase as the values of these parameters increase. This finding is consistent with the literature wherein the dissolution performance of API-excipient complexes were explained by these parameters.[44] **Chapter 3** has previously shown that cocrystals of LEF demonstrate improved dissolution rate over LEF. However, in this study a similar effect has only been observed with respect to lactose as an excipient, which improved the dissolution at different rates for different cocrystals. DCP, on the other hand, has a detrimental effect resulting in lower dissolution of cocrystal formulations when compared to neat LEF and its cocrystals. The excellent correlation observed between the results of MD simulations and experimental observations validates the role of MD simulations in the selection of suitable excipients for development of novel cocrystal-based formulations. Furthermore, the ever-growing computational power and advances in force fields further contribute to reducing simulation time and help in the quest for suitable excipients for development of cocrystal-based formulations.

Chapter 5 Quantum Crystallographic Studies of LEF Cocrystals

Chapter 5 herein introduces the quantum crystallographic consideration of LEF cocrystals, and how both experimental data and theoretical intermolecular energetic calculations thereof can provide a route to inform the nature of cocrystal interactions, their composition and, consequently, their decomposition in solution.

These studies will provide both qualitative and quantitative data to inform the understanding of the effect of cocrystallisation on the atom–atom interactions, molecule–molecule interactions, crystal packing, lattice energies, as well as a number of other significant factors that influence the nature and physicochemical properties of these cocrystals.

This will serve as a progression from **Chapter 3** as these investigations will be more explicit, rather than simply a holistic view of the crystal structure as a whole entity – as per the principles of crystal engineering – i.e. focusing on both the nature *and* type of intermolecular interactions and how they in turn affect the overall system.

Relating back to the 6 key objectives of this study, this chapter aims to address the following statement:

3. Elucidate the effect of different coformers on the electronic distributions and how this can be related to both physicochemical properties and API/cocrystal-excipient interactions.
4. Combine and complement both qualitative and quantitative approaches towards a quantum crystallographic understanding of these cocrystals.

5.1 Approach

As mentioned above, this chapter will combine, compare, and contrast both qualitative and quantitative breakdowns of theoretical molecule-molecule interactions within these cocrystal systems.

Thorough analysis of the breakdowns of these theoretical molecular pair interactions, using inferences from crystal structure, geometry, and conformation can offer insights into the specific atom-atom interactions, thus providing an in-depth inference of how the molecules interact, e.g. API and coformer. This enables an identification of the strong hydrogen-bonds that dominate the overall molecular pair interactions, and how these strong hydrogen-bonds dictate these

interactions, subsequently the overall cocrystal assembly and thus the underlying susceptibility for lattice breakdown as a result of melting or dissolution, i.e. the effect on physicochemical properties.

Where experimental electron density distributions (EDDs) gained from high-resolution studies would succeed in providing detailed, localised intermolecular interaction analysis, theoretical molecule-molecule interaction energy calculations can serve as an alternative, complementary approach. Intermolecular interactions are considered as a whole; however they can be deconstructed to their constituent components: coulombic (E_{coul}), polarisation (E_{pol}), dispersion (E_{disp}), and repulsion (E_{rep}). While not considered as in-depth, due to being more generalised towards the molecule as a whole, it provides a chance to investigate a wider range of interactions and strengths, i.e. the more numerous, weaker interactions that overall make up the majority of the intermolecular interaction energy – not just the strong, dominating hydrogen-bonds – many of which will be comprised of constituent components such as dispersion effects that therefore cause them to be considered weaker individually, yet overall give the greatest contribution.

5.2   Theoretical Molecular Pair Interactions

5.2.1   Interaction Components

The nature and strength of the intermolecular interactions within a crystal system can be extracted from the crystal structure data. The Crystal Explorer package,[94] implemented by Spackman *et al.* allows for a calculation of the interaction energies through determination of B3LYP/6-31G(d,p) monomer wavefunctions using the Gaussian tool.[95,96]

Calculated Crystal Explorer interaction energies can be deconstructed into their respective energetic components in relation to their contribution toward the total energy, i.e. Coulombic, polarisation, dispersion, and repulsion energies, and their respective magnitudes assigned. This can provide insight into the nature of individual molecular pair interactions: whether they are indicative of strong hydrogen-bonding (high Coulombic contribution), or more moderate-to-weaker strength van der Waals' interactions (dominated by dispersive forces), and also the general breakdown between the constituent components in all molecular pair interactions involved in the cocrystal as well as the general trade-off between attractive (favourable) and repulsive (unfavourable) forces.

Figure 5.1 shows the percentage breakdown of the energetic contributions of all individual molecular pair interactions with respect to the overall total energy of all four cocrystals.
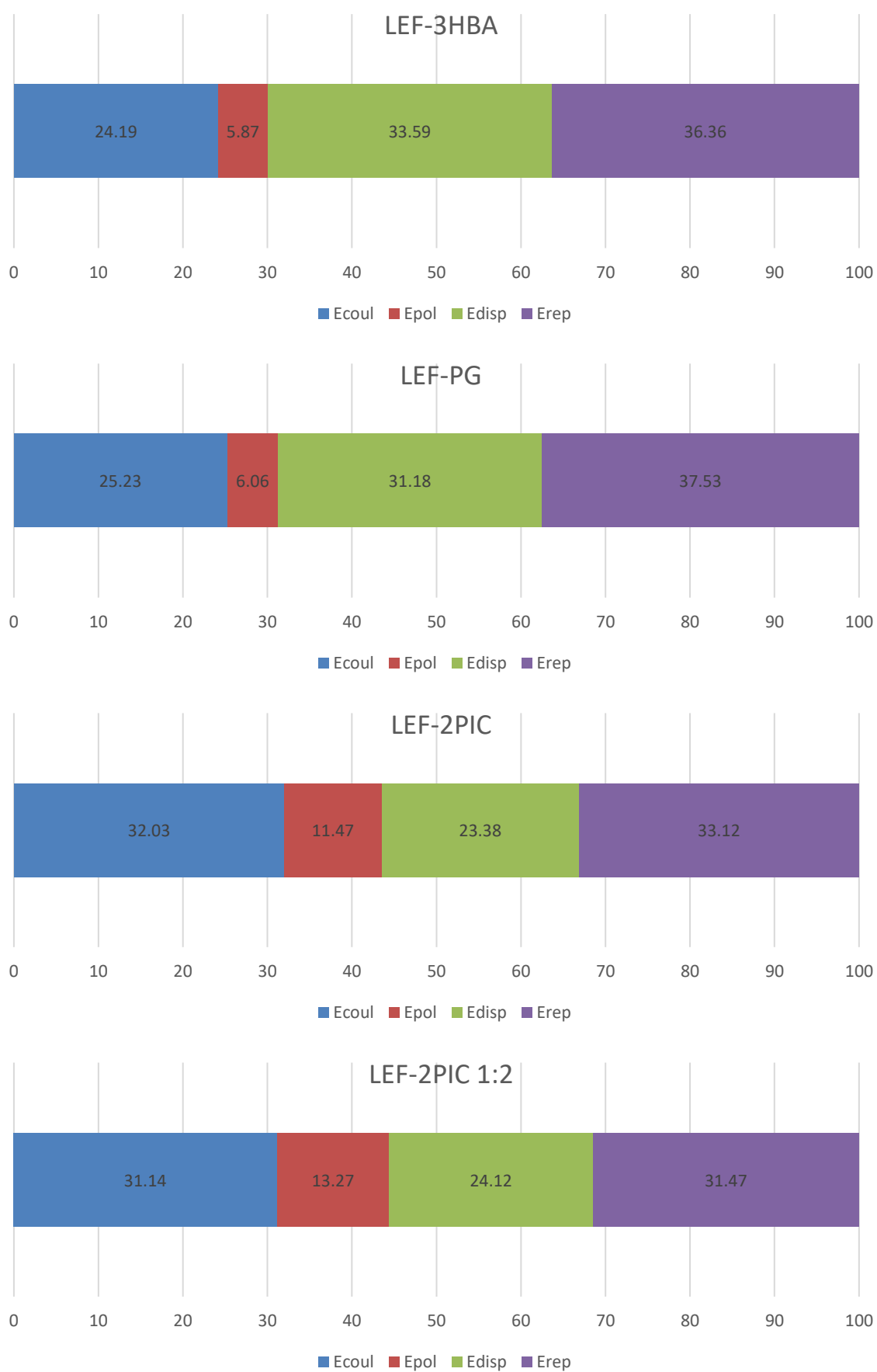
Figure 5.1 Contributions of the individual energy components (Coulombic, polarisation, dispersion, and repulsion) to the total energy of the four cocrystals

A significantly increased Coulombic component is seen in LEF-2PIC and LEF-2PIC 1:2 when compared to LEF-3HBA and LEF-PG. This is to be expected as the intramolecular proton transfer that occurs in the 2PIC coformer of each of these cocrystals results in a strong, charge-assisted hydrogen-bond that will manifest itself in the Coulombic component of the interaction energy.

Nevertheless, conventional hydrogen bonds themselves – displaying the expected D–H···A composition and retaining the D–H covalent bond – which are seen in all four of the cocrystals are also considered strong interactions that evidence themselves in the Coulombic energy component. This builds a logical case for the pairwise comparison between the LEF-2PIC and LEF-2PIC 1:2 cocrystals (Chapter 5.2.4.1) due to the ability to negate the charge-related element of the hydrogen-bond strength between the cocrystals, as well as the potential for assessment of stoichiometric effects. Similarly, **Chapter 5.2.4.2** will discuss the coformer structural similarities and differences between LEF-3HBA and LEF-PG with respect to their effects on the intermolecular interactions present.

While this breakdown provides a holistic view of the molecular pair interactions of each cocrystal system, which gives an indication of the overall general natures and strengths of interactions present in the cocrystals, it does not identify the specific molecular pair interactions that contribute greatest to the cocrystal composition. Deconstructing this view further into specific molecular pair interactions allows for an assessment of the interplay between those strong hydrogen bonds, that are generally considered "structure directing" and integral to cocrystal composition, and the moderate-to-weaker van der Waals' interactions that, while not structure directing, have an important role in the stabilisation of the crystal lattice.

Calculated CE interaction energies provide specific molecule···molecule interaction energies, broken down into their constituent components, and can be identified and compared quantitively through matching the corresponding colour-coded molecules in the energy calculation output to the graphical display (**Figure 5.2**). However, a simpler yet more informative visualisation of the specific molecular pair interactions and their comparative associated strengths can be obtained using the Energy Frameworks view. By representing energies between molecular pairs as cylinders joining the centroids of each pair, with the cylinder radius proportional to the magnitude of the interaction energy, this offers a unique way to view the directionality as well as energetic magnitude of the intermolecular interactions.
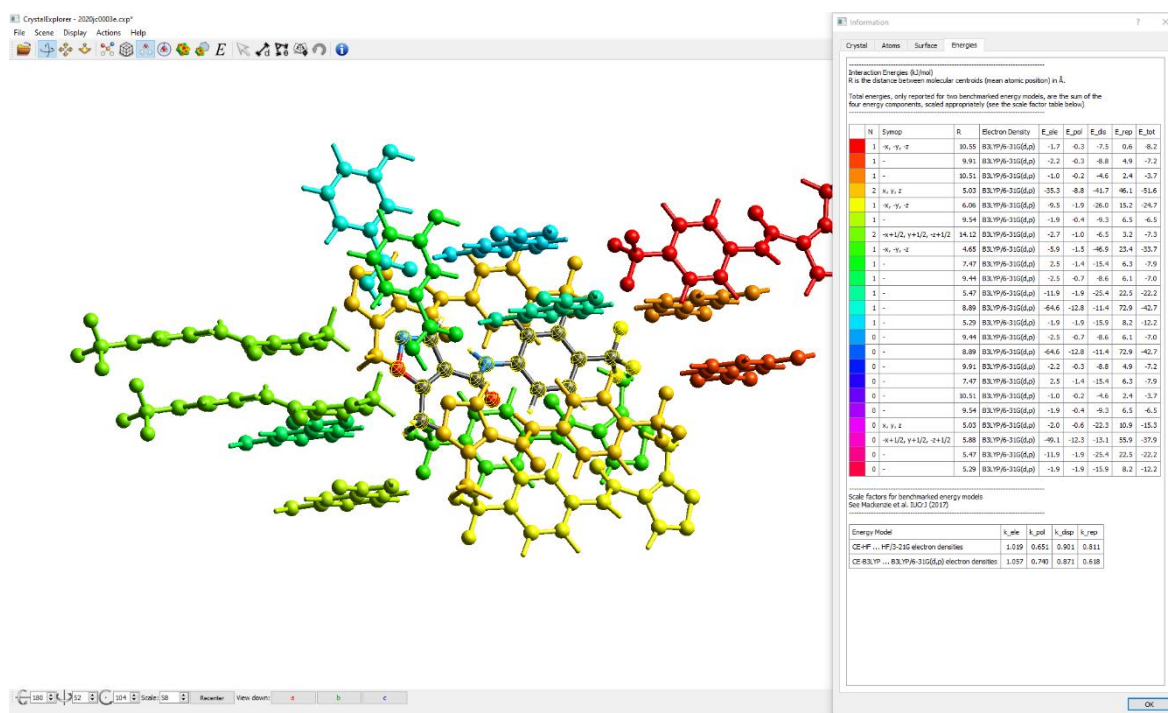
Figure 5.2 Graphical output of Crystal Explorer interaction energy calculation with energy component values displayed and colour coded for each individual molecular pair

5.2.2 Energy Frameworks

As mentioned, calculated CE interaction energies can be graphically represented in relation to their constituent contributing components toward the total energy, i.e. Coulombic (red cylinders) and dispersion (green cylinders) energies, and their respective magnitudes. These energy frameworks provide a graphical, qualitative depiction of the quantitative molecular pair interaction energy values and allows for a visual analysis and comparison of relative contributions of individual energetic components within a particular molecule-molecule interaction, as well as a clear indication of the involved molecules.

This technique is useful to highlight notable molecular pair interactions and begin to make inferences into their nature and effects on overall cocrystal composition, and possibly physicochemical properties. Additionally, this somewhat simplified initial exploration can identify potential avenues for deeper investigation of energetic components, atom pair interactions, electron density distributions and electrostatic potentials.

5.2.2.1 LEF-3HBA Energy Frameworks

The energy framework representation of a single unit cell of LEF-3HBA, viewed along the *b*-axis, displaying the Coulombic energy component is shown in **Figure 5.3**. Here it is clear to see that there is a significant contribution towards the total molecular pair 3HBA···3HBA interaction, likely arising from 3HBA dimer formation via a $3HBA_{hydroxyl}$···$3HBA_{carboxyl}$ hydrogen-bonding interaction. Alongside this, the Coulombic energy has a large influence on the total energy seen in the LEF···3HBA API···coformer interaction, which rudimentary visual analysis of the crystal structure suggests to emanate from the LEF $N_{isoxazole}$···$3HBA_{carboxyl}$ interaction. It can be noted that the same individual 3HBA molecule is involved in both of these notable interactions, which leads to an interpretation that this enables the formation of an extended hydrogen bonding network, consisting of connecting LEF···3HBA···3HBA···LEF··· etc. interactions. The proliferation of this network will allow for the distribution of charge beyond the two interacting molecules and throughout the crystal lattice, providing a net stabilisation effect and thus a rationalisation for the large favourable observed interaction energies.

Figure 5.4 shows the same energy framework representation of LEF-3HBA, displaying the dispersion energy component. There is a relatively large dispersion contribution present in two interactions within the offset stacking of LEF···LEF molecular pairs when compared to the remaining interactions seen. Visual assessment of the molecular geometry of the crystal structure here suggests that these LEF···LEF molecular pair interactions, and their dispersion contributions, arise from the π···π interactions between neighbouring LEF aromatic rings.
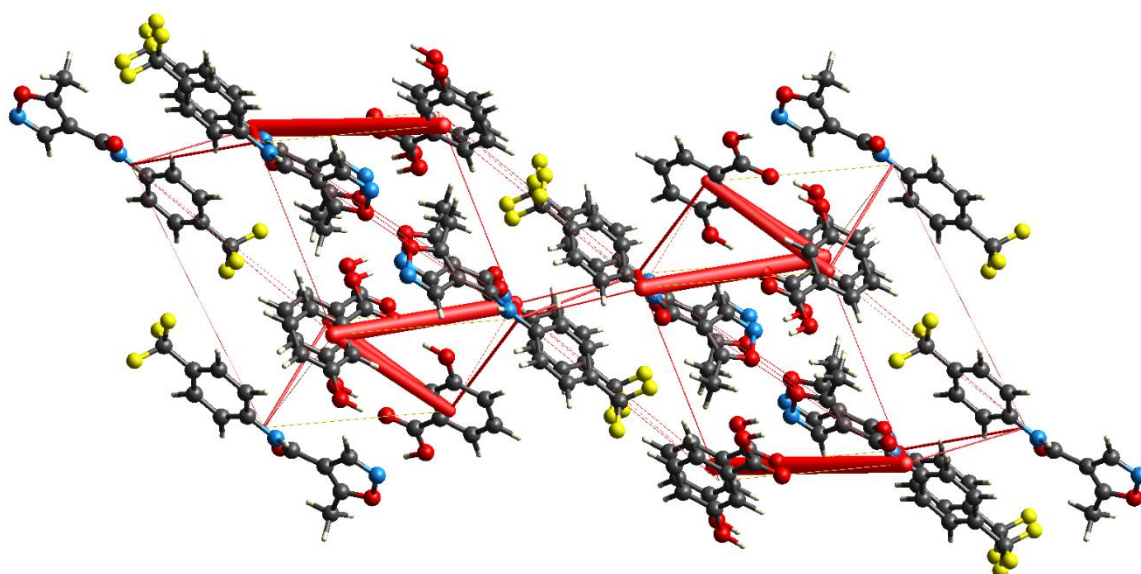
Figure 5.3 Energy framework representation of LEF-3HBA, viewed along the *b*-axis, with the Coulombic energy component highlighted

Cylinder sizes were set to an arbitrary value of 50
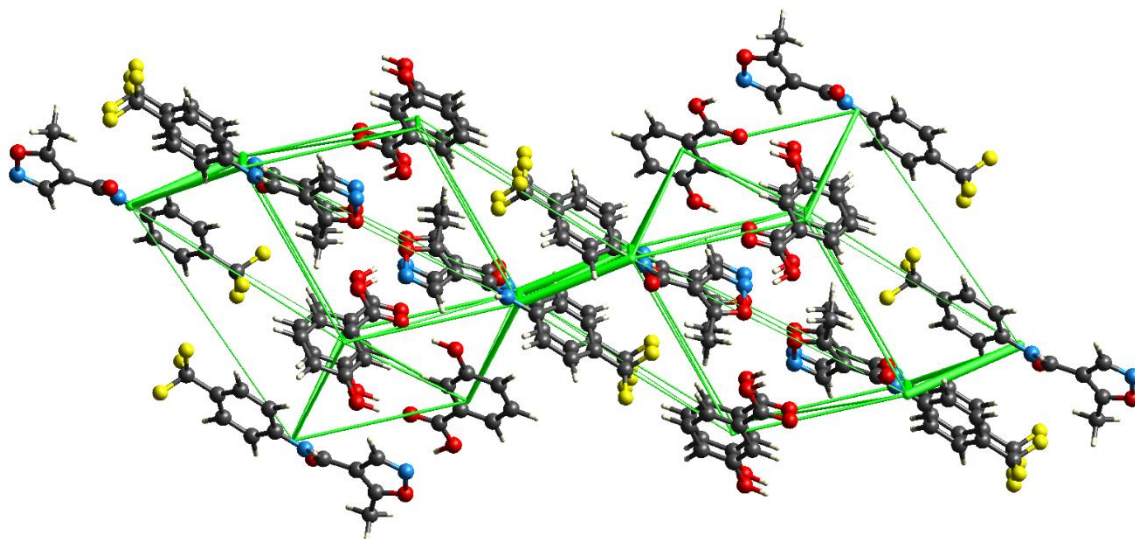
Figure 5.4 Energy framework representation of LEF-3HBA, viewed along the *b*-axis, with the dispersion energy component highlighted

Cylinder sizes were set to an arbitrary value of 50

The dispersion energy is distance dependent, and therefore considerably reduces in strength with increasing distance. Therefore, the molecule-molecule centroid distance of this notable interaction would be expected to be small, which also provides an explanation for the reduced contribution of dispersion energy to the total energy seen in the remaining molecular pair interactions of LEF-3HBA. The weak to moderate strength associated with interactions that possess a comparatively large dispersion coefficient is generally associated with those that do not arise from hydrogen-bonding and are thus not "structure directing" but are nevertheless integral to the cocrystal composition as part of the interplay/trade-off between the aforementioned strong LEF⋯3HBA "directional" hydrogen-bonds.

5.2.2.2   LEF-PG Energy Frameworks

Figure 5.5 displays the Coulombic component of the energy framework of LEF-PG, viewed along the *c*-axis. There are multiple noteworthy E_{coul} contributions towards the total molecular pair interaction energies involving the PG coformer, including both PG⋯PG and LEF⋯PG molecular pairs. Within these molecular pairs, the coformer displays a $PG_{hydroxyl}$⋯$PG_{hydroxyl}$ hydrogen-bond that is suggested to occur between neighbouring PG molecules at the 1- and 3- positions, respectively. This strong hydrogen-bond therefore manifests itself in the Coulombic component of the total energy, and forms part of a series of identical interactions that serve as part of a chain of coformer molecules that propagate throughout the unit cell along the *c*-axis. Simultaneously these same PG molecules participate in a bifurcated LEF⋯PG hydrogen-bond to the amide functionality of LEF, with this likely arising from the 2-position of PG and possessing both donor, PG_{OH}⋯$LEF_{C=O}$, and acceptor, LEF_{NH}⋯PG_{OH}, modalities. The magnitude of the Coulombic component

Figure 5.5 Energy framework representation of LEF-PG, viewed along the *c*-axis, with the Coulombic energy component highlighted

Cylinder sizes were set to an arbitrary value of 50

is greater in the LEF$_{NH}$···PG$_{OH}$ interaction, suggesting the balance of charge from this bifurcated hydrogen-bond is weighted towards the coformer molecular, thus creating a net accumulation of electron density about PG. Therefore, the aforementioned chain of PG···PG molecular pair interactions provides a vital charge redistribution opportunity, thus stabilising the crystal lattice. A final API···coformer molecular pair interaction can be seen, involving the orthogonal PG molecules to the previous LEF···PG interaction. An intuitive chemical assessment of the molecular and centroid-centroid geometries suggests that the atom···atom interaction involved here is a PG-donating PG$_{OH}$···LEF$_N$ hydrogen-bond between the 3-hydroxyl PG and LEF isoxazole atoms. Once again, the strength and nature of the interaction can be inferred from the magnitude of its Coulombic component. This can be seen with respect to the associated dispersion energy for this interaction – and all other suggested hydrogen-bonds – shown in Figure 4.5.

Figure 5.6 displays an energy framework representation of LEF-PG, highlighting the dispersion energy component as a function of its contribution to the total molecular pair interaction energy, E$_{tot}$. The prominent interaction that displays a notable dispersive nature involves a LEF···LEF molecular pair. These are part of an 'ABAB' alternating stack of LEF molecules along the crystallographic *c*-axis, with the respective benzene and isoxazole aromatic rings aligning, suggesting the nature of interaction involved. The fact that this interaction is dominated by dispersion further substantiates this inference as, as previously established, aromatic π···π interactions are of moderate strength with the majority of the total interaction energy being contributed by the dispersion energy.
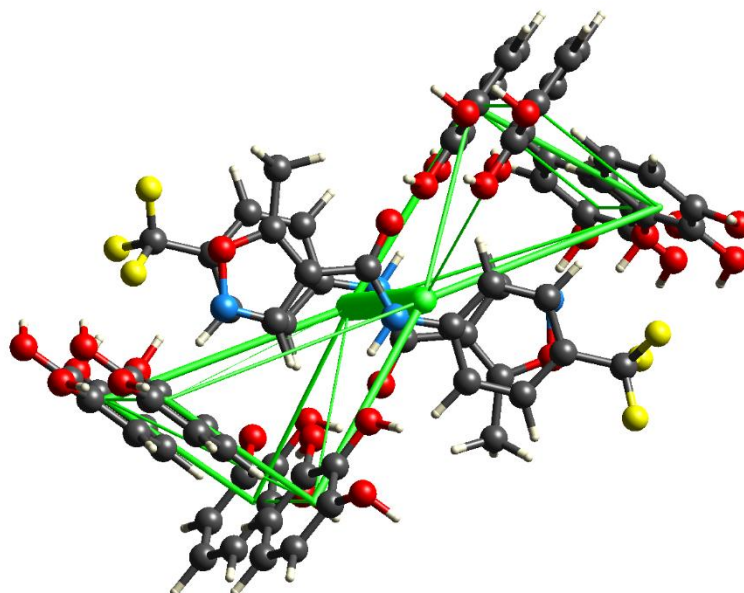
Figure 5.6 Energy framework representation of LEF-PG, viewed along the *c*-axis, with the dispersion energy component highlighted

Cylinder sizes were set to an arbitrary value of 50

5.2.2.3   LEF-2PIC Energy Frameworks

The energy framework, concerning the Coulombic energy component, for LEF-2PIC is shown in **Figure 5.7**. Here there are clearly two interactions with a significant Coulombic contribution to the total molecular pair interaction energy. These consist of one API···coformer interaction and one coformer···coformer interaction. The most notable of these is a 2PIC···2PIC interaction between facing 2PIC molecules. Its large Coulombic contribution is, of course, indicative of a strong hydrogen-bond, however the exceptional magnitude of this component suggests potentially something more. **Chapter 3.7.3** shows that the coformer 2PIC molecule undergoes an intramolecular proton transfer upon cocrystallisation that results in COO^- and NH^+ functional groups. These are then available to participate in charge-assisted hydrogen-bonds, which will possess a greater strength of interaction. Using this knowledge, it is reasonable to deduce that this 2PIC···2PIC dimer interaction arises from the charge-assisted $2PIC_{COO-}$···$2PIC_{NH+}$ hydrogen-bond. Interestingly, this dimer formation creates both hydrogen-bond donating (NH^+) and accepting (COO^-) sites on each 2PIC molecule, allowing for a reciprocation of the charge-assisted $2PIC_{COO-}$···$2PIC_{NH+}$ hydrogen-bond across the molecular pair, further increasing the strength of this interaction as well as stabilising the electron density distribution between the molecules.

The enhancement of interaction strength also seems to be present in the remaining LEF···2PIC molecular pair interaction showing a significant Coulombic contribution, with an understanding that this involves the LEF amide N–H group as a hydrogen-bond donor to the 2PIC COO^- group.
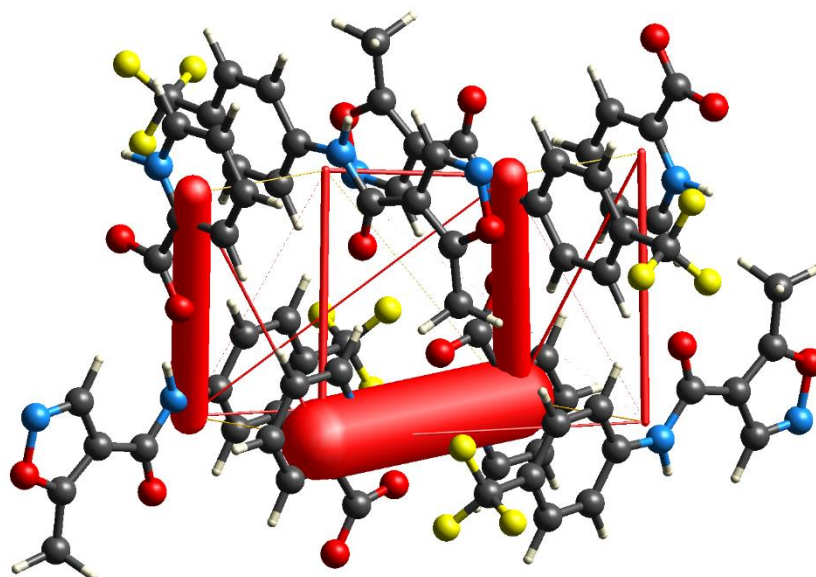
Figure 5.7 Energy framework representation of LEF-2PIC, viewed along the *a*-axis, with the

Coulombic energy component highlighted
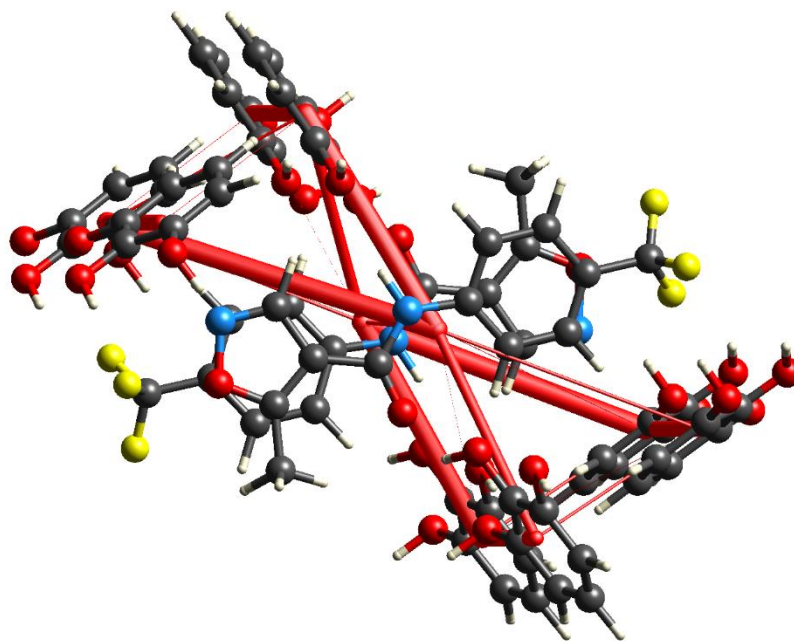
Cylinder sizes were set to an arbitrary value of 50

Comparatively, this interaction would be expected to, and does, exhibit a lower total interaction

energy than the 2PIC⋯2PIC interaction, as there is only one such atom⋯atom interaction

occurring between LEF and 2PIC.
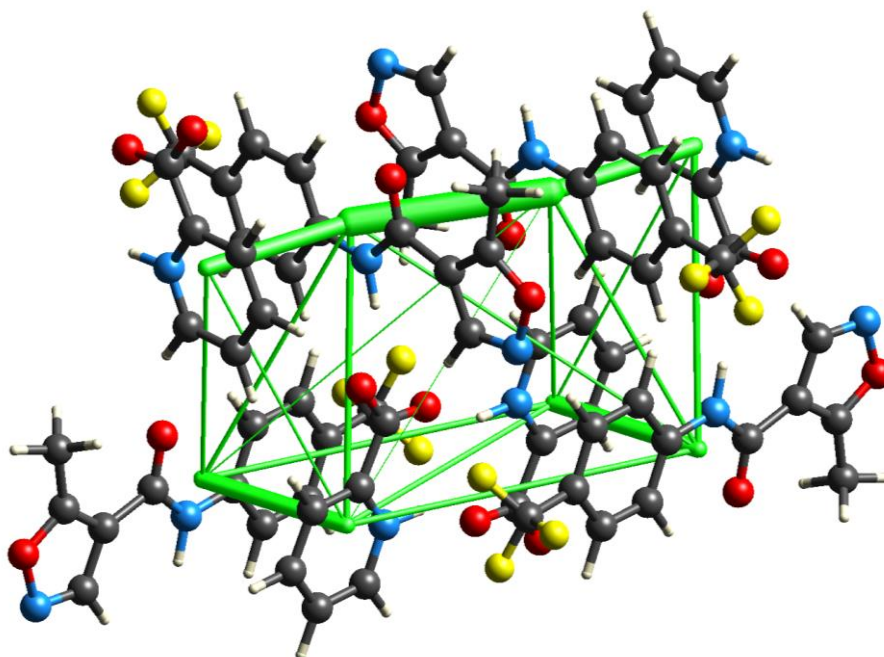
Figure 5.8 Energy framework representation of LEF-2PIC, viewed along the $\frac{(a+c)}{2}$-axis, with

the dispersion energy component highlighted

Cylinder sizes were set to an arbitrary value of 50

5.2.2.4   LEF-3HBA Molecular Pair Interaction Energies

Table 5.1 shows the energy components, with respect to molecule-molecule centroid distances, for each individual molecular pair interaction calculated for LEF-3HBA. **Figure 5.9** also shows an example output from the energy calculations that this data is drawn from, using first LEF as the central molecule interacting to any molecules within a 3.8 Å radius.

From this Table, and the corresponding colour coded interactions between the central LEF and surrounding molecules, it is apparent that the LEF-3HBA API···coformer interaction identified in the energy frameworks as having a large Coulombic component of the total energy involves a contribution of -64.6 kJ mol^{-1} (light blue/cyan 3HBA molecule interacting with central LEF molecule in **Figure 5.2**, and the Coulombic energy component circled in red in **Table 5.1**).

Table 5.1 Energy components with respect to centroid distances for the individual molecular pair interactions of LEF-3HBA determined from Crystal Explorer calculations

	Energy/kJmol^{-1}				
	E$_{coul}$	**E$_{pol}$**	**E$_{disp}$**	**E$_{rep}$**	**E$_{tot}$**
LEF···3HBA	10.55	-1.7	-0.3	-7.5	0.6	-8.2
LEF···3HBA	9.91	-2.2	-0.3	-8.8	4.9	-7.2
LEF···3HBA	10.51	-1	-0.2	-4.6	2.4	-3.7
LEF···LEF	5.03	-35.3	-8.8	-41.7	46.1	-51.6
LEF···3HBA	6.06	-9.5	-1.9	-26	15.2	-24.7
LEF···3HBA	9.54	-1.9	-0.4	-9.3	6.5	-6.5
LEF···3HBA	14.12	-2.7	-1	-6.5	3.2	-7.3
LEF···LEF	4.65	-5.9	-1.5	-46.9	23.4	-33.7
LEF···3HBA	7.47	2.5	-1.4	-15.4	6.3	-7.9
LEF···3HBA	9.44	-2.5	-0.7	-8.6	6.1	-7
LEF···3HBA	5.47	-11.9	-1.9	-25.4	22.5	-22.2
LEF···3HBA	8.89	-64.6	-12.8	-11.4	72.9	-42.7
LEF···3HBA	5.29	-1.9	-1.9	-15.9	8.2	-12.2
3HBA···3HBA	5.03	-2	-0.6	-22.3	10.9	-15.3
3HBA···3HBA	5.88	-49.1	-12.3	-13.1	55.9	-37.9

Similarly, the interactions highlighted in **Chapter 5.2.2.1** possessing the large dispersion energy component relating to LEF···LEF aromatic π···π stacking interactions can be seen in the energy calculation outputs in **Table 5.1** and **Figure 5.2**. There are two such interactions present between the central LEF molecule and surrounding LEF molecules within the 3.8 Å radius (light orange/yellow and pea green LEF molecules in **Figure 5.2**) that, accordingly, show significant dispersion contributions of -41.7 and -46.9 kJ mol^{-1}, respectively towards the total energy (dispersion energy components circled in red in **Table 5.1**). As the table shows, these interactions possess a short molecular pair centroid distance, R, which enables the dispersion coefficient to dominate.

Interestingly however, the LEF···LEF interaction that exhibits a dispersion energy component value of -41.7 kJ mol^{-1} also has a significant contribution towards the total energy from the coulombic component. This strong coulombic component is therefore indicative of hydrogen-bonding, rather than dispersive van der Waals'/ π···π interactions and would be expected to correspond to a strong LEF N_{amide}···LEF O_{amide} interaction. Along with the strong LEF···3HBA and 3HBA···3HBA hydrogen-bonds discussed in **Chapter 5.2.2.1**, this interaction forms part of the significant extended hydrogen-bonding network throughout the crystal lattice that acts as the driving force behind the cocrystal composition, as well as providing stabilisation of these strong interactions through charge redistribution within the network.

5.2.3   Comparing LEF to cocrystals

Comparison of the individual and total molecular pair interaction energies, and their respective components, of both LEF and its cocrystals allows for a rationalisation of some of the factors affecting their compositions, and by relation, their formation as well as an insight into the influence they have on the observed physicochemical properties. CE B3LYP/6-31G(d,p) molecular pair interaction energies.

5.2.3.1   Structure Assembly and Property Rationalisation

Using Crystal Explorer to compare molecular pair interaction energies shows that fewer, weaker ones exist in the single component leflunomide, with more strong/favourable interactions occurring in the cocrystals (**Figure 5.9**).

Although the stronger intermolecular interactions seen in the cocrystal systems might initially point towards their aqueous solubility being lower than that of the single-component LEF, it is important to note that solubility, in this instance as it is measured, is a thermodynamically dependent process as time is allowed for solution equilibrium to be reached. The factors affecting
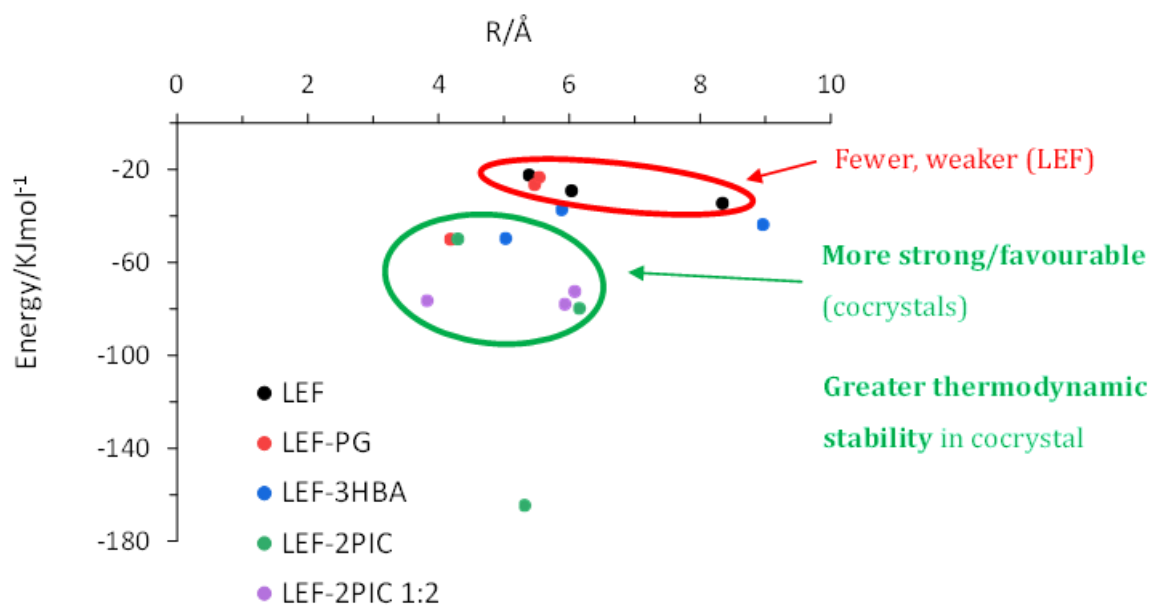
Figure 5.9 Crystal Explorer B3LYP/6-31G(d,p) total molecular pair interaction energies (E_{tot}) as a function of molecule-molecule distance (R) for LEF and cocrystals

thermodynamic solubility, as opposed to kinetic solubility (which is represented in supersaturated solutions where the amount of solute exceeds the equilibrium, or thermodynamic, solubility amount and is generally deemed and inaccurate impression on solubility) include interactions between solute (drug/cocrystal) and solvent, as well as drug-drug interactions. The stronger intermolecular interactions seen in the cocrystals, and the relationship between these and the increase in cocrystal solubility is understood to be due to the increased solubility of the coformers, or the effect of its dissociation over the time taken to reach equilibrium.

As well as the implications this has on physicochemical properties, this also has indications when considering cocrystal formation. The greater thermodynamic stability of the cocrystals, indicated by the greater intermolecular interaction strength seen in **Figure 5.9**, points towards a greater thermodynamic stability of these systems, suggesting a preference for formation of cocrystals in solution crystallisation processes. As for the effect on melting points, strong intermolecular interactions required for melting, such as hydrogen bonds, primarily manifest themselves in the Coulombic energy component. It is apparent here that this is generally increased in the cocrystals. The rationalisation for this comes from the fact that there are also many more moderate strength interactions, which are dominated by dispersion energy (**Table 5.2**). These also provide a barrier to melting, suggesting therefore that the dispersion energy here, and the lower barrier (and therefore energy required to overcome this) seen in the cocrystals impacts the observed melting point and potentially outweighs that of the coulombic energy in these cases.

Table 5.2 Coulombic and dispersion energy components for LEF and cocrystals determined from Crystal Explorer energy calculations

Sample	E_{coul} p/molecule/kJmol^{-1}	E_{disp} p/molecule/kJmol^{-1}
LEF	-55.5	-106.1
LEF-PG	-35.0	-50.9
LEF-3HBA	-91.4	-50.1
LEF-2PIC	-108.2	-46.9
LEF-2PIC 1:2	-79.0	-67.2

5.2.4 Comparing Cocrystals

Further investigation and rationalisation of the structure assemblies and properties of these cocrystals can be enabled by pairwise comparison of cocrystal systems based upon factors that create similarity, and thus reasonable and systematic comparison. The two factors chosen in this study are:

1. Stoichiometric effects: LEF-2PIC and LEF-2PIC 1:2 contain the same coformer, however the increased stoichiometric ratio of coformer to API can be explored as to its effect on the electronic distribution and thus the molecular-pair interactions.
2. Structural similarities: the coformers of LEF-PG and LEF-3HBA are structurally similar, minimising differences due to steric effects, therefore examination of how the nature and type of molecular-pair interactions differ will be predominantly due to electronic effects.

5.2.4.1 Stoichiometric Effects

In both cocrystals, the strongest values of E_{tot} stem from 2PIC: either homomolecular 2PIC-2PIC or heteromolecular LEF-2PIC interactions (**Figure 5.10**). However, the increased 2PIC:LEF ratio (stoichiometry) creates further opportunities for 2PIC-2PIC interactions in the 1:2 cocrystal. However, in order to understand their differing physicochemical properties, it must be noted that these interactions are charge assisted due to the intramolecular proton transfer occurring.

These are hydrogen-bonds and are, as expected, dominated by the coulombic component of the interaction energy. These interactions are highly favourable and contribute the greatest towards the overall energy, as seen in **Table 5.3** and **Table 5.4**.
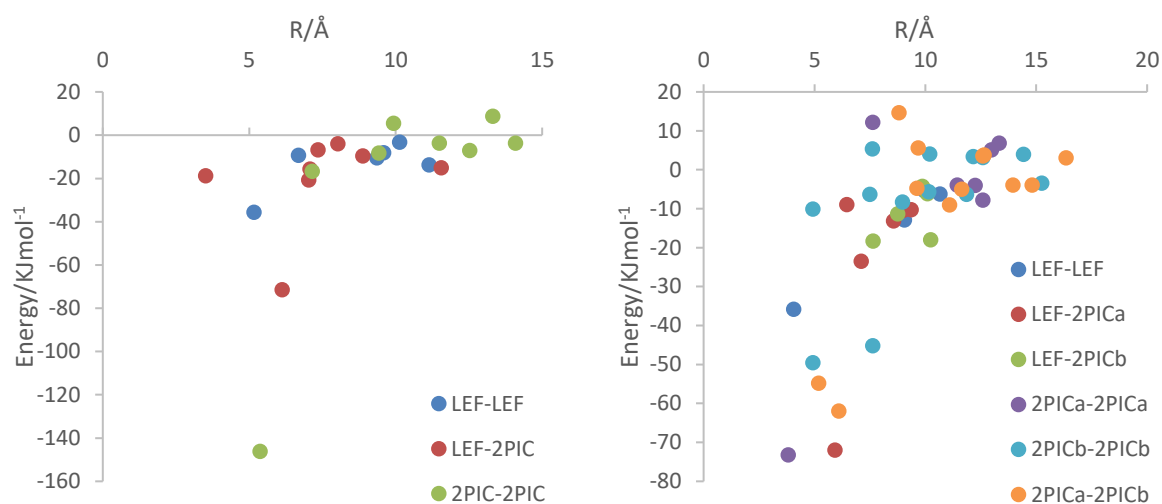
Figure 5.10 Crystal Explorer B3LYP/6-31G(d,p) total molecular pair interaction energies (E_{tot}) as a function of molecule-molecule distance (R) for LEF-2PIC and LEF-2PIC 1:2

Their strength and abundance is explanatory for the cocrystal assembly and stability as well as, particularly in the case of LEF-2PIC 1:2, the physicochemical properties. LEF-2PIC 1:2 exhibits a much lower overall solubility and dissolution rate compared to LEF-2PIC.

This significant increase in observed strong, coulombic-dominated intermolecular interactions will create a greater energetic barrier to dissociation of the LEF and 2PIC components, thus delaying the release of LEF into solution. Conversely, there is a single, strong molecular-pair interaction in LEF-2PIC. However, this is a homomolecular 2PIC-2PIC dimer interaction, that will not affect the dissociation of LEF from the crystal lattice – which leaves amorphous LEF that lacks strong intermolecular interaction capabilities to maintain and thus exhibits an observed increase in solution concentration – the aforementioned "spring effect" discussed in **Chapter 3.10.1**.

Table 5.3 Coulombic and dispersion energy components for LEF-2PIC determined from Crystal Explorer energy calculations

	Energy/kJmol^{-1}				
	E_{coul}	E_{pol}	E_{disp}	E_{rep}	E_{tot}
LEF-LEF	-34.6	-18.5	-141.6	83.2	-111.4
LEF-2PIC	-120.9	-60.5	-108.5	128	-161.9
2PIC-LEF	-121.9	-50.3	-71.1	100	-143.2
2PIC-2PIC	-197.1	-69.4	-45.1	111.1	91.3
Total	-474.5	-198.7	-366.3	422.3	-325.2

Table 5.4 Coulombic and dispersion energy components for LEF-2PIC 1:2 determined from Crystal Explorer energy calculations

	Energy/kJmol^{-1}				
	E_{coul}	E_{pol}	E_{disp}	E_{rep}	E_{tot}
LEF-LEF	-26.8	-10.8	-118.7	55.2	-101.3
LEF-2PICa	-118.7	-51.4	-77.4	109.6	-138.1
2PICa-LEF	-36.2	-19	-50.2	39.4	-66.1
2PICa-2PICa	-76.9	-29.8	-52.8	34	-125.4
LEF-2PICb	-6.3	-16.3	-38.2	23.8	-62.7
2PICb-LEF	-25.4	-10.2	17.1	17	-44.4
2PICb-2PICb	-135	-61.1	-84.4	96.7	-183.5
2PICa-2PICb	-122.7	-64.6	-35.9	110.7	-112.4
2PICb-2PICa	-64.4	-33.1	-16.5	56.4	-57.6
Total	-612.4	-296.3	-457.0	542.8	-891.5

5.2.4.2   Structural Similarities

In both LEF-PG and LEF-3HBA cocrystals, there are strong LEF-LEF interactions – with large (>30 kJ mol^{-1}) values of E_{tot} (**Figure 5.11**). The strong LEF-LEF interactions in LEF-3HBA have a greater E_{tot} and is dominated by the coulombic component, whereas there is a very small coulombic contribution to the overall LEF-LEF interaction energies seen in LEF-PG. As discussed, coulombic-
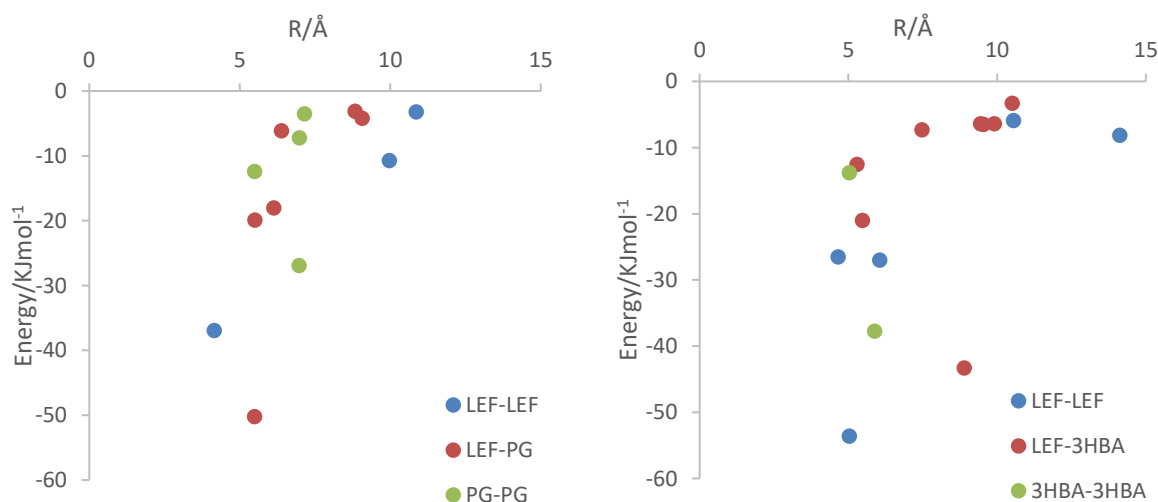
Figure 5.11 Crystal Explorer B3LYP/6-31G(d,p) total molecular pair interaction energies (Etot) as a function of molecule-molecule distance (R) for LEF-PG and LEF-3HBA

dominated interactions are indicative of structure-directing/defining hydrogen-bonds as these strong interactions are beneficial to the total energy.

The larger relative dispersive contribution towards E_{tot} of the LEF-LEF interactions in LEF-PG suggests that, although moderate contributors to the overall molecular pair interaction energies, these are only slightly favourable interactions that are not necessarily structure/composition defining and pose a lower restriction to lattice decomposition in thermal degradation environments. Dispersion is most likely to arrive from $\pi\cdots\pi$ interactions – this is seen in the LEF-PG crystal structure as the alternating oriented chains of LEF molecules are interconnected via $\pi\cdots\pi$ stacking, whereas in LEF-3HBA self-assembles via N–H⋯O hydrogen-bonds. As discussed in **Chapter 5.2.2.2**, the energy frameworks model for the LEF-PG unit cell, representing only the dispersion energy, clearly shows the dominance of dispersion interactions throughout the crystal lattice. This is seen quantitatively in **Table 5.5**. It has been highlighted how these LEF-LEF molecular pair dispersion energy contributions arise from interactions between neighbouring LEF molecules – most likely via $\pi\cdots\pi$ stacking from benzene and imidazole moieties. These are moderate strength interactions and, as the major contributors to the overall molecular pair interaction energies, therefore do not constitute a major driving force behind cocrystal assembly and thus a significant barrier to decomposition during melting.

Combining qualitative and quantitative data in this investigation is again helpful. Energy framework representation of cocrystal molecular pair interactions clearly aid the visualisation of their different components, and the absolute values from the deconvolution of interaction energies provide a more detailed view on the more subtle differences between interactions, their nature, and contributors. For example, the non-dissociating cocrystal LEF-3HBA, which **Table 5.6** shows has a greater Coulombic contribution to LEF-LEF interactions, has a significant Coulombic contribution in the observed API–coformer interactions between LEF and 3HBA.

Table 5.5 Coulombic and dispersion energy components for LEF-PG determined from Crystal Explorer energy calculations

|	Energy/kJmol^{-1}				
	E_{coul}	E_{pol}	E_{disp}	E_{rep}	E_{tot}
LEF-LEF	-33.6	-15.4	-151	98.2	-101.6
LEF-PG	-116	-49.2	-93.6	130.8	-128
PG-LEF	-73.6	-34	-63.9	93.6	-77.7
PG-PG	-78	-32.6	-86.4	100.7	-96.5
Total	-301.2	-131.2	-394.9	423.3	-403.8

Table 5.6 Coulombic and dispersion energy components for LEF-3HBA determined from Crystal Explorer energy calculations

	Energy/kJmol^{-1}				
	E_{coul}	E_{pol}	E_{disp}	E_{rep}	E_{tot}
LEF-LEF	-87.9	-31.2	-153.9	89.9	-182.8
LEF-3HBA	-70.5	-35.2	-92.8	91.9	-106.7
3HBA-LEF	62.7	16.6	-78.9	87.4	-94.3
3HBA-3HBA	-78.8	-31.8	-70	77.6	-103
Total	-174.5	-81.6	-395.6	346.8	-486.8

As is the case, the strong Coulombic involvement in this interaction is indicative of a strong hydrogen-bond – something that would be expected to be a driving force behind cocrystal formation, as well as providing a significant barrier to decomposition, i.e. during dissolution. The solubility and dissolution effects seen in these cocrystals is also accounted for by the significant disparity in PG and 3HBA coformer solubilities: 625 vs 7.57 g L^{-1} respectively.

5.3   Conclusions

This chapter has utilised quantum crystallographic approaches to understanding the cocrystal systems in this study. By investigating beyond standard resolution geometrical analysis, the types, strengths, and natures of a number of interactions in each cocrystal system have been analysed and their effects on cocrystal assembly has been elucidated, as well as sound arguments made for their formation and physicochemical properties. The deconvolution of molecular-pair interaction energies has served to explain the observed differences in physicochemical properties, such as solubility, dissolution rate, and melting point.

In line with the objectives outlined in **Chapter 2.3**, both qualitative and quantitative approaches towards this quantum crystallographic understanding of these cocrystals have been combined and complemented. Graphical depictions of energy frameworks have allowed for a qualitative analysis of molecular pair interactions, and the relative contributions of the individual energetic components within each interaction, along with a depiction of the interacting molecules, and, using inferences based on geometry and chemical intuition, an indication of the functional groups involved.

LEF-3HBA was found to be dominated by coformer···coformer molecular pair interactions, likely arising from 3HBA dimer formation via a 3HBA$_{hydroxyl}$···3HBA$_{carboxyl}$ hydrogen-bonding. The 3HBA

coformer is key to structure assembly of this cocrystal as it is also involved in other coulombic-dominated interactions, LEF $N_{isoxazole} \cdots 3HBA_{carboxyl}$ interactions, and helps to form an extended LEF$\cdots$3HBA$\cdots$3HBA$\cdots$LEF$\cdots$ etc. hydrogen bonding network, providing a route for charge distribution throughout the crystal lattice and thus overall stabilisation of the large favourable observed interaction energies.

The strong, structure-directing interactions in LEF-PG were also seen to arise from co former$\cdots$coformer molecular pair interactions. $PG_{hydroxyl} \cdots PG_{hydroxyl}$ hydrogen-bonds, again manifesting largely in the coulombic component of the total energy, form chains of coformer molecular-pair interactions propagating throughout the unit cell, providing vital charge redistribution from an electronic accumulation about the PG molecule, and thus stabilising the crystal lattice.

Both LEF-2PIC cocrystals, LEF-2PIC and LEF-2PIC 1:2, contain a number of strong molecular-pair interactions. However, these are strengthened by the fact that an intramolecular proton transfer that occurs upon cocrystallisation, resulting in COO_- and NH_+ functional groups.

Pairwise comparison of sub-sets of cocrystal systems – based upon stoichiometric differences and structural similarities – has allowed for a systematic approach to be taken when considering the coformer effect upon physicochemical properties.

Investigation into the effect of differing stoichiometries has demonstrated that the additional 2PIC coformer molecule in the crystal lattice created an increase in strong, coulombic-dominated intermolecular interactions, that served to create a higher energetic barrier to dissociation of the LEF and 2PIC components, thus delaying the release of LEF into solution in LEF-2PIC 1:2 compared to LEF-2PIC.

Considering structural similarities, a comparison of the cocrystals containing the structurally similar PG and 3HBA coformers, LEF-PG and LEF-3HBA, displayed how the individual contributions of the total molecular-pair interaction energies can affect cocrystal formation as well as physicochemical properties. The greater contribution towards the total energy from the coulombic component seen in LEF-3HBA are seen to be not only structure defining/directing, but also providing a greater barrier to decomposition than the dispersive energy-dominated interactions of LEF-PG when thermal degradation/melting is a factor.

Chapter 6 Conclusions and Further Work

6.1 Conclusions

The work presented in this thesis is a study of the low-solubility API leflunomide. The study involved the synthesis and comprehensive characterisation and investigation of a number of novel multicomponent systems of leflunomide.

The synthesis of new cocrystal systems of leflunomide was aided by undertaking a knowledge-based design approach, which used judicious selection of coformers based upon crystal engineering principles, to identify a range of coformers likely to form cocrystals with leflunomide to use in the screening process. The successful screening generated five new cocrystals with all coformers possessing functional groups identified as having a high propensity to interact with those of leflunomide.

These cocrystals were structurally characterised using single-crystal x-ray diffraction techniques, and then subjected to a comprehensive evaluation of their physicochemical properties, such as thermal properties, stability, dissolution rate and solubility. These were performed alongside that of LEF, in order to compare the physicochemical behaviour of the cocrystals with their parent API, with the cocrystals found to possess improved solubilities and dissolution rates.

Formulation aspects of cocrystals were also considered. Two of the cocrystals were also studied by molecular dynamics simulations, identifying associated factors key in determining the dissolution properties of cocrystal formulations, and probing the relationship between cocrystal-excipient interactions in water. These formulations were experimentally evaluated for their dissolution rates and solubilities; properties which appeared to be influenced by their formulation and the experimental hierarchies of dissolution performance were compared with those predicted from molecular dynamics simulations.

The structure assembly, and inferences into formation and physicochemical properties of the cocrystals were also explored through quantum crystallographic methods. Properties such as electronic distributions, related intermolecular interaction energies, and their individual energetic contributions were analysed via systematic, pairwise comparisons based upon structural and stoichiometric similarities and differences, respectively.

6.2 Revisiting the Objectives

At the outset of this thesis, six key research objectives were identified and aimed to be undertaken. These aims were summarised by the following statements:

1. Apply the principles of crystal engineering to successfully inform a knowledge-based design approach to cocrystallisation.
2. Assess the subsequent impact of cocrystallisation upon the structural and physicochemical properties of a low-solubility API.
3. Elucidate the effect of different coformers on the electronic distributions and how this can be related to both physicochemical properties and API/cocrystal-excipient interactions.
4. Combine and complement both qualitative and quantitative approaches towards a quantum crystallographic understanding of these cocrystals.
5. Employ theoretical molecular dynamics simulations to shed light on certain indicative properties of an API/cocrystal that impact its solution behaviour and assess its success relative to experimental observations.
6. Acquire a particle-level perspective on cocrystal-excipient interactions from atomic- and electronic-level data and compare to experimentally derived parameters.

Throughout the work presented above, these objectives have been addressed through a systematic approach to designing, synthesising, and studying a subset of leflunomide cocrystals. More comprehensively, the aforementioned research goals were individually attained; details of this are discussed in the following subsections.

6.2.1 Design of Cocrystals Using Knowledge-Based Design and Crystal Engineering Principles

The first aim of this study was to use judicious coformer selection to synthesise a number of these cocrystal systems. As discussed in **Chapter 1**, the primary aim of cocrystal synthesis in a pharmaceutical context is ultimately to improve their pharmaceutical profiles. In this study, a knowledge-based design approach has been adopted, utilising a detailed analysis of the molecular structure and intermolecular interaction capabilities of leflunomide, using the CCDC modules Isostar and Mercury. These have enabled a range of functional groups potentially favourable for its cocrystallisation, and thus a selection of coformers possessing these, to be identified.

Representative "central groups" were chosen from the Isostar library based on their resemblance to the main functional hydrogen-bonding groups present in leflunomide. Searches of their most commonly occurring interactions within the CSD enabled a determination of the most preferential contacts for each functional group, indicative of those that could occur between leflunomide and potential coformers. These were found to be groups containing an aromatic component, such as NH_2, H, and OH groups bonded to an aromatic carbon. Alongside these, polar X–H groups (X=N, O or S) were also found to be commonly occurring contacts for all central groups.

The motif searching function in Mercury was also employed to more accurately investigate the contacts between contact groups and leflunomide, not only by tailoring the central groups to more precisely represent LEF, but also by defining the nature of interaction, i.e. separation into donor and acceptor atoms. Again, the results from this search identified amide and aromatic hydroxyl (and carboxyl) groups, as well as amine contacts.

The information obtained from this searching process allowed for a library of favourable functional groups for cocrystal design be compiled, representing the possibility for formation of a number of well-known supramolecular synthons with the functional groups of leflunomide. A library of diverse coformers was then compiled from a list of those commonly used in cocrystal screening experiments, against which the Mercury Molecular Complementarity search tool was utilised, giving a list of coformer "hits" to be used in the solid-form screening process.

Ultimately, this rational selection of coformers has resulted in five new pharmaceutically acceptable cocrystals of leflunomide, with the successful coformers, 2-picolinic acid (2PIC), 2-aminopyrimidine (2APYM), 3-hydroxybenzoic acid (3HBA), and pyrogallol (PG) all containing functional groups identified as favourable in the design process: aromatic –OH, –COOH, and –NH_2 groups.

6.2.2 Assess the Impact of Cocrystallisation on the Structural and Physicochemical Properties of Leflunomide

Following on from the first objective, and in line with the ultimate goal of cocrystallisation in a pharmaceutical aspect, outlined in **Chapter 1**, leflunomide and its cocrystal systems were subjected to a thorough investigation of their structural and physicochemical properties. In particular, the solution properties of solubility and dissolution rate were evaluated, and comparisons were drawn between cocrystal and parent, single-component LEF. As a counterpart to the examination of solution properties, the thermal properties, such as melting point and thermal stability, and accelerated storage and solution stability were measured to further assess to the pharmaceutical applicability and potential of the cocrystal systems.

In analysing the crystal structures of the cocrystals, a number of supramolecular synthons identified in the design process in **Chapter 3.4** were displayed. These included amine···amide, COOH···amide and COOH···isoxazole motifs, giving credence to the accuracy and importance of a knowledge-based approach in cocrystal design and selection of coformers.

With regards, to their physicochemical properties, the four pharmaceutically acceptable cocrystals: LEF-PG, LEF-3HBA, LEF-2PIC, and LEF-2PIC 1:2 were found to possess melting points different to that of the parent single-component leflunomide. LEF-PG and LEF-2PIC displayed melting points falling within the range of LEF and its coformer, while the LEF-3HBA cocrystal displayed a higher melting point than both respective components. LEF-3HBA was the only cocrystal found to be stable under both accelerated and slurry conditions, as characteristic peaks of the single-component LEF were observed in the PXRD patterns of LEF-PG both LEF-2PIC cocrystals after 24-hour slurry experiments – indicative of dissociation.

However, when solubility was considered, LEF-PG and LEF-2PIC exhibited the highest calculated solubilities of all samples, with the aforementioned dissociation posited to be due to a "spring effect": a mechanism described in **Chapter 3.10.1**. The dissolution rates of the cocrystals were also enhanced with respect to LEF.

These reasoning behind these studies was two-pronged. Firstly, the evaluation of these properties served to mirror the process that which is followed when screening for cocrystal systems in the pharmaceutical industry and provide an educated, thorough recommendation for promising cocrystal systems of LEF for further development. Secondly, and most importantly for this study, knowledge of these properties allowed for a direct point of comparison when the effects and differences in electronic distributions, intermolecular interactions, and assemblies of the leflunomide systems were investigated in **Chapter 5**.

6.2.3   Compare Experimental Solution Behaviour with Calculated Properties from Molecular Dynamics Simulations

In this chapter, the goal was to further compare and complement the approaches of experimental and theoretical work in order to garner a deeper understanding of the molecular-level interactions between drug, excipient, and water. This was to enable the formation of "hierarchies" of predicted solution performance and use this to prepare, and eventually compare, experimental solution performance of prototype formulated cocrystals of leflunomide. In detail, this chapter identified and investigated underlying mechanisms and key indicative properties in affecting the dissolution of LEF formulations, which in turn were used to rationalise the experimental observations.

Molecular dynamics simulations were shown to unearth key information regarding molecule-molecule interactions within cocrystal formulations: their nature, number, and strength. A number of key parameters, such as solvent-accessible surface area, number of hydrogen bonds between an API or cocrystal in formulations with water, and interaction energy between an API or cocrystal in formulation and water were demonstrated to be governing factors in the elucidation of dissolution performance of leflunomide and its cocrystal system formulations.

In the presence of formulation excipient lactose, theoretically derived trends in dissolution performance of LEF < LEF-3HBA < LEF-2PIC were in direct agreement with the experimental observations and were also shown to be enhanced by the addition of lactose as an excipient when compared to their pure, unformulated counterparts. Conversely when DCP was considered as an excipient, the predicted dissolution performance follows the trend LEF < LEF-2PIC < LEF-3HBA, which was hypothesised to be explained by the ionic nature enabling stronger interactions between the coformer and excipient reducing those between cocrystal complex and water when compared to LEF-3HBA. Again, this theoretical hierarchy was found to be in good agreement with the experimentally observed dissolution trend.

6.2.4 Analyse the Effect of Coformers on Electronic Distributions, Intermolecular Interactions, and Physicochemical Properties

The work described in Chapter 5 used a quantum crystallographic approach and combined both qualitative and quantitative breakdowns of theoretical molecule-molecule interactions within LEF and the LEF cocrystal systems in order to elucidate the effect of different coformers on the electronic distributions and relate to both physicochemical properties and to rationalise cocrystal structure and formation.

Qualitative analysis, using energy frameworks of molecular-pair interactions, provided a route to viewing the molecules involved in individual interactions, their energies, the relative contributions of the individual energetic components within each interaction. This allowed for the strength and nature of the interactions to be related to the molecules involved, as well as an inference of the functional groups involved using chemical intuition based on the geometries of the interacting molecules.

A quantitative approach utilised the breakdown of molecular-pair interaction energies into the respective individual energetic components: coulombic, polarisation, dispersion, and repulsion. This provided insight into the nature of the molecular-pair interactions of LEF cocrystals and whether they were dominated by coulombic energetic contributions – indicative of strong hydrogen-bonding, or dispersive forces – more moderate-to-weaker strength van der Waals'

interactions, as well as the breakdown between the constituent components in all molecular pair interactions involved in the cocrystal as well as the general trade-off between attractive (favourable) and repulsive (unfavourable) forces.

Comparison of LEF to the cocrystals, as well as pairwise comparison of cocrystals – based upon stoichiometric differences and structural similarities – focusing on these energetic components allowed for a systematic approach to be taken when considering the factors influencing cocrystal assemblies, potentially their formations, and their physicochemical properties with respect to leflunomide and each other.

Concerning stoichiometric effects, comparison of LEF-2PIC and LEF-2PIC 1:2 found that the additional 2PIC coformer molecule in the crystal lattice had a negative impact on solution performance, which was related to the observed increase in strong, coulombic-dominated (charge-assisted) intermolecular interactions, which thus created a higher energetic barrier to dissociation of the LEF and 2PIC components.

When investigating structural similarities, LEF-PG and LEF-3HBA were chosen for pairwise comparison to demonstrate how subtle differences in coformer structure, and the inherent steric and electronic effects therein, impact upon the total molecular-pair interaction energies, their individual energetic contributions, and how this can affect cocrystal structure, assembly, and physicochemical properties. It was found that the main molecular-pair interactions in LEF-3HBA possessed a greater component of the coulombic energy compared to that of LEF-PG. These types of interactions were noted to be more influential to the structure and cocrystal assembly than the moderate-to-weaker strength interactions dominated by dispersive forces, which were more common in LEF-PG. In addition, the strong, coulombic-dominated molecular-pair interactions were also highlighted as providing a greater barrier to decomposition, a factor concerning melting points, and was evidenced in the higher observed melting point of LEF-3HBA.

6.3   Further Work

In line with the aims of the project further work would aim to build upon the results obtained from screening and quantum crystallographic studies of leflunomide cocrystals (**Chapter 3** and **Chapter 5**), focusing on the nature of particles within a system, i.e. cocrystals and excipient, with respect to their size, morphologies, and interactions. With an objective to use insights gained from theoretical molecular pair energies, these would supplement both experimental observations of morphology, from methods such as Scanning Electron Microscopy (SEM) and crystal face-indexing, as well as theoretical predictions of these properties, obtained from morphology calculations of cocrystals (using packages such as Mercury BDFH, HABIT/SHAPE). In

both experimental and computational studies, select cocrystals and excipients would be compared, along with that of their single component API leflunomide, to provide insight into the effect of both cocrystallisation and the particle-level influences formulation has on the physicochemical profile of leflunomide.

The aim here would be to relate their "interior" crystal properties to "exterior" face-to-face interparticle properties and behaviours through an understanding of hydrogen-bonding natures, electron densities, and intermolecular interactions. Such characteristics would be reasonably expected to affect how crystals and particles interact with one another in a practical context and thus their physicochemical properties. Again, experimental (diffractometer-mounted crystal face-indexing) and theoretical (BDFH and attachment energy) morphologies would be used as the basis, and the marrying of the two approaches would be key, tying in with the overall theme and title of this work.

Appendix D.3 contains example SEM images of powder samples of leflunomide, and the cocrystals studied in **Chapter 4** in the computational and experimental studies of leflunomide formulations. These samples were ground and sieved to a size of 53-90 μm to ensure a uniform particle size for a consistent comparison across the systems. These particles and their morphologies, along with the experimental morphologies obtained from face-indexing of mounted single crystals used for high-resolution X-ray diffraction studies and quantum crystallographic investigations (**Chapter 5**), would therefore be used as the experimental counterpart to those obtained theoretically using attachment energy calculations in the program HABIT along with overlays of crystal structure within Mercury BDFH morphology calculations.

Further to this qualitative comparison of experimental vs theoretical morphologies, a quantitative approach, entailing the calculation of electronic density distributions of leflunomide and cocrystals and the subsequent analysis of their effects on atom-atom and molecule-molecule interactions, along with the molecular pair interaction energies discussed in **Chapter 5.2**, would be employed. These properties, when coupled with the knowledge of morphologies (both experimental and theoretical) would be used to predict the nature of particle faces, where electronic density distributions are used as an indicator of potential interactions between particles. To complement this experimental knowledge of potential interparticular interactions, theoretical calculations of morphology using HABIT will also enable the calculation of properties such as surface and attachment energies, and indications of roughness at "exterior" crystal faces. Calculated properties such as anisotropy factors can be derived through these processes, which can indicate the potential for strong interactions between particles. For example, a low anisotropy factor (defined as the slice energy – the attachment energy at certain d-spacings in 0.1 d-spacing

steps – divided by the total lattice energy) is indicative of the breaking of strong intermolecular synthons at a particle surface, therefore creating a likelihood of strong interactions forming with neighbouring particles in order to stabilise this exposed slice energy. This could provide a particle-level view of the similar approach to that used in **Chapter 5** when considering molecule-molecule interactions, and therefore an understanding of how particles behave with respect to each other and thus their physicochemical properties.

Ultimately, the further work outlined here addresses final objective outlined in **Chapter 2.3**:

6. Acquire a particle-level perspective on cocrystal-excipient interactions from atomic- and electronic-level data and compare to experimentally derived parameters.

Appendix A　　LEF Experimental

LEF was purchased from Biotain Pharma Co., Ltd., China, while all coformers were purchased from Sigma-Aldrich, Singapore, and used as received without any further purification. Analytical grade solvents were used for the crystallisation experiments.
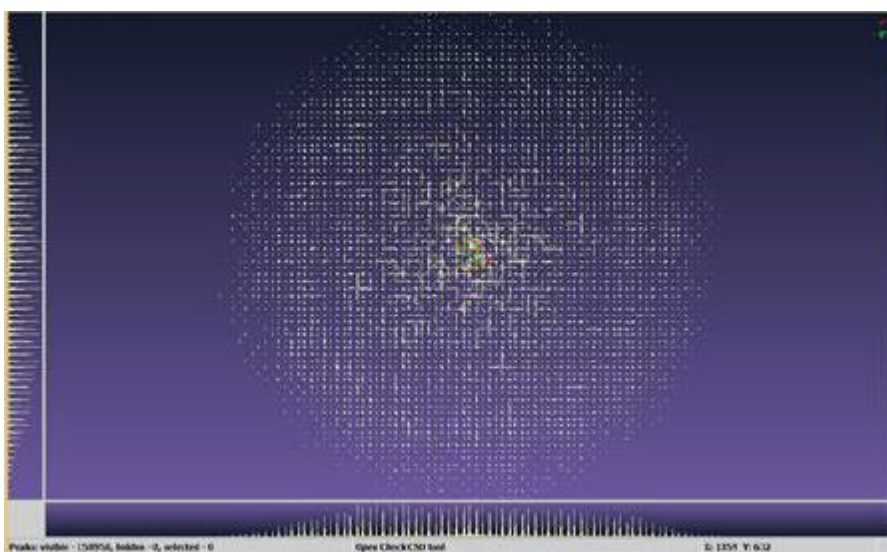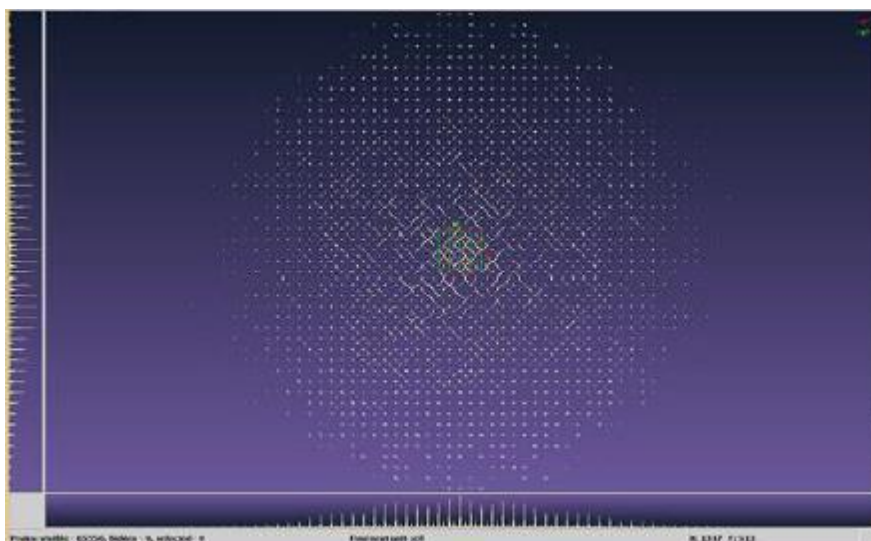
A.1.1　　　LEF-PG Crystal Structure

The crystal structure of the LEF-PG cocrystal presented herein is modelled in the I–4 space group. Examination of the raw data indicates a degree of commensurate modulation. After testing a variety of space groups, from triclinic to tetragonal crystal systems, it was decided that the I–4 space group symmetry gives a model which is a close approximation to the true commensurate structure (for more details see the Supporting Information).
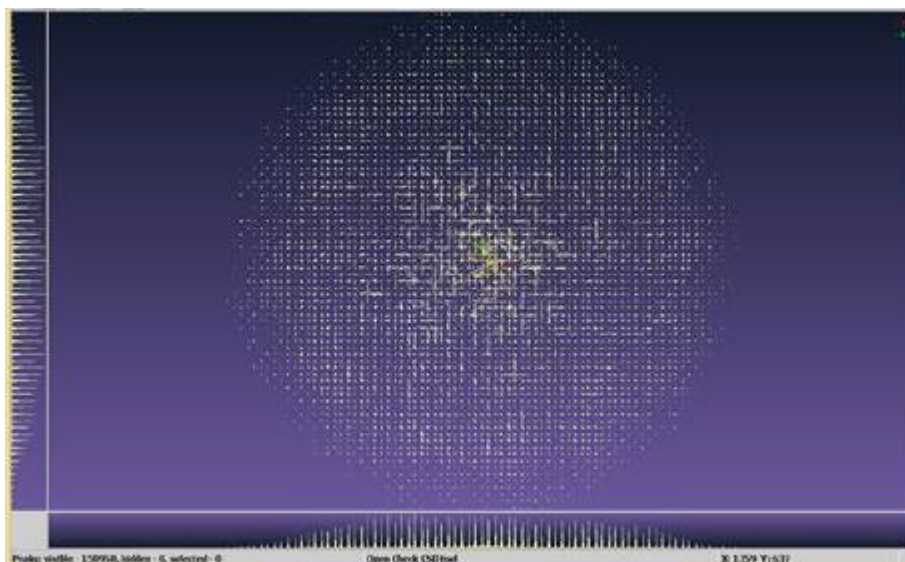
The crystal structure of the LEF-PG cocrystal presented herein is modelled in the I–4 space group, using the following cell parameters: a = 22.5725(4), b = 22.5725(4), c = 7.0280(2); α = 90, β = 90, γ = 90. Examination of the raw data shows that there are additional weaker peaks with half indices in the a and b directions. During data collection, solution, and refinement the LEF-PG structure appeared to show signs of modulation (with a doubling in the length of the a and b unit cell axes). This is consistent with a model of commensurate modulation and effects of this nature can be seen in the precession image down the c-axis (see **Figure A.1**). The data was also indexed using a larger cell of 31.6, 31.6, 7.0; 90, 90, 90, but all efforts to obtain a good solution failed (the precession image down the c-axis is shown in **Figure A.2** for comparison). Examination of the data indicated a range of possible symmetry elements across different systems. After testing a variety of space groups, from triclinic to tetragonal crystal systems, it was decided that the I–4 space group symmetry gives a model which is a close approximation to the true commensurate structure. The above is valid for the room temperature data collected. However, attempts to solve the structure in the I–4 space group with low temperature (100 K) data completely failed, and no appropriate solution could be obtained in any space group. This indicates that there is a stronger effect of the modulation at lower temperatures and this can also be seen in the precession image down the c-axis (**Figure A.3**).The room temperature I–4 LEF-PG model presented herein is suitable for the purposes of this thesis and, given that considerable efforts to collect and solve further data under different conditions and space groups were undertaken, it was decided not to pursue this case any further at this stage. The raw data images for the room temperature data collection

have been deposited in the Zenodo repository (https://doi.org/10.5281/zenodo.2585778) so that
the interested reader can x(re)examine as they see fit.

A.1.2 CF₃ Disorder

The crystal structure of LEF-PG, LEF-3HBA, LEF-2PIC and LEF-2PIC 1:2 cocrystals contain disorder about the LEF CF3 group due to thermal rotation of the F-atoms about C. In each case this disorder was modelled using a number of constraints and restraints. The CF_3 group was split into two parts (A and B) and two models were resolved for each CF_3 group – containing approximate A:B occupancy ratios refined to 61:39, 51:49, 50:50 and 51:49 respectively. A distance restraint, SADI, was placed on the carbon atom of this group to restrain C–F and F–F distances within each group to be equal. An enhanced rigid bond restraint, RIGU, was also applied to the anisotropic displacement parameters of each CF_3 part individually.

A.1.3 High-Resolution Data

High-resolution data collection for LEF, LEF-3HBA, LEF-2PIC, LEF-2PIC 1:2, and LEF-PG was run exclusively on a Rigaku rotating anode source (FRE+ SuperBright Molybdenum X-Ray generator) diffractometer fitted with a HyPix-600HE detector and an AFC12 goniometer. This has a highly focused beam (70µm) achieved with the VariMax VHF (Very High Flux) optics. Data was collected at 100K with the aid of an Oxford Cryosystems Cobra. Each data set was collected under slightly different conditions for each crystal, but in all instances a full sphere of data was collected to a resolution of ≥0.50 Å. Data reduction was performed using CrysalisPro software, with each experiment treated separately. Experimental parameters are detailed in **Table A1** below.

Table A1 Crystal structure data and experimental parameters for the data collection of LEF and cocrystals

Compound reference	LEF	LEF-PG	LEF-3HBA	LEF-2PIC	LEF-2PIC 1:2
Crystal data					
Chemical formula	$C_{12}H_9F_3N_2O_2$	$C_6H_6O_3 \cdot C_{12}H_9F_3N_2O_2$	$C_{12}H_9F_3N_2O_2 \cdot C_7H_6O_3$	$C_6H_5NO_2 \cdot C_{12}H_9F_3N_2O_2$	$2(C_6H_5NO_2) \cdot C_{12}H_9F_3N_2O_2$
Mr	270.21	396.32	408.33	393.32	516.43
Crystal system	Monoclinic	Tetragonal	Monoclinic	Monoclinic	Monoclinic
Space group	$P2_1/c$	I–4	$P2_1/n$	$P2_1/c$	$P2_1/c$
a/Å	12.148(0)	22.3977 (1)	11.78065 (7)	9.8742 (2)	23.72955 (10)
b/Å	13.71750(10)	22.3977 (1)	5.02808 (4)	14.9085 (2)	12.59793 (6)
c/Å	14.03910(10)	6.9617 (1)	29.8635 (2)	12.4247 (2)	7.62509 (5)
α/°	90	90	90	90	90
β/°	102.31(0)	90	92.5247 (6)	112.753 (2)	95.7180 (4)
γ/°	90	90	90	90	90
Cell volume/Å^3	2285.73(2)	3492.39 (6)	1767.22 (2)	1686.70 (5)	2268.13 (2)
Z	8	8	4	4	4

Data Collection

Diffractometer	Rigaku FRE+	Rigaku FRE+	Rigaku FRE+	Rigaku FRE+	Rigaku FRE+
Temperature/K	100	100	100	100	100
Radiation type	Mo Kα	Mo Kα	Mo Kα	Mo Kα	Mo Kα
Wavelength, λ /Å	0.71073	0.71073	0.71073	0.71073	0.71073
Resolution / Å					
Exposure /s					
Redundancy					
No. of reflections measured	597196	379006	512830	269299	415615
No. of independent reflections	27440	19993	20039	269299	25795
R_{int}	0.046	0.096	0.045	0.061	0.060
Completeness					

Refinement

GoF, S	1.04	1.52	1.17	1.02	1.15
Final R_1 [I> 2σ(I)]	0.037	0.138	0.064	0.057	0.059
$wR(F^2)$ [I> 2σ(I)]	0.123	0.361	0.185	0.174	0.176

A.2   Physicochemical Properties Measurements

A.2.1   Differential Scanning Calorimetry

A Mettler Toledo DSC 822e module was used for the DSC analysis. In each experiment, the sample size was 2–5 mg, the temperature range was typically 25–250 °C, and the heating rate was 10 °C min^{-1}. The samples were purged with a stream of flowing nitrogen (20 mL min^{-1}). The instrument was calibrated using Indium as the reference material.

A.2.2   Stability Studies

The stability of all the pharmaceutically acceptable cocrystals was evaluated under accelerated storage conditions (40 °C and 75% relative humidity (RH)) over a period of 13 weeks in an MMM Climacell 111 humidity incubator. Samples of approximately 100 mg size were stored under the test conditions and tested periodically using XRPD to identify the samples' identity.

For the slurry experiments, excess powder samples of the cocrystals were left stirring in water at 37 °C for 24 h before filtering and drying in ambient conditions, and the resulting powders were analysed by XRPD.

A.2.3   Dissolution Rate

The dissolution rate of all samples was tested using an Agilent 708-DS dissolution sampling apparatus. Samples containing equivalent to 25 mg LEF in a 500 mg corn starch tablet were pressed for 30 s at 1 kN using an FT-IR press and placed in an ultrapure water dissolution medium (900 mL) with a rotation speed of 100 rpm at 37 °C. Sampling was conducted by withdrawing 2 mL aliquots of sample from the vessel and filtered through a 45 µm syringe tip filter for analysis by HPLC. This was conducted at 5, 10, 15, 30, 45, 60, 90, 120, 180, 240, 300 and 360 mins. In order to maintain the dissolution volume, samples were immediately replaced with an equivalent fresh dissolution medium.

A.2.4   Solubility

Solubility was measured by stirring excess amounts of powder samples in 5 mL of ultrapure water at 37 °C for 24 h, filtering the resultant slurry through a 45 µm syringe filter and analysing by HPLC. The concentration of the final solution was calculated using predetermined calibration data.

A.2.5 High Performance Liquid Chromatography

HPLC was used to quantify LEF concentration in the samples obtained from solubility and dissolution experiments. HPLC instrument was equipped with a ZORBAX ECLIPSE XDB-C18 column (4.6 mm x 250 mm x 5 μm) and run at 37 °C. The mobile phase consisted of acetonitrile and water (50:50 v/v) with a flow rate of 1 mL min^{-1} and 15 min run time. A sample injection volume of 50 μL was used. The detection wavelength was set to 262 nm. The retention time of LEF was 7.4 mins, and the retention times of the coformers PG, 3HBA and 2PIC were 2.6, 2.8 and 2.2 mins, respectively.

Appendix B   LEF Cocrystal Design

B.1   Characterisation of the Bulk LEF Powder
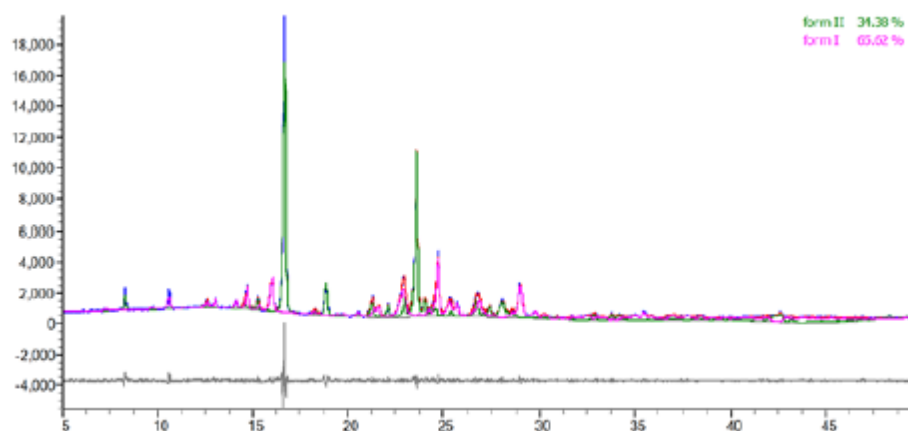
Figure B.1 Rietveld analysis of the bulk LEF powder pattern (black) with the reference simulated

powder patterns of Form I (pink) and Form II (green)

This shows that the bulk powder is a mixture of the two polymorphs

B.2   CSD Analysis of Leflunomide Interactions

B.2.1   Isostar Searching Using Predefined Contact Groups

The functional groups present in LEF, and the propensity to which they interact with other groups

can be understood through statistical analysis of the CSD. Selecting ligands, representative of the

functional groups in LEF, and possible contact groups from a pre-set list available in Isostar v2.2.5

enabled the determination of the most preferential contacts for each functional group. LEF

contains a number of functional groups with potential for intermolecular interactions, mainly an

amide group (bonded either side to aromatic rings), an isoxazole ring (methyl substituted), and a

trifluoromethyl group. These were initially modelled using select ligands available in the Isostar

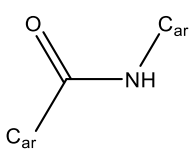library and denoted the central group (**Figure B.2**).
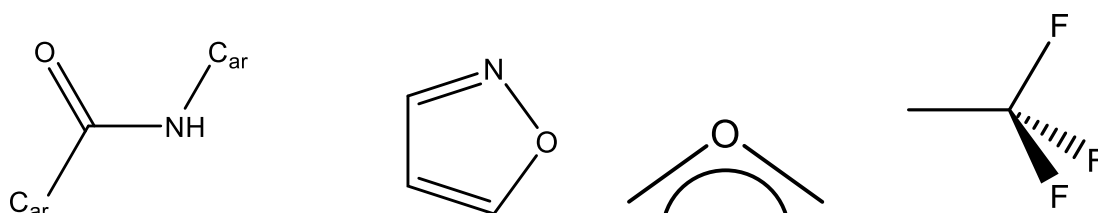
Figure B.2 Chemical diagrams of the predefined ligands used to represent LEF functional

groups in contact searching

Isostar searching based on these central groups, with respect to a variety of common functional groups (contact groups), gave statistical information on the number of crystal structures containing both the central and contact groups, and the number of these structures in which the central and contact group form a contact with distance (R) less than the sum of the van der Waals' radii (V).
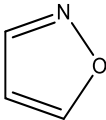
Table B.1 shows the interactions preferred in aromatic-aromatic amide central group, with the contact groups present in most structures (and with contact between the two groups) highlighted in green.

Table B.1 Isostar search results for preferred interactions of the aromatic-aromatic amide central group with predefined contact groups, showing the number of structures containing both groups and those with contact between the groups

aromatic-aromatic amide	structures have both groups present	structures have both groups and contact between them	%
any polar X-H (X= N, O or S)	2754	1375	49.93
any alkyl C-H	1547	689	44.54
any aromatic C-H	2750	1009	36.69
any NH	2754	907	32.93
any uncharged NH	2809	866	30.83
amide NH	2754	734	26.65
uncharged $C(sp^2)/C(ar)$-NH_2	62	36	58.06
any OH	780	539	69.10
alcohol OH	125	88	70.40
phenol OH	141	59	41.84
water	389	338	86.89
aromatic or sp^2 N	1116	210	18.82
any terminal O	2754	1413	51.31
any C=O	2754	1267	46.01
amide C=O	2754	670	24.33
carboxylate	38	15	39.47

The most favourable groups to form interactions with this central group are OH and O groups – including alcohol/phenol OH and carboxylic acid/carboxylate groups – showing up to a 70% propensity to form contacts when both groups are present. As well as these, uncharged NH_2 and X–H groups show preference to form contacts (49-58%). Containing these functional groups, the contact groups mentioned are indicative of most alcohol/carboxylic acid/amine/amide containing compounds.

Table B.2 Isostar search results for preferred interactions of the unsubstituted isoxazole central group with predefined contact groups, showing the number of structures containing both groups and those with contact between the groups

isoxazole	structures have both groups present	structures have both groups and contact between them	%
any polar X-H (X= N, O or S)	352	158	44.89
any alkyl C-H	597	382	58.96
any aromatic C-H	559	329	58.86
any NH	249	85	34.14
any uncharged NH	146	45	30.82
amide NH	58	11	18.97
uncharged $C(sp^2)$/C(ar)-NH_2	32	16	50.00
any OH	171	79	46.20
alcohol OH	64	27	42.19
phenol OH	41	11	26.83
water	40	21	52.50
aromatic or sp^2 N	743	112	15.07
any terminal O	516	122	23.64
any C=O	422	89	21.09
amide C=O	58	7	12.07
carboxylate	17	4	23.53

The exact 5-methyl substituted isoxazole fragment present in LEF is not present in the Isostar pre-set list of ligands and ring systems, therefore the two fragments were selected as the central group for the specific contact search in order to give a good indication of the behaviour of the 5-methylisoxazole fragment – the structurally similar unsubstituted isoxazole fragment, and two representative aromatic O and N fragments.

In **Table B.2** the data for the unsubstituted isoxazole central group shows a preference for contact to alkyl and aromatic C–H groups (59%), slightly more so than that with uncharged sp2 hybridised/aromatic C–NH$_2$ groups (50%). Also showing a preference are OH, alcohol and polar X–H groups. This data suggests a preference for aromatic containing compounds, with (mostly polar) hydrogen-bond donating groups further enhancing the probability of contact.
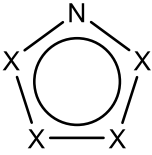
Searching using the other central group used to denote the 5-methyl isoxazole group in LEF, the aromatic O group, generally resulted in a higher number of structures containing both central and contact groups (**Table B.3**). However, this was coupled with a significantly lower percentage of these structures having contact between groups, such as only a 12% contact incidence rate for uncharged sp^2 hybridised/aromatic C–NH$_2$ groups – as opposed to 50%. Firstly, this reduction in occurrence suggests that, in the majority of contacts involving the LEF isoxazole group the N atom will be more involved in the intermolecular interactions. Secondly, the similar trend in occurrence of contacts between the isoxazole and aromatic O central groups supplements the proposed preference for aromatic and hydrogen-bond donor containing compounds.

In order to further investigate the isoxazole functional group contact preferences, and whether the N-atom dominates the contributions in intermolecular interactions, a third representative ligand was chosen for Isostar statistical searching. This "aromatic N, in 5-rings" ligand enabled analysis of the tendency for interactions to occur between the contact groups and central group no containing O-atoms. Table C.4 contains the results for this interaction search, which show consistency with the contact frequencies for the isoxazole central group. A greater percentage of structures contain contacts between both groups for the OH-containing contact groups and C–NH$_2$ groups than for the aromatic O central group. This supports the idea that the N-atom of the LEF isoxazole is more involved in any intermolecular interactions arising.

Table B.3 Isostar search results for preferred interactions of the aromatic O central group with predefined contact groups, showing the number of structures containing both groups and those with contact between the groups

aromatic O	structures have both groups present	structures have both groups and contact between them	%
any polar X-H (X= N, O or S)	3943	425	10.78
any alkyl C-H	7060	783	11.09
any aromatic C-H	7138	733	10.27
any NH	2285	186	8.14
any uncharged NH	1316	61	4.64
amide NH	508	19	3.74
uncharged C(sp^2)/C(ar)-NH$_2$	189	23	12.17
any OH	2255	247	10.95
alcohol OH	880	56	6.36
phenol OH	324	15	4.63
water	482	94	19.50
aromatic or sp^2 N	4560	213	4.67
any terminal O	6195	329	5.31
any C=O	4512	156	3.46
amide C=O	508	21	4.13
carboxylate	131	12	9.16
aromatic O	9999 (subset from 10084 structures)	250	2.50

Table B.4 Isostar search results for preferred interactions of the aromatic N, in 5-rings central group with predefined contact groups, showing the number of structures containing both groups and those with contact between the groups
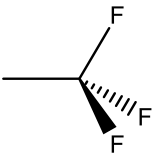
aromatic N, in 5-rings	structures have both groups present	structures have both groups and contact between them	%
any polar X-H (X= N, O or S)	9999 (subset from 11623 structures)	2854	28.54
any alkyl C-H	9999 (subset from 12918 structures)	819	8.19
any aromatic C-H	9999 (subset from 13992 structures)	967	9.67
any NH	9318	2315	24.84
any uncharged NH	7121	1661	48.17
amide NH	956	216	22.59
uncharged $C(sp^2)/C(ar)-NH_2$	379	149	39.31
any OH	5730	2662	46.46
alcohol OH	1775	842	47.44
phenol OH	903	225	24.92
water	2128	1172	55.08
aromatic or sp^2 N	9999 (subset from 18863 structures)	229	2.29
any terminal O	9373	355	3.79
any C=O	7283	250	3.43
amide C=O	956	55	5.75
carboxylate	351	24	6.84
aromatic O	1313	7	0.53

LEF also contains a trifluoromethyl functional group, which could be accurately modelled in the Isostar contact searching. Examination of **Table B.5** shows that this central group forms contacts most frequently with uncharged sp^2 hybridised/aromatic C–NH$_2$ groups (61%), amide NH (59%) and aromatic C–H groups. Also showing reasonable propensity for contact are the polar X–H, NH and CONH$_2$ groups. These contact percentages suggest that an ideal contact for LEF trifluoromethyl group would be an aromatic, nitrogen-containing (preferably a primary amide or amine) moiety.

Table B.5 Isostar search results for preferred interactions of the trifluoromethyl central group with predefined contact groups, showing the number of structures containing both groups and those with contact between the groups

| trifluoromethyl	structures have both groups present	structures have both groups and contact between them	%
any polar X-H (X= N, O or S)	2442	1371	56.14
any alkyl C-H	1727	903	52.29
any aromatic C-H	1714	1034	60.33
any NH	1407	734	52.17
any uncharged NH	557	251	45.06
amide NH	149	88	59.06
uncharged C(sp^2)/C(ar)-NH$_2$	67	41	61.19
CONH2	27	14	51.85
any OH	2442	1013	41.48
alcohol OH	212	99	46.70
phenol OH	101	44	43.56
water	620	430	69.35
aromatic or sp^2 N	547	112	20.48
any terminal O	2442	811	33.21
any C=O	2442	781	31.98
amide C=O	149	53	35.57
carboxylate	1007	305	30.29

Statistical analysis of intermolecular contacts in the Isostar v 2.2.5 database has allowed for a primary evaluation of the preferred interactions between the functional groups of LEF and potential coformers. All five separate central groups have shown a general high affinity for contacts with groups containing an aromatic component, such as C(ar)-NH$_2$, aromatic C–H, and phenol OH groups. In addition to these, polar X–H groups were amongst the highest occurring contacts for all central groups, with specifically OH groups displaying a high affinity for contact with the aromatic-aromatic amide, isoxazole and aromatic N central groups, and N–H groups likewise for the aromatic N and trifluomethyl central groups. This leads to three initial preferences in coformer structure and functional groups for the design of LEF cocrystallisation: aromatic region, OH groups, and either amide or amine NH groups.

B.2.2 Specific Contact Searching Using Mercury

With Isostar interaction search providing an initial insight into the nature and preference of interactions in the various functional groups of LEF, specific contact searching using the motif search tool integrated in Mercury allowed for more defined contacts to be searched. Rather than investigating contacts between predefined ligands and groups, each functional group could be tailored to more accurately represent those involved in LEF and its possible contacts (**Figure B.3**). In addition to this, the nature of interactions could be defined, such as separation into donor atoms and acceptor atoms.

As mentioned in **Appendix B.2**, specific contact searching of the substituted isoxazole proved slightly difficult due to the uncommon nature of the fragment in the CSD and the fact that Isostar searching uses only a pre-set selection of ligands. Several structurally similar fragments were chosen as central groups to represent the behaviour of isoxazole fragment as closely as possible. Where possible, default central and contact groups present in the motif search tool of Mercury were chosen in order to maximise the popularity of the representative fragments and thus the number of results. The only exception to this was the trifluoromethyl group, which was defined using the sketch tool.
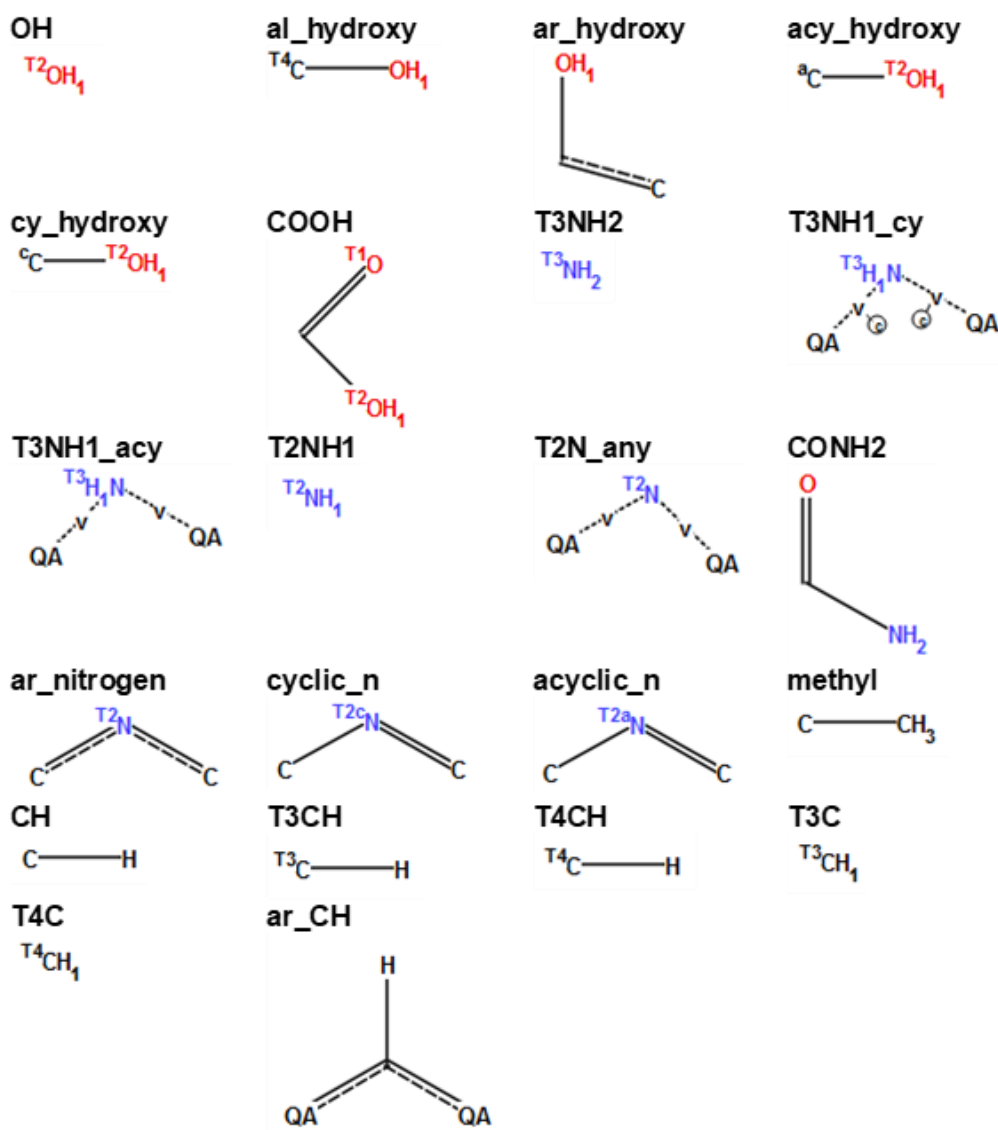
Figure B.3 Chemical diagrams of the contact groups and their abbreviated names used in specific contact searching
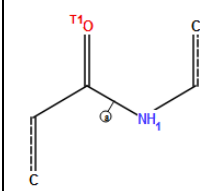
QA represents any non-hydrogen element

Similar to the Isostar search, an aromatic-aromatic amide was used to accurately portray this moiety in LEF (**Table B.6**). In this case the dominant contact group is some variant of the CH (79.7%), with more specifically the aromatic CH group showing high frequency of up to 66%. This is followed by primary amine groups (T3NH2) which occur in almost 50% of cases, with all of these contacts involving the amide carbonyl group. The amide NH group shows highest affinity for contacts with carboxylic acid carbonyl (42%) and aliphatic hydroxy groups (34%), but interestingly this is not reflected in a high frequency of contacts between amide NH and carboxylic acid OH groups (3.5%). Visualisation of the few structures displaying these contacts suggests that the steric hindrance presented by the trans-configuration of aromatic groups either side of the amide

creates a barrier for interactions to occur, something that is not as present with the more frequently occurring motif involving the amide CO and NH2 of an amide contact group (57%).

Table B.6 Specific contact search results for the ar_ar_amide motif with various functional groups, showing the number of structures containing the motif and frequency

Bold indicates the atoms involved in the motif

	amide **C=O**		amide **NH**	
contact group	no. of structures	% frequency	n. of structures	% frequency
OH	154	27.8	92	16.6
al_hydroxy	84	38.0	74	33.50
ar_hydroxy	54	28.1	8	4.17
acy_hydroxy	96	25.9	81	21.8
cy_hydroxy	58	28.2	12	5.83
CO**OH**	20	11.6	6	3.49
COOH	5	2.91	72	41.9
T3NH2	57	49.1	8	6.9
T3NH1_cy	20	8.47	1	0.424
T3NH1_acy	954	28.5	42	1.26
T2NH1	0	0	0	0
T2N_any	12	0.853	125	8.89
CO**NH2**	8	57.1	0	0
CONH2	0	0	1	7.14
ar_nitrogen	4	0.319	121	9.64
cyclic_n	5	7.14	1	1.43
acyclic_n	1	4.17	0	0
methyl	131	10.3	3	0.236
CH	2708	79.7	256	7.54
T3CH	2247	66.3	135	3.98
T4CH	1108	52.3	125	5.9
T3C	1472	43.4	202	5.96
ar_CH	2255	66.4	144	4.24

Following these groups, the various hydroxyl contact groups show moderate frequencies with the amide at both the carbonyl and NH positions. Of these hydroxyl groups, aliphatic hydroxyls occur most often to both CO and NH positions (33-38%), and aromatic and cyclic OH groups possess a 28% percentage of formation to the amide carbonyl group specifically. These detailed contact results suggest a preference in the aromatic amide group for interactions with aromatic, amide, and hydroxyl moieties, with the majority of these involving the amide carbonyl group.

Table B.7 shows the frequency of occurrence for each motif in relation to the LEF isoxazole group – the default central group chosen from Mercury is the unsubstituted version of this functional group. CH contacts dominate both at both the N and O positions this instance (62-66%), with notably aromatic CH groups again occurring in relative abundance (32-37%). Other favourable interactions include primary and cyclic secondary amines (33%) and aliphatic and acyclic hydroxyl groups (35-39%). This is consistent with the results from Isostar searching, and additionally shows a clear domination of the isoxazole N atom when motifs involving heteroatom-containing contact groups. Hence, the proposal that any intermolecular interactions occurring at the LEF isoxazole will stem from its nitrogen atom is further substantiated.

Noticing that the isoxazole N is the interacting atom in the majority of motifs found for this central group, further investigation into the preferences of structurally similar functional groups was warranted. The isoxazole moiety creates a cyclic, aromatic environment about its nitrogen atom. In **Table B.8**, the frequencies of motifs involving both an aromatic and a cyclic nitrogen are presented. Both forms show highest frequencies with OH groups in general, as almost all of the most commonly occurring motifs involve the various hydroxyl groups. More specifically carboxylic acid OH (50-65%) groups show preference in both cases.

Table B.7 Specific contact search results for the isoxazole motif with various functional groups, showing the number of structures containing the motif and frequency
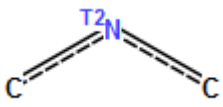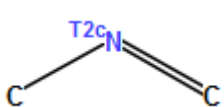
Bold indicates the atoms involved in the motif

	isoxazole			
	isoxazole **N**		isoxazole **O**	
contact group	no. of structures	% frequency	no. of structures	% frequency
OH	44	28.8	4	2.61
al_hydroxy	25	38.5	1	1.54
ar_hydroxy	6	13.6	1	2.27
acy_hydroxy	21	35.6	1	1.69
cy_hydroxy	20	20.8	2	2.08
CO**OH**	6	27.3	0	0
COOH	0	0	1	4.55
T3NH2	21	33.3	4	6.35
T3NH1_cy	24	33.3	3	4.17
T3NH1_acy	39	23.1	3	1.78
T2NH1	0	0	0	0
T2N_any	11	1.34	12	1.47
CO**NH2**	1	20	0	0
CONH2	0	0	0	0
ar_nitrogen	0	0	0	0
cyclic_n	0	0	0	0
acyclic_n	0	0	0	0
methyl	9	1.62	28	5.03
CH	544	66.5	507	62
T3CH	316	42.5	257	34.5
T4CH	310	41.3	294	39.2
T3C	78	10.5	97	13
ar_CH	231	36.7	204	32.4
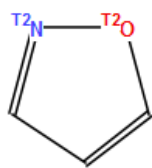
Table B.8 Specific contact search results for ar and cyclic n (representing the isoxazole motif) with various functional groups, showing the number of structures containing the motif and frequency Bold indicates the atoms involved in the motif
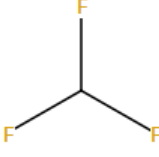
contact group	ar_nitrogen		cyclic_n	
	no. of structures	% frequency	no. of structures	% frequency
OH	5609	51.4	2506	46.4
al_hydroxy	1945	41.1	1544	43.5
ar_hydroxy	1334	45.1	281	21.3
acy_hydroxy	3649	51	1575	42
cy_hydroxy	1732	43	828	29.6
CO**OH**	2252	64.9	563	50
T3NH2	2160	45.8	1522	43.3
T3NH1_cy	1608	21.5	1844	19.3
T3NH1_acy	1409	18.5	682	23.6
T2NH1	5	10.4	9	10.1
T2N_any	696	1.32	361	1.23
CO**NH2**	129	20.4	109	38.9
CONH2	4	0.632	0	0
ar_nitrogen	558	1.06	17	0.511
cyclic_n	17	0.511	275	0.941
acyclic_n	3	0.352	1	0.151
methyl	347	1.75	170	1.22
C**H**	23435	44.7	12373	42.9
T3C**H**	17098	33.2	7617	27.5
T4C**H**	9433	25.6	6445	26.7
T4CH	2064	5.61	1289	5.35
T3C	6988	13.6	2460	8.9
ar_C**H**	16242	31.7	5802	25.7

Results for the trifluoromethyl group were dominated by CH motifs, as expected following from the Isostar search results (**Table B.9**). However, one striking difference is the decrease in frequencies of motifs occurring between CF3 and the heteroatom contact groups. This could be due to the fact that the Isostar contact search only requires the two groups form a contact with a

distance less than the sum of the van der Waals radii, whereas the Mercury motif search is more specific in defining the donating and accepting atoms involved, e.g. OH donating.

Table B.9 Specific contact search results for the trifluoromethyl group with various functional groups, showing the number of structures containing the motif and frequency

Bold indicates the atoms involved in the motif

	trifluoromethyl	
contact group	number of structures	% frequency
OH	465	11.7
al_hydroxy	215	7.59
ar_hydroxy	50	10.15
acy_hydroxy	304	11.8
cy_hydroxy	105	9.21
CO**OH**	116	18.3
COOH	71	11.2
T3NH2	117	12.7
T3NH1_cy	271	9.6
T3NH1_acy	90	3.04
T2NH1	4	7.69
T2N_any	494	5.44
CO**NH2**	18	11.8
CONH2	11	7.19
ar_nitrogen	113	4.93
cyclic_n	43	3.49
acyclic_n	10	2.13
methyl	6750	32.9
CH	33651	87.5
T3CH	23093	69.9
T4CH	24081	72.6
T3C	16072	48.7
ar_CH	21712	71.3

B.2.3   Molecular Complementarity and Selection of Coformers

Based on the most frequently occurring intermolecular interactions, involving central groups representative of those in LEF and a variety of contact groups, a library of favourable functional groups for cocrystal design was formed. These functional groups include primary amine, amide, and hydroxyl groups, with an additional preference for aromaticity when CH groups are considered. Interestingly these functional groups represent the possibility for formation of a number of well-known supramolecular synthons. In addition, the potential for COOH/hydroxyl–aromatic nitrogen heterosynthon formation involving the isoxazole moiety of LEF provides an argument for carboxylic acid functional groups to be considered.

Using knowledge of these preferred functional groups a number of coformers were chosen from a list of those commonly used in cocrystal screening experiments, ensuring a wide range of structures to encompass the varying types of motifs shown to be favourable. These were checked against a library of coformers from the CCDC, provided within the Molecular Complementarity search tool implemented in Mercury. Any coformers that were not already present within this library were added. The molecular complementarity search uses analysis of properties such as coformer shape, size, and polarity, amongst other factors, to generate a list of potential hits for a particular molecule. Results for these predictions (**Table B.10**) in turn allowed for a selection of coformers to be used in the solid form screening of LEF, with as many as possible tested, providing they were available. Consistent with those from the interaction searches, these results predicted a high complementarity of LEF with aromatic O−H, N−H, and heteroatom containing coformers, as well as a number of dicarboxylic acids.

Table B.10 Summary of results of molecular complementarity search

Coformer	Hit Rate/%	Coformer	Hit Rate/%
(+)-camphoric_acid	0	acetic_acid	0
(-)-camphorsulfonic_acid	0	acetophenone_oxime	100
2-amino-5-methylbenzoic_acid	100	acetylenedicarboxylic_acid	100
3-methylpyridine	100	adipic_acid	100
4-acetamidobenzoic_acid	100	alitame	100
4-aminobenzoic_acid	100	apigenin	100
4-hydroxybenzoic_acid	100	azelaic_acid	100
aspirin	100	benzoic_acid	100
2-aminopyiridne	100	biotin	100
2-aminopyrimidine	100	caprolactam	0
isophthalic acid	100	capsaicin	100
2-hydroxybenzoic acid	0	cholic_acid	100
2,4,6-triaminopyridine	N/A	citric_acid	0
3-hydroxybenzoic acid	100	ethylparaben	100
pyridoxine	0	folic_acid	100
4-dimethylaminopyridine	100	fumaric_acid	100
benzamide	100	gentisic_acid	0
catechol	0	glutaric_acid	100
D-alanine	0	glycine	0
D-glucuronic_acid	0	glycolic_acid	0
D-pantothenol	100	hesperetin	100
EDTA	100	hippuric_acid	100
gallic acid	100	hydrocinnamic_acid	0
isoniazid	100	imidazole	0
isonicotinic acid	100	isonicotinamide	100
L-arginine	100	ketoglutaric_acid	100
L-aspartic_acid	0	lactobionic_acid	0
L-aspartic_acid_z	0	lactose	100
L-glutamic_acid	100	maleic_acid	100
L-glutamic_acid_z	0	malic_acid	0
L-glutamine	0	malonic_acid	0
L-glutathione	100	maltitol	0
L-lactic_acid	0	mannitol	0
L-leucine	0	methanesulfonic_acid	0
L-mandelic_acid	100	methylparaben	100

L-methionine	100	monobutyrin	100
L-phenylalanine	100	nicotinamide	100
L-proline	0	oxalic_acid	0
L-serine	0	pamoic_acid	100
L-tartaric_acid	0	phthalamide	0
L-tryptophan	100	pimelic_acid	100
L-tyrosine	100	piperazine	0
N-ethylacetamide	100	propylparaben	100
nicotinic acid	100	pyrazine	0

B.3   Coformers Used in Solid-Form Screening

Based on the results of the molecular complementarity search, a wide range of coformers were screened for LEF cocrystal formation (**Table B.11**).

Table B.11 Coformers used in the solid-form screening of Leflunomide
Bold text indicates successful cocrystal formation

1,2-phenylenediacetic acid	Isonicotinic acid
2,4,6-triaminopyrimidine	Isoniazid
2,5-dihydroxybenzoic acid	Isophthalic acid
2-amino-4-chlorobenzoic acid	Kojic acid
2-aminopyridine	L-arabinose
2-aminopyrimidine	L-arginine
2-chloro-4-nitrobenzoic acid	L-glutamic acid
2-picolinamide	L-mandelic acid
2-picolinic acid	L-phenylalanine
2-piperidone	L-proline
3,5-dihydroxybenzoic acid	L-tryptophan
3,5-dinitrobenzoic acid	L-tyrosine
3-aminobenzoic acid	Malonic acid
3-hydroxybenzoic acid	Melamine
4-aminobenzamide	Methyl gallate
4-aminobenzoic acid	Methylparaben
4-hydroxy-3-methoxybenzoic acid	myo-inositol
4-dimethylaminopyridine	N-cyclohexylsulfamic acid
4-hydroxybenzamide	Nicotinamide
4-hydroxybenzoic acid	Orotic acid

5-methyl-2-pyridone	Oxalic acid
5-methylresorcinol	Pamoic acid
Adipic acid	Paracetamol
Aspirin	p-coumaric acid
Benzamide	Phloroglucinol
Benzoic acid	Phthalic acid
Betaine monohydrate	Piperazine
Caffeine	Propylparaben
Catechol	Pyridine-2-carboxamide
D-mannitol	Pyridoxine
D-tartaric acid	**Pyrogallol**
Ethylmalonic acid	Resorcinol
Ethylparaben	Salicylamide
Gallic acid	Salicylic acid
Glutaric acid	Syringic acid
Glutathione	Valpromide
Hydroxyurea	Vanillic acid
Isonicotinamide	Vanillin

B.4 Successful Solid-Form Screening

B.4.1 Coformer Structure

XRPD analysis of the products of solid-form screening allowed identification of coformers that show potential cocrystal formation with LEF. Three of the chosen coformers, 2-picolinic acid (2PIC), 2-aminopyrimidine (2APYM) and 3-hydroxybenzoic acid (3HBA) were identified as hits from the molecular complementarity search, with pyrogallol (PG) falling into the fail list. The chemical structures of these coformers are shown in **Figure B.4**.

B.4.2 XRPD Patterns

The XRPD patterns of the solvent drop grinding products that showed cocrystal formation were plotted and compared to that of their individual coformers, and the simulated pattern of the cocrystal obtained from the crystal structure.
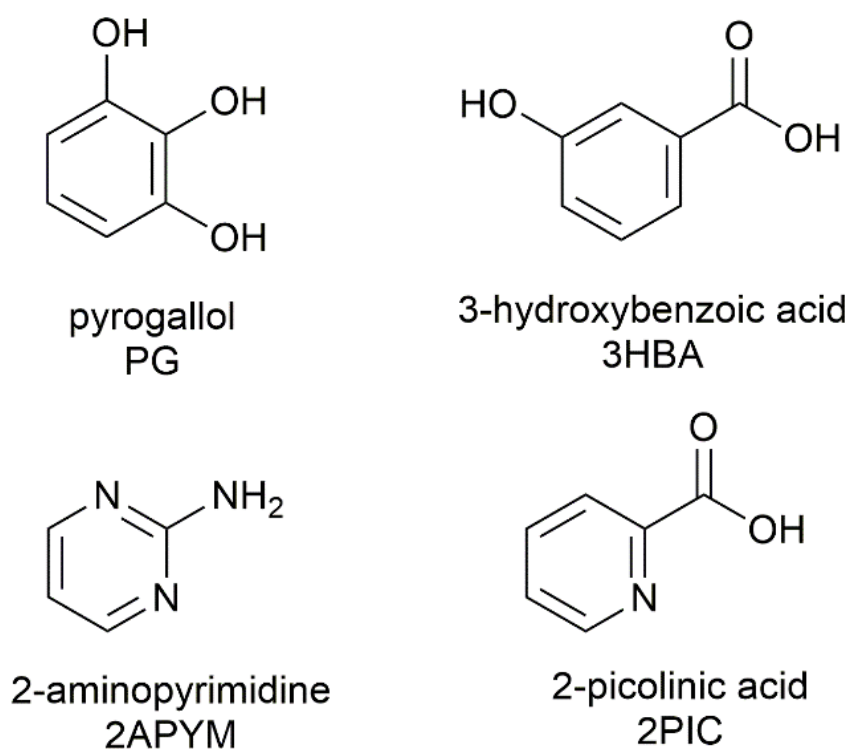
Figure B.4 Chemical diagram of the coformers that solid-form screening by grinding indicated successful cocrystal formation
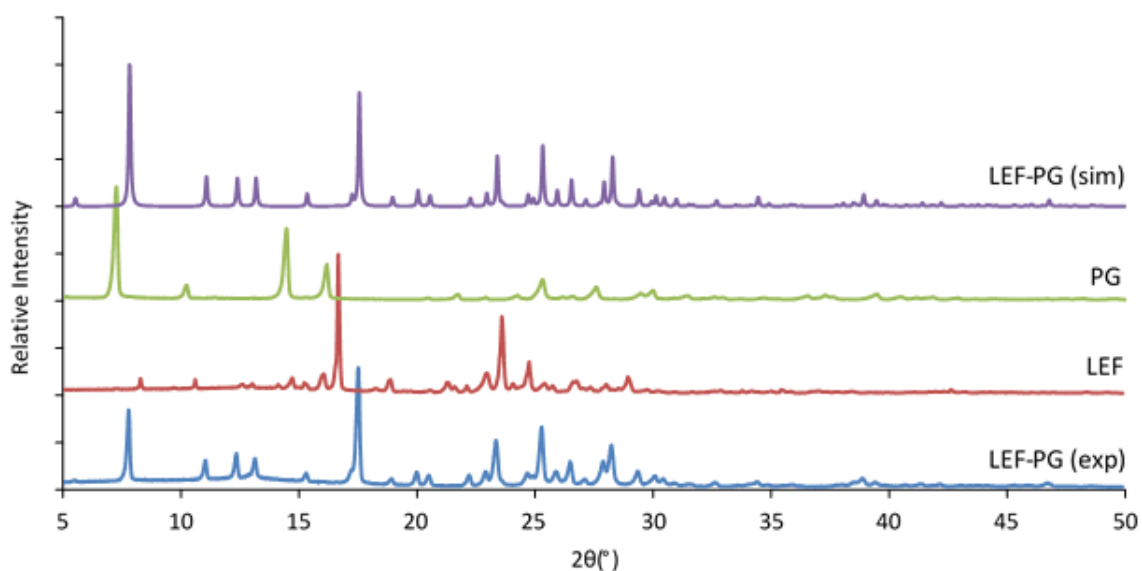
Figure B.5 XRPD pattern of the LEF-PG solvent drop grinding product with reference to the patterns of LEF and PG and the calculated pattern obtained from the LEF-PG cocrystal
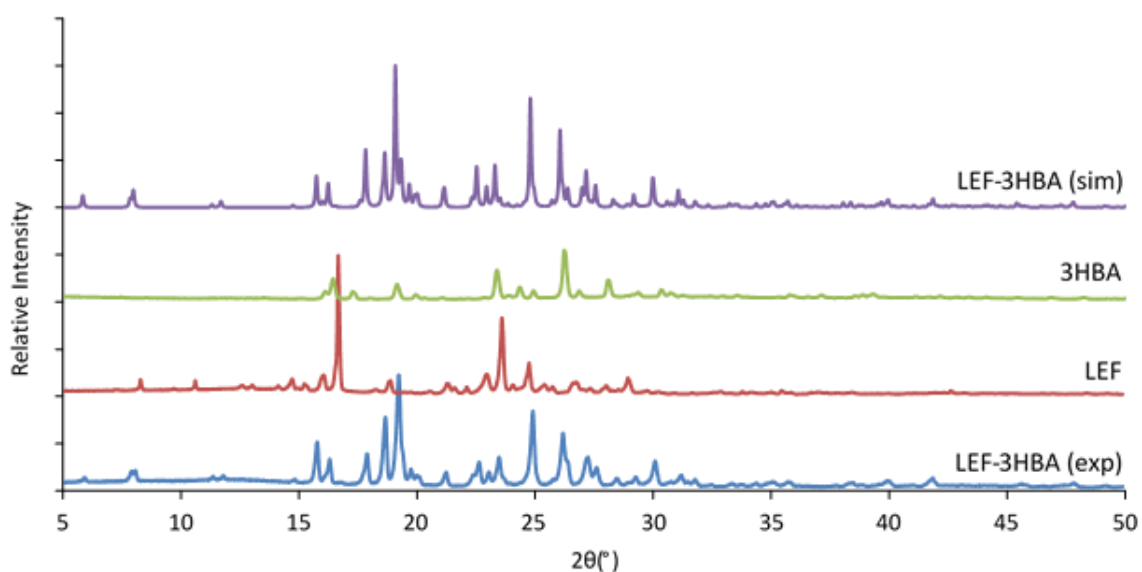
Figure B.6 XRPD pattern of the LEF-3HBA solvent drop grinding product with reference to the patterns of LEF and 3HBA and the calculated pattern obtained from the LEF-3HBA cocrystal
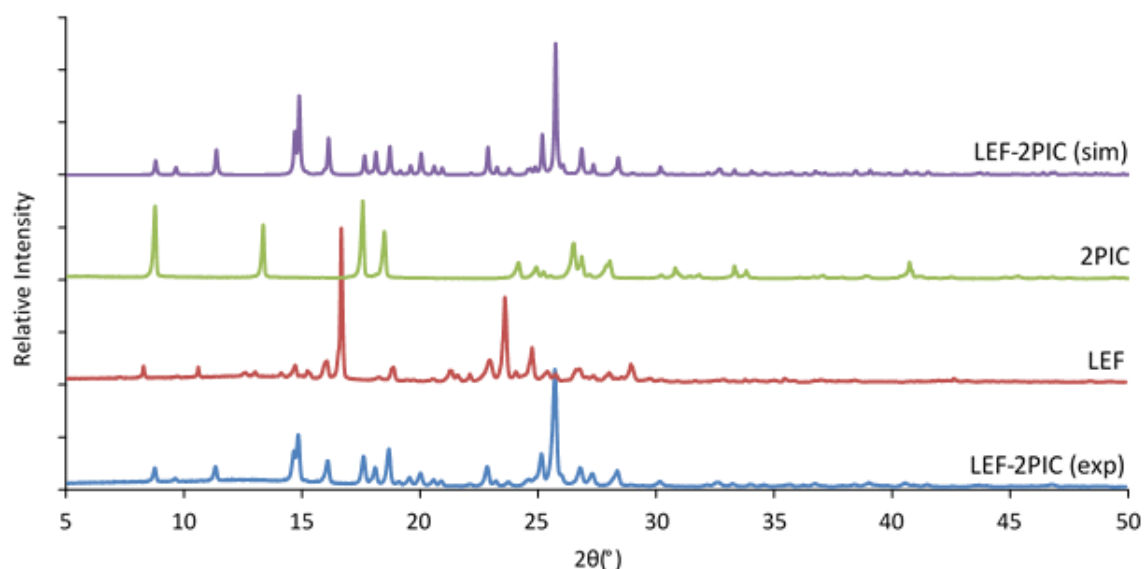
Figure B.7 XRPD pattern of the LEF-2PIC solvent drop grinding product with reference to the patterns of LEF and 2PIC and the calculated pattern obtained from the LEF-2PIC cocrystal
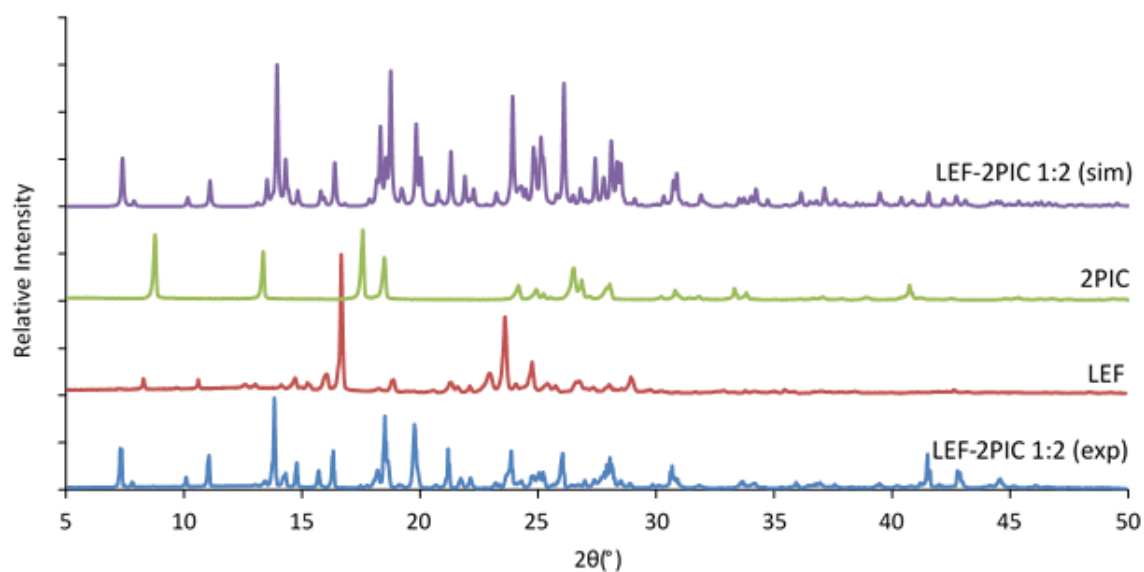
Figure B.8 XRPD pattern of the LEF-2PIC 1:2 solvent drop grinding product with reference to the patterns of LEF and 2PIC and the calculated pattern obtained from the LEF-2PIC 1:2 cocrystal
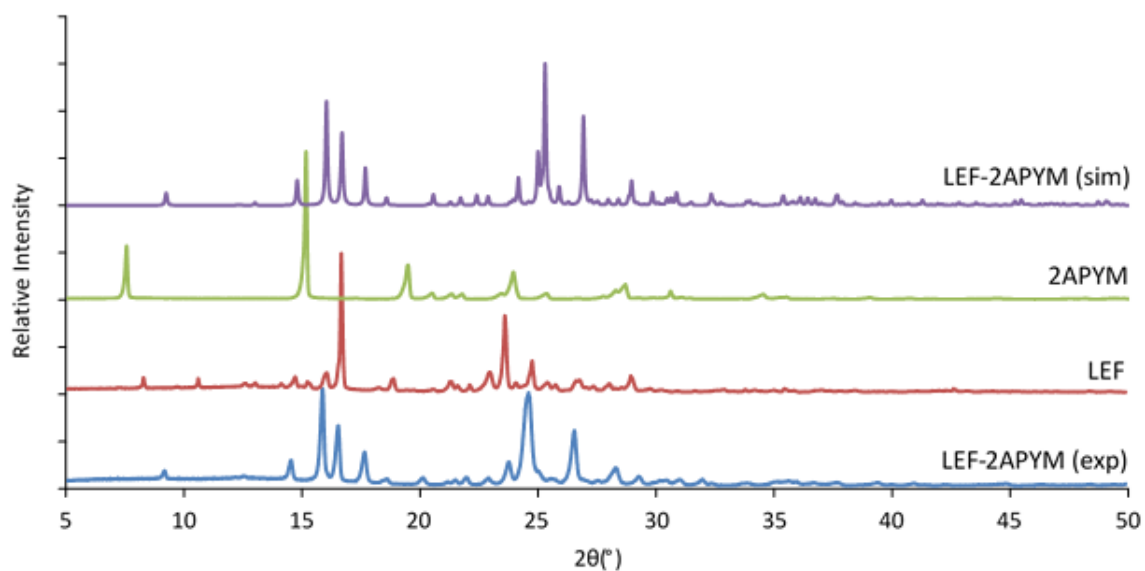
Figure B.9 XRPD pattern of the LEF-2APYM solvent drop grinding product with reference to the patterns of LEF and 2APYM and the calculated pattern obtained from the LEF-2APYM cocrystal

B.5   Crystal Structure Parameters

Table B 12 Crystal structure data and experimental parameters for the standard resolution data collection of LEF cocrystals

Compound reference	LEF-PG	LEF-3HBA	LEF-2PIC	LEF-2PIC 1:2
Crystal data				
Chemical formula	$C_6H_6O_3 \cdot C_{12}H_9F_3N_2O_2$	$C_{12}H_9F_3N_2O_2 \cdot C_7H_6O_3$	$C_6H_5NO_2 \cdot C_{12}H_9F_3N_2O_2$	$2(C_6H_5NO_2) \cdot C_{12}H_9F_3N_2O_2$
Mr	396.32	408.33	393.32	516.43
Crystal system	Tetragonal	Monoclinic	Monoclinic	Monoclinic
Space group	I−4	$P2_1/n$	$P2_1/c$	$P2_1/c$
a/Å	22.5725(4)	12.0099(2)	10.5890(3)	23.9960(4)
b/Å	22.5725(4)	5.0426(1)	14.3057(3)	12.6923(2)
c/Å	7.0280(2)	30.2491(4)	12.5434(3)	7.6691(1)
α/°	90	90	90	90
β/°	90	91.391(1)	108.513(3)	95.341(1)
γ/°	90	90	90	90
Cell volume/Å^3	3580.89(16)	1831.38(5)	1801.78(8)	2325.59(6)
Z	8	4	4	4

Data Collection

	Agilent Technologies Dual Source Supernova	Agilent Technologies Dual Source Supernova	Agilent Technologies Dual Source Supernova	Agilent Technologies Dual Source Supernova
Diffractometer				
Temperature/K	297	297	297	297
Radiation type	Mo Kα	Cu Kα	Mo Kα	Cu Kα
Wavelength, λ /Å	0.71073	1.54184	0.71073	1.54184
No. of reflections measured	5423	9794	25280	13048
No. of independent reflections	3075	3591	3181	4749
R_{int}	0.014	0.021	0.016	0.02
Completeness	96.31	99.94	99.84	99.98

Refinement

GoF, S	1.062	1.041	1.068	1.177
Final R_1 [I> 2σ(I)]	0.0831	0.049	0.039	0.066
$wR(F^2)$ [I> 2σ(I)]	0.22	0.144	0.112	0.196

B.6   Hydrogen Bond Tables

Table B13 Hydrogen bond tables for the LEF cocrystals

Sample	D–H⋯A[a]	H⋯A/Å	D⋯A/Å	D–H⋯A/°	Symmetry code
	N(2)–H(2)⋯O(4)	2.14	2.980(5)	146	3/2-x,1/2-y,1/2+z
	O(3)–H(3)⋯O(4)	2.32	2.643(6)	104	
	O(4)–H(4)⋯O(2)	2.03	2.749(6)	146	x,y,1+z
	O(4)–H(4)⋯O(5)	2.31	2.759(5)	115	
	O(5)–H(5)⋯O(3)	2.27	2.852(5)	129	x,y,1+z
	C(1)–H(1)⋯O(3)	2.57	3.388(6)	147	3/2-x,1/2-y,1/2+z
	C(4) –H(4B)⋯O(2)	2.49	3.064(8)	118	
	C(7)–H(7)⋯O(2)	2.31	2.902(6)	121	
	C(10)–H(10)⋯F(3A)	2.39	2.722(16)	101	
LEF-PG	C(11)–H(11)⋯O(4)	2.58	3.194(7)	124	3/2-x,1/2-y,1/2+z
	N(2)–H(2)⋯O(2)	2.18	2.9755(18)	157	x,1+y,z
	O(3)–H(3)⋯O(4)	1.80	2.735(2)	169	3/2-x,1/2+y,3/2-z
	O(5)–H(5)⋯N(1)	1.87	2.784(2)	174	
LEF-3HBA	C(7)–H(7)⋯O(2)	2.43	2.922(2)	113	
	N(2)–H(2)⋯O(3)	2.02	2.8927(18)	160	x,y,1+z
	N(3)–H(3)⋯O(4)	2.336	2.6824(19)	102	
	N(3)–H(3)⋯O(4)	1.84	2.666(2)	151	1-x,1-y,2-z
	C(1)–H(1)⋯O(3)	2.47	3.205(2)	131	x,y,1+z
	C(10)–H(10)⋯F(3)	2.37	2.708(11)	100	
	C(10)–H(10)⋯F(3A)	2.40	2.75(2)	101	
	C(11)–H(11)⋯O(2)	2.23	2.840(2)	120	
LEF-2PIC	C(17)–H(17)⋯O(2)	2.40	3.111(2)	132	x,y,1+z
	N(2)–H(2)⋯O(3)	1.94	2.8477(1)	169	x,1+y,z
	N(3)–H(3)⋯O(5)	1.78	2.6492(1)	159	x,1/2-y,-1/2+z
	N(4)–H(4)⋯O(4)	1.85	2.7028(1)	158	
	N(4)–H(4)⋯O(5)	2.27	2.6305(1)	103	
	C(1) –H(1)⋯O(3)	2.39	3.2453(1)	152	x,1+y,z
	C(7)–H(7)⋯O(2)	2.27	2.8509(1)	120	
	C(8)–H(8)⋯F(2A)	2.37	2.6986(1)	101	
	C(11)–H(11)⋯O(3)	2.38	3.1435(1)	140	x,1+y,z
	C(16)–H(16)⋯O(2)	2.57	3.1360(1)	120	
	C(17)–H(17)⋯O(2)	2.48	3.0991(1)	124	
LEF-2PIC 1:2	C(23)–H(23)⋯O(6)	2.24	3.0126(1)	139	x,y,-1+z

[a]D = Donor, A = Acceptor

B.7 Thermal Properties
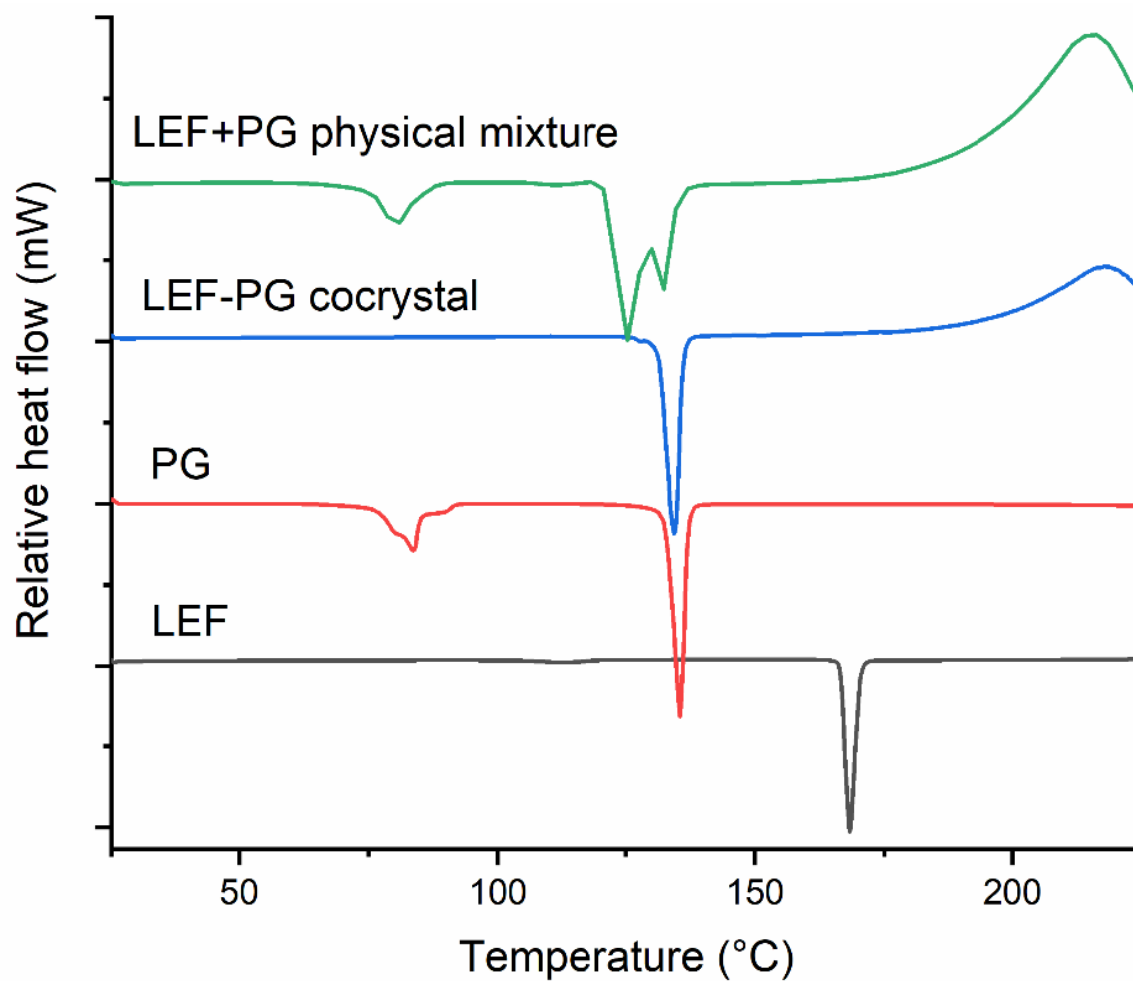
Figure B.10 Comparison of DSC plots of LEF and PG with the corresponding cocrystal (LEF-PG) and physical mixture

An endotherm at 80 °C in the thermogram of PG is due to water loss from the crystal lattice
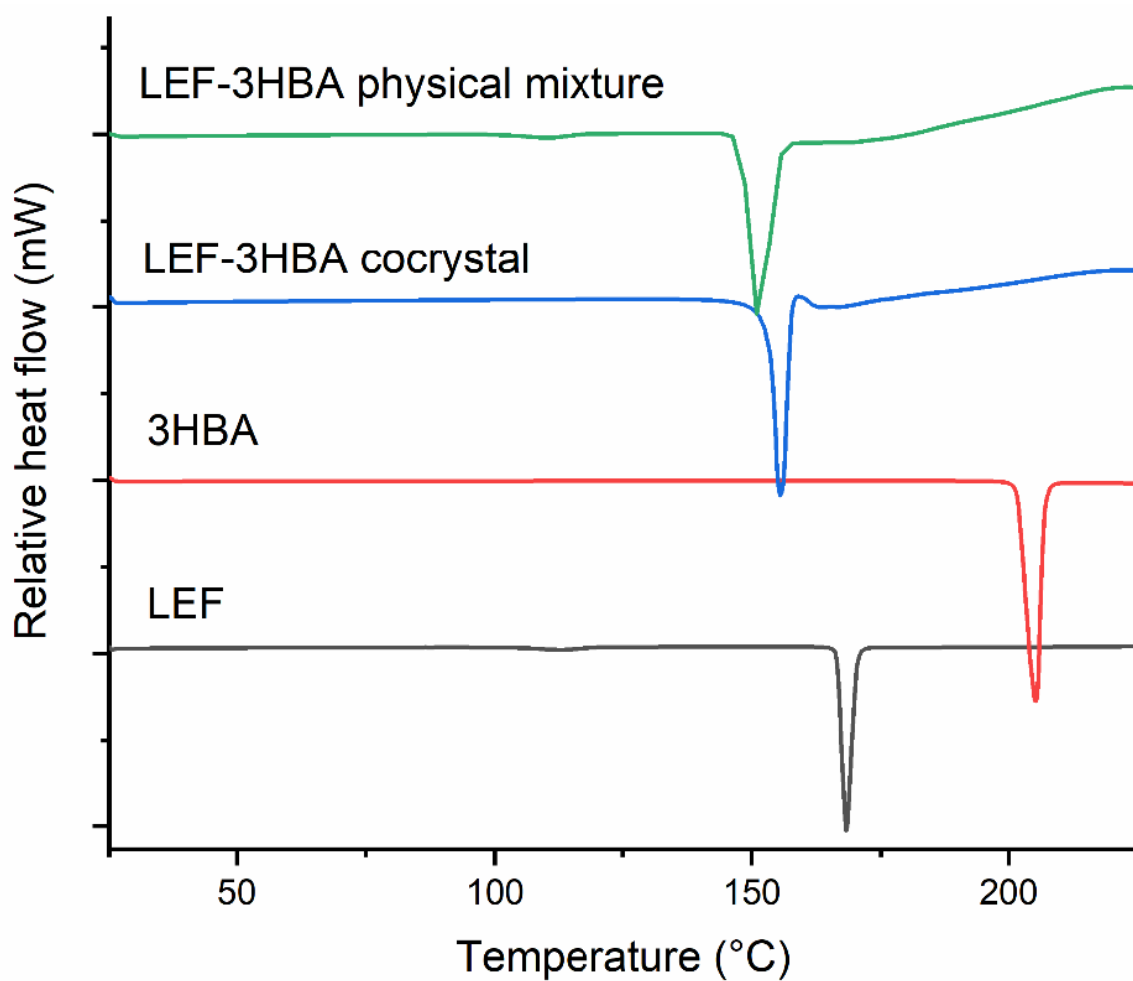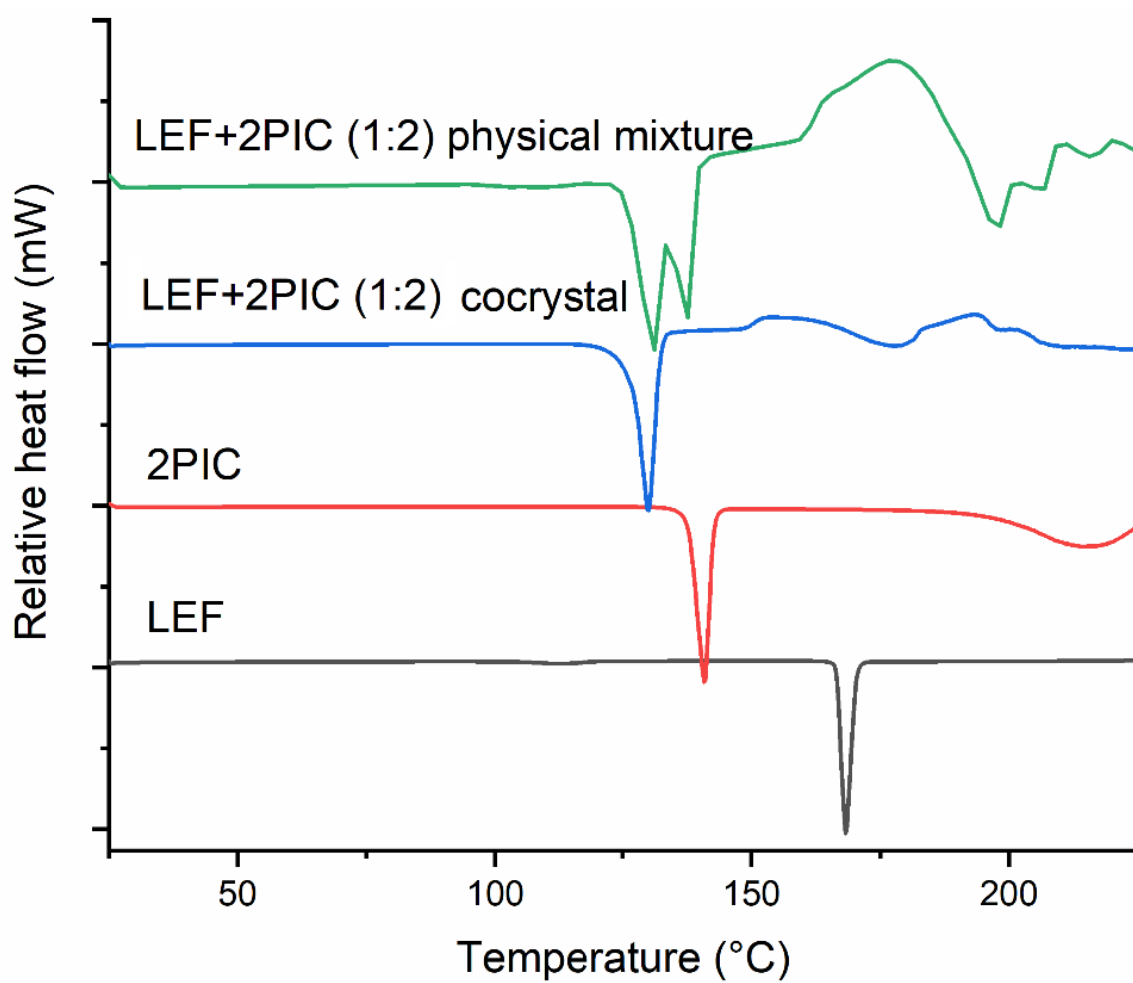
Figure B.11 Comparison of DSC plots of LEF and 3HBA with the corresponding cocrystal (LEF-3HBA) and physical mixture

The thermogram of the physical mixture shows an endothermic transition at 110 °C for the phase transformation of LEF Form I to II and a single melting endotherm at 148 °C, which could be due to the formation of a eutectic composition
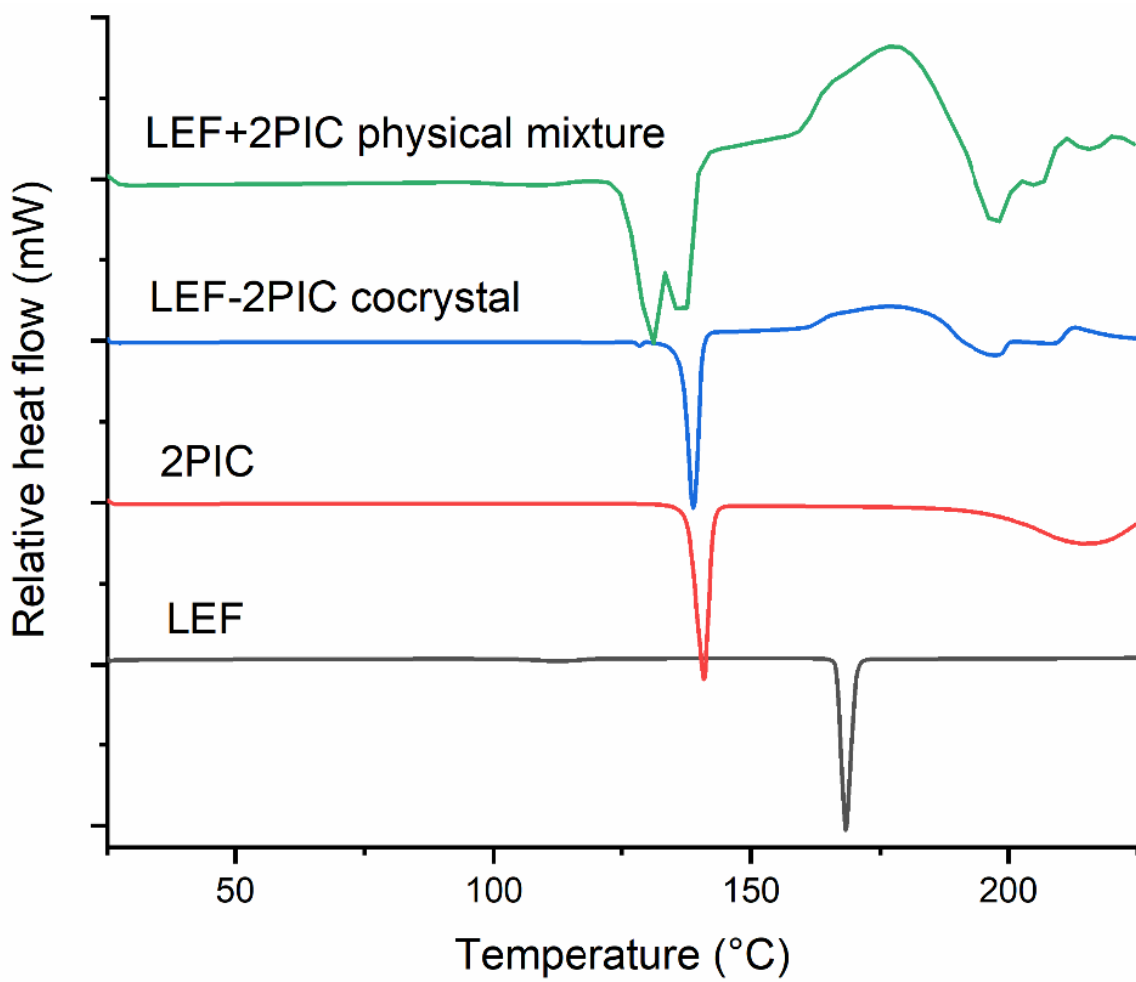
Figure B.12 Comparison of DSC plots of LEF and 2PIC with the corresponding cocrystal (LEF-2PIC) and physical mixture

Figure B.13 Comparison of DSC plots of LEF and 2PIC with the corresponding cocrystal (LEF-2PIC (1:2)) and physical mixture
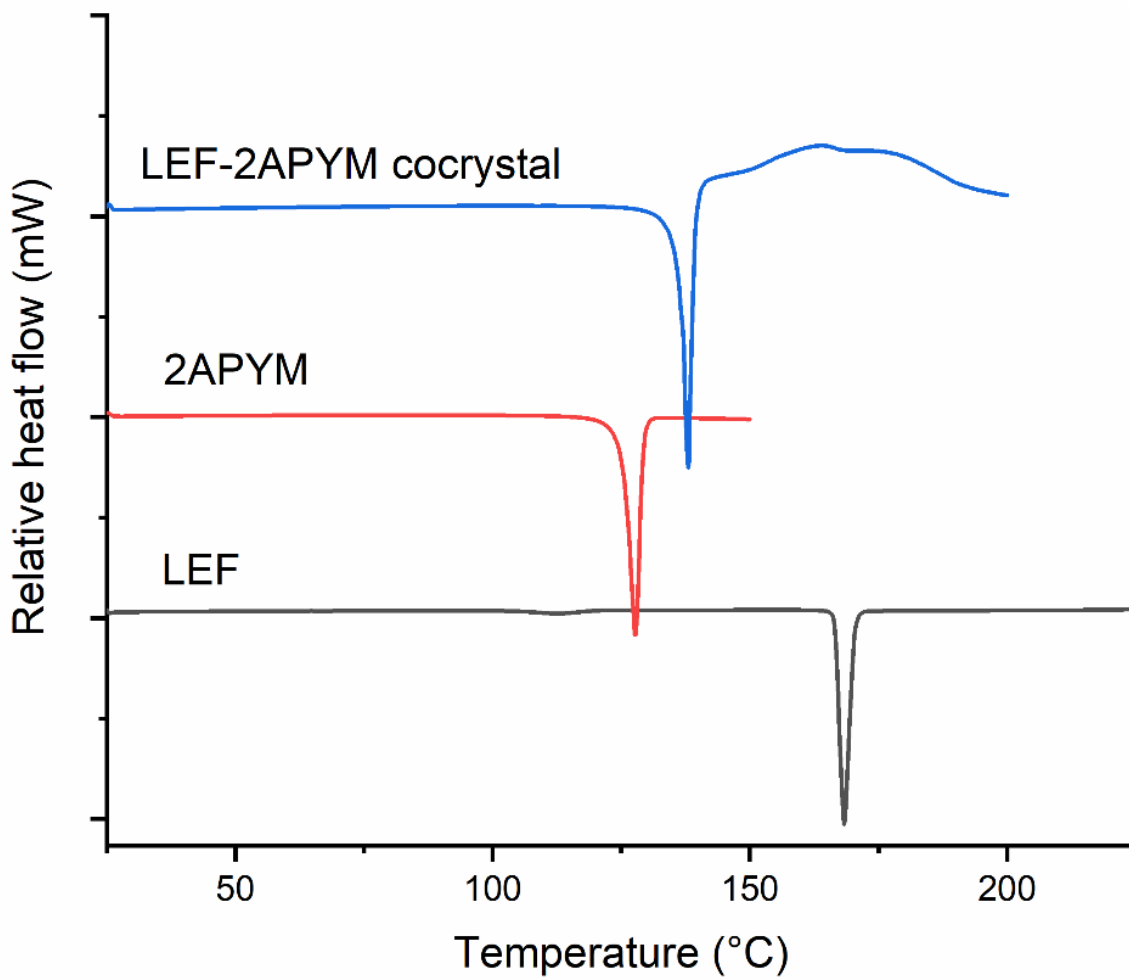
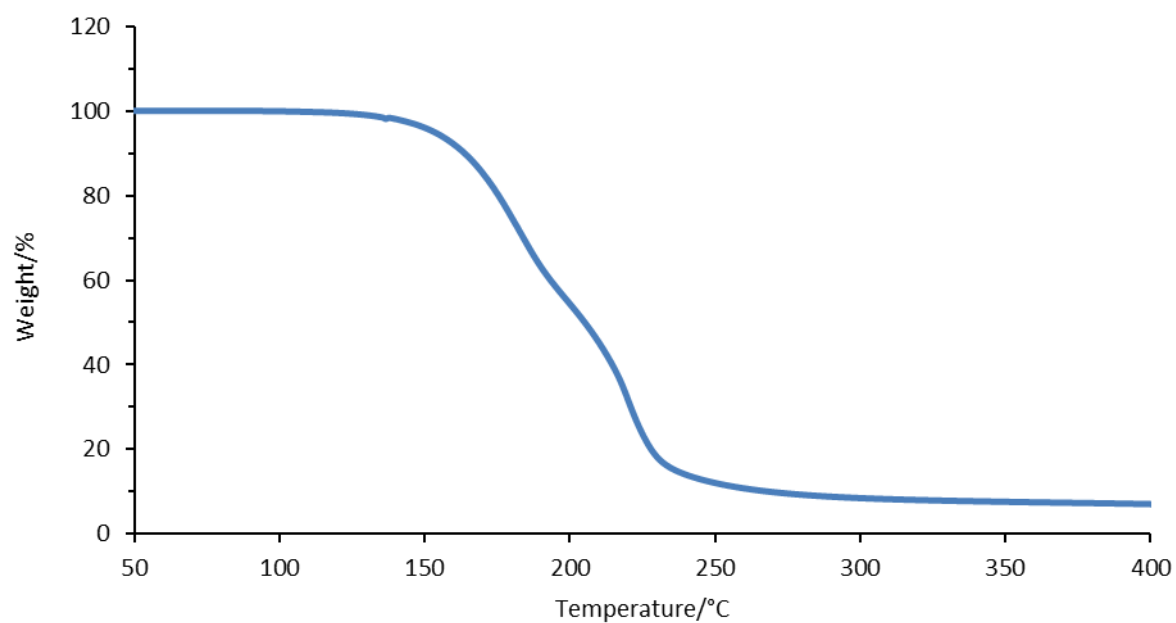**Figure B.14** Comparison of DSC plots of LEF and 2APYM with the corresponding cocrystal (LEF-2APYM)
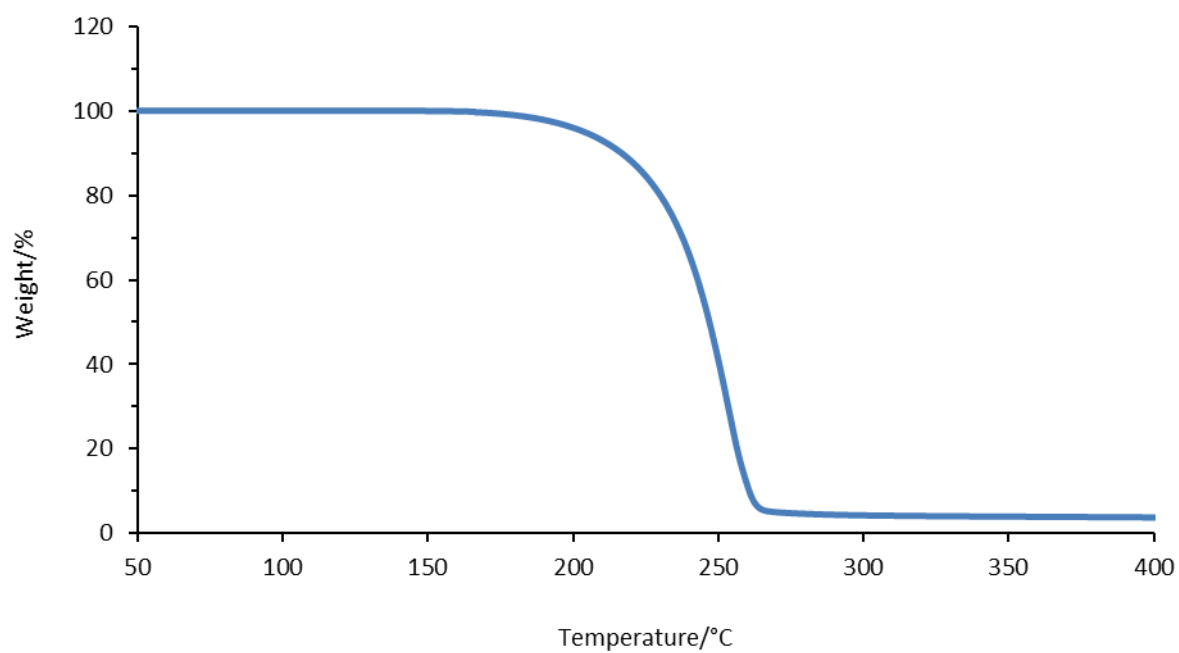
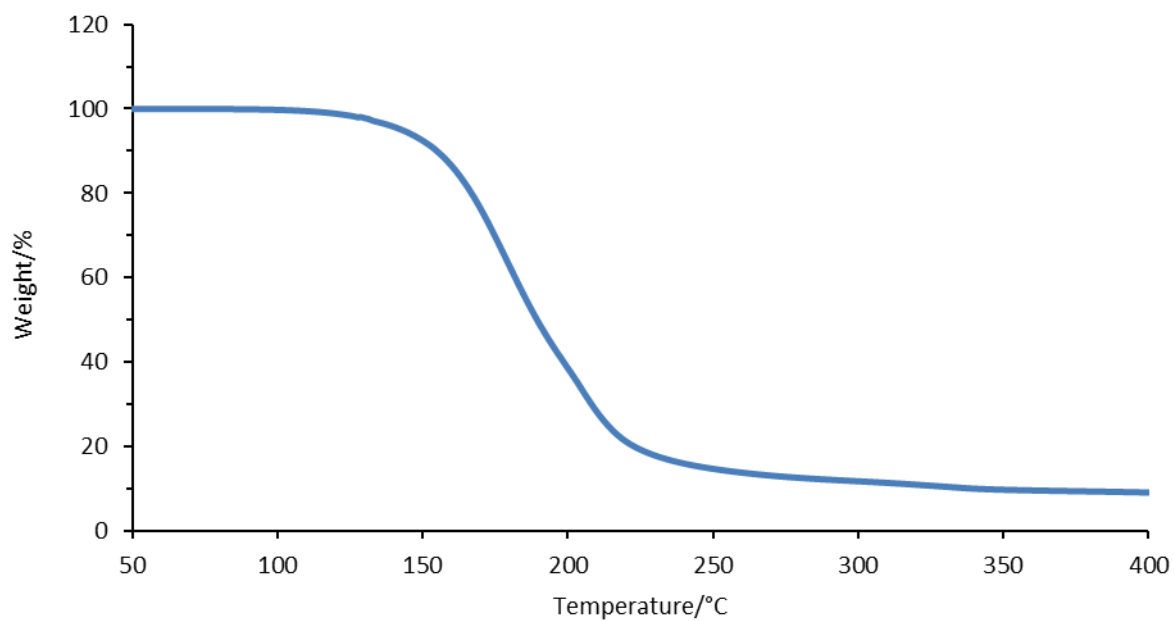**Figure B.15** TGA plot for LEF over the range 50-400°C
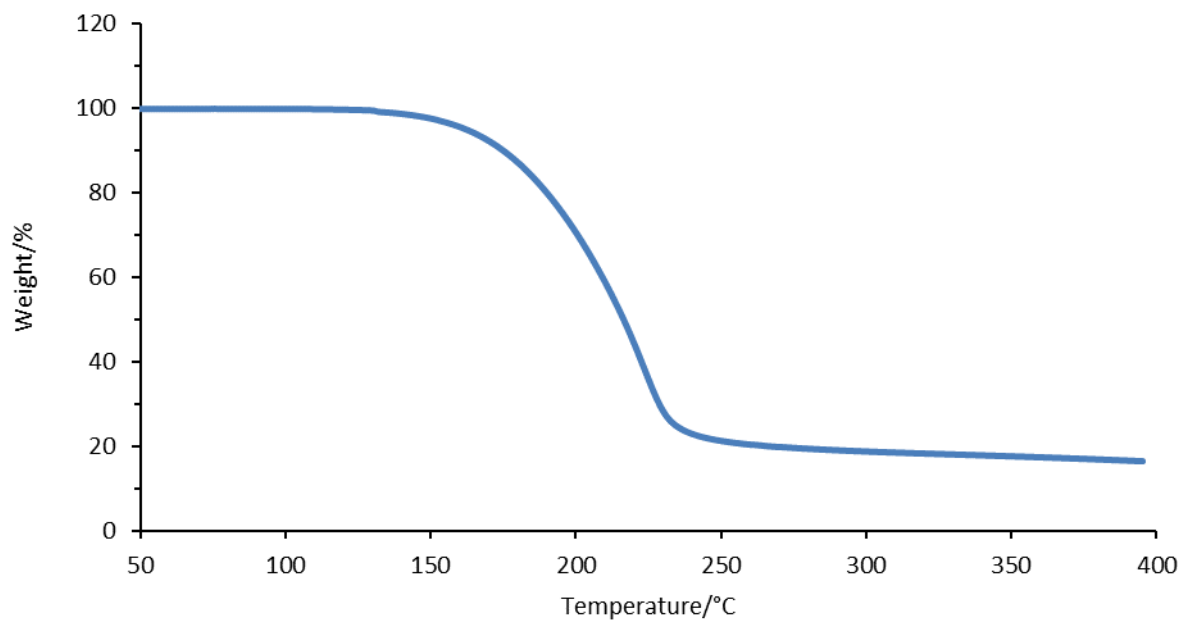
Figure B.16 TGA plot for LEF-PG over the range 50-400°C
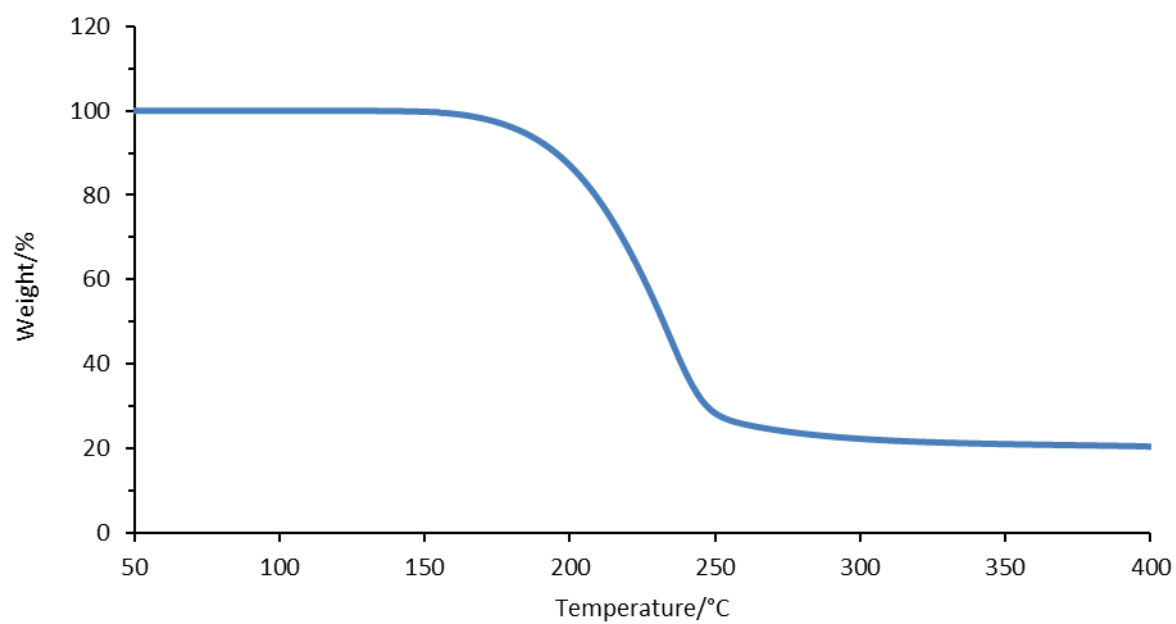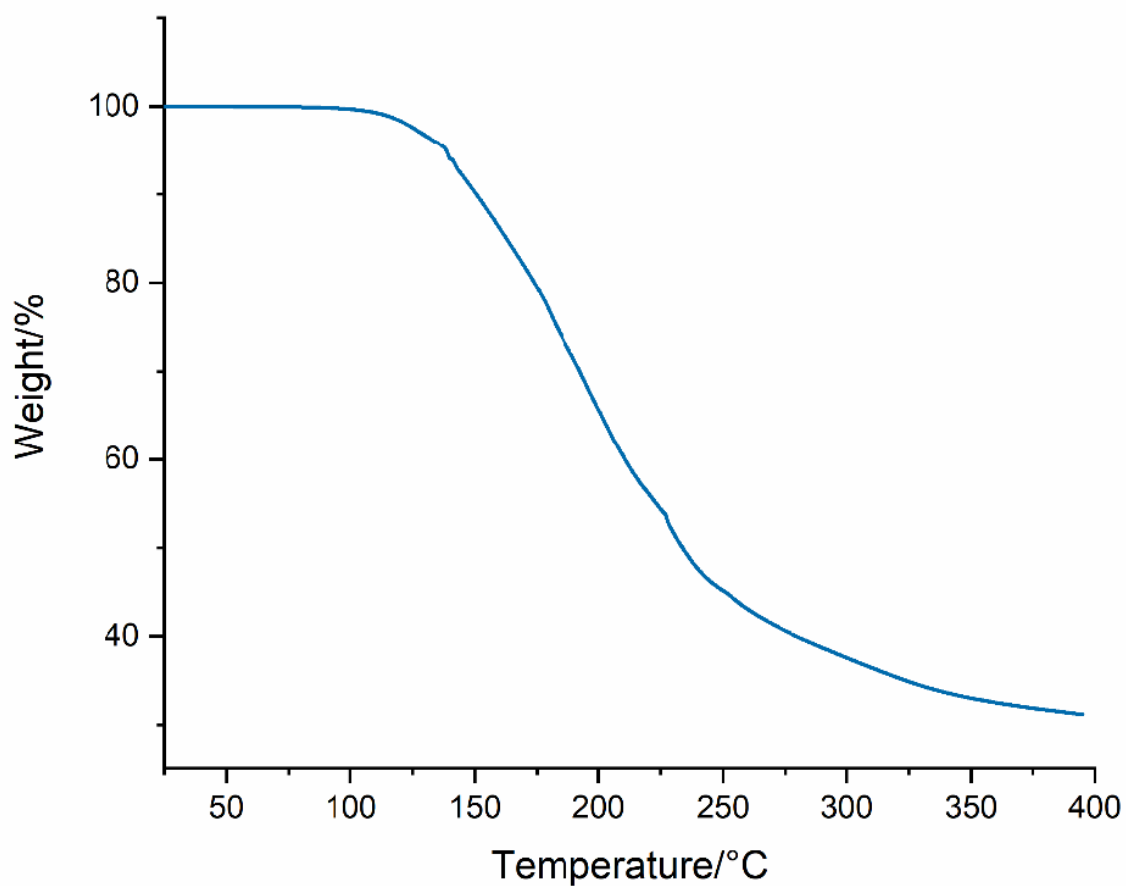
Figure B.17 TGA plot for LEF-3HBA over the range 50-400°C

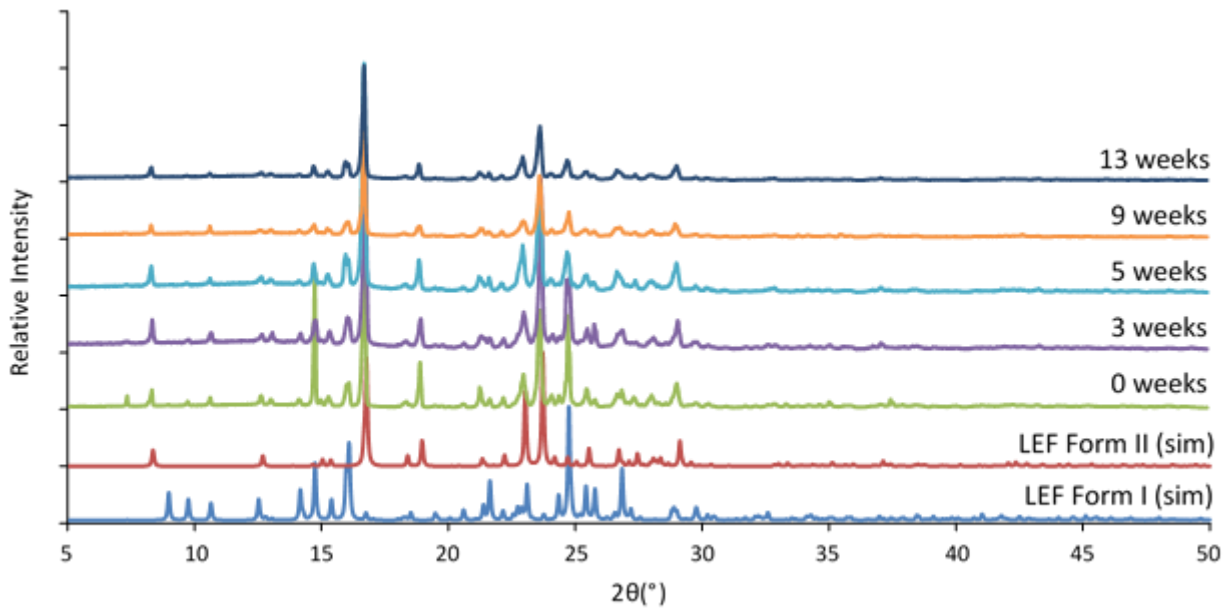**Figure B.18** TGA plot for LEF-2PIC over the range 50-400°C

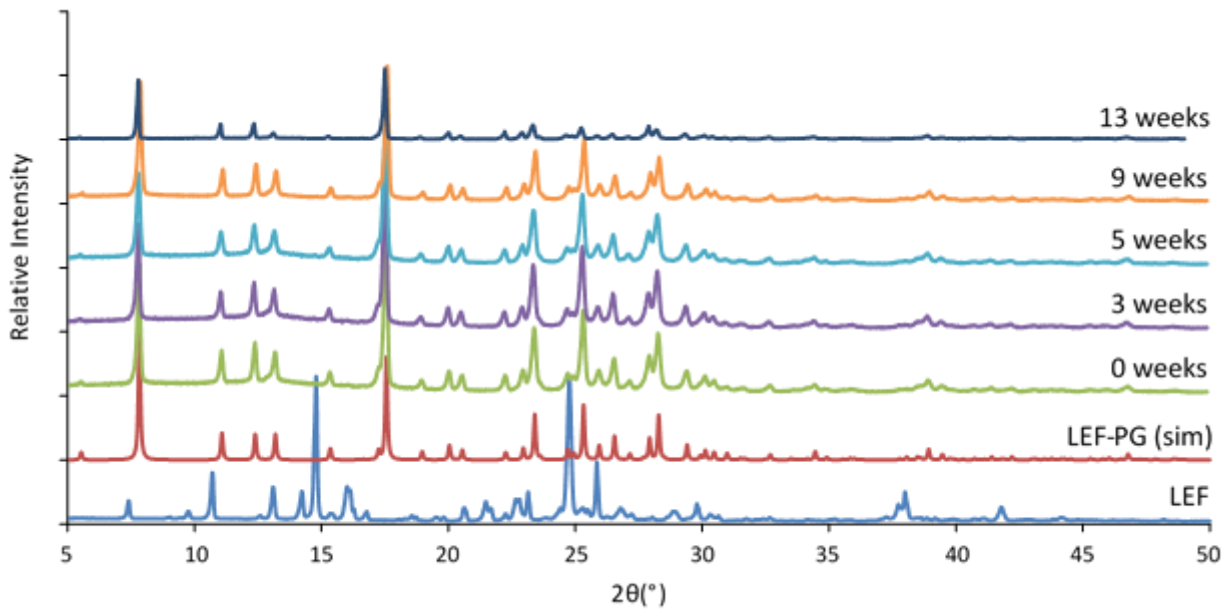**Figure B.19** TGA plot for LEF-2PIC 1:2 over the range 50-400°C

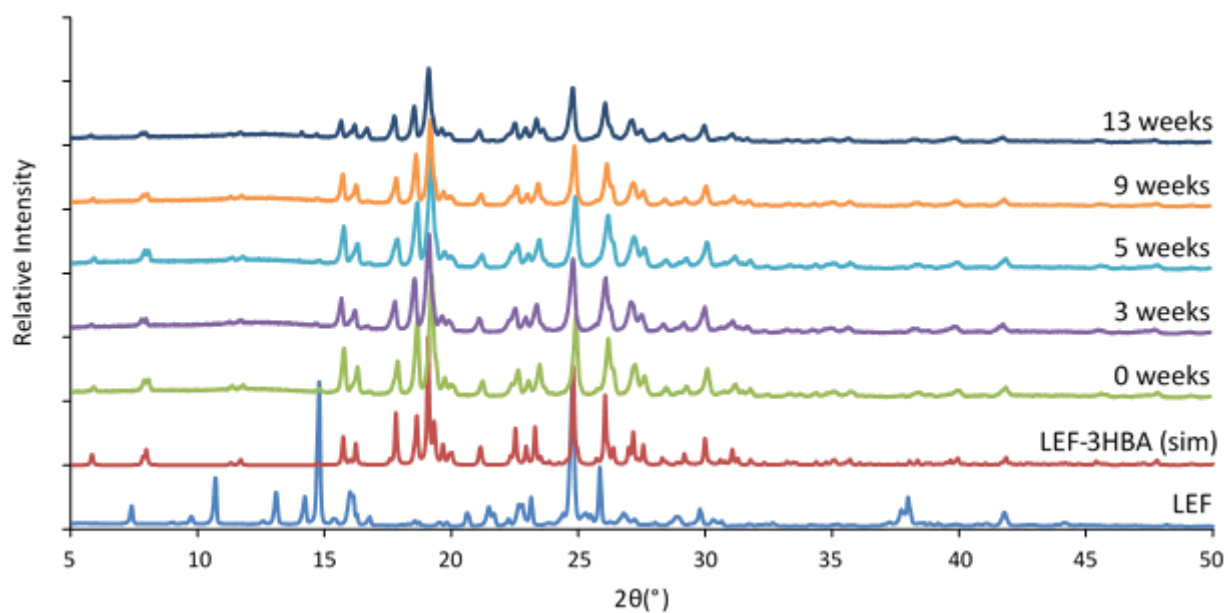**Figure B.20** TGA plot for LEF-2APYM over the range 25-400°C
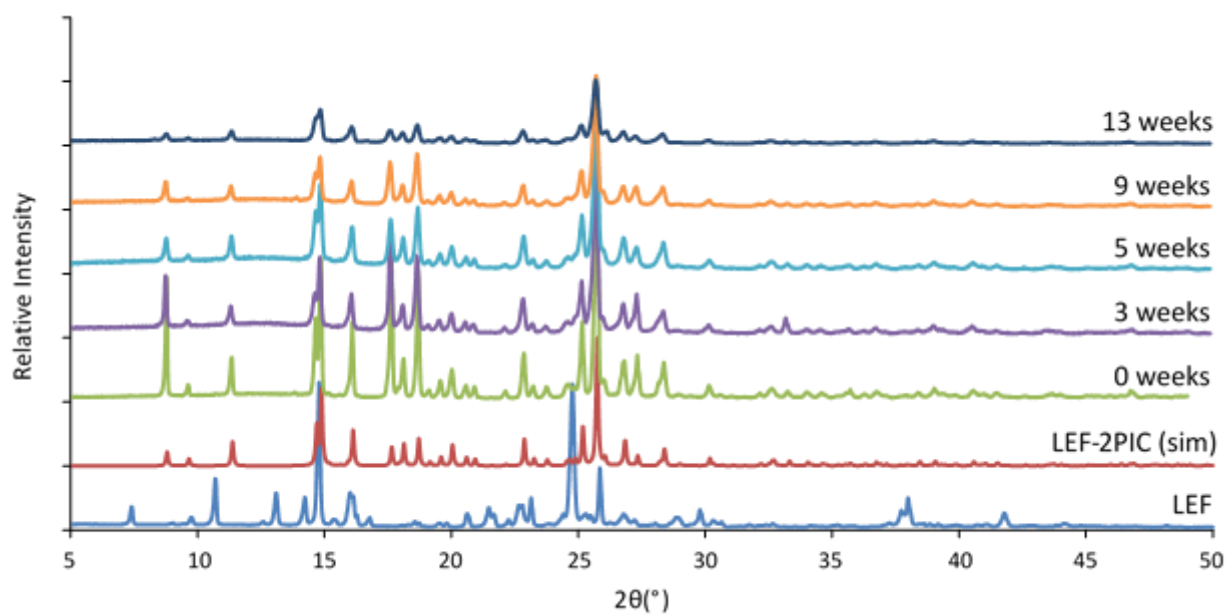
B.8   Stability

Figure B.21 XRPD patterns of LEF obtained under accelerated storage conditions, with reference to the simulated patterns of LEF Form I and Form II

Figure B.22 XRPD patterns of LEF-PG obtained under accelerated storage conditions, with reference to LEF and the simulated pattern of LEF-PG

Figure B.23 XRPD patterns of LEF-3HBA obtained under accelerated storage conditions, with reference to LEF and the simulated pattern of LEF-3HBA
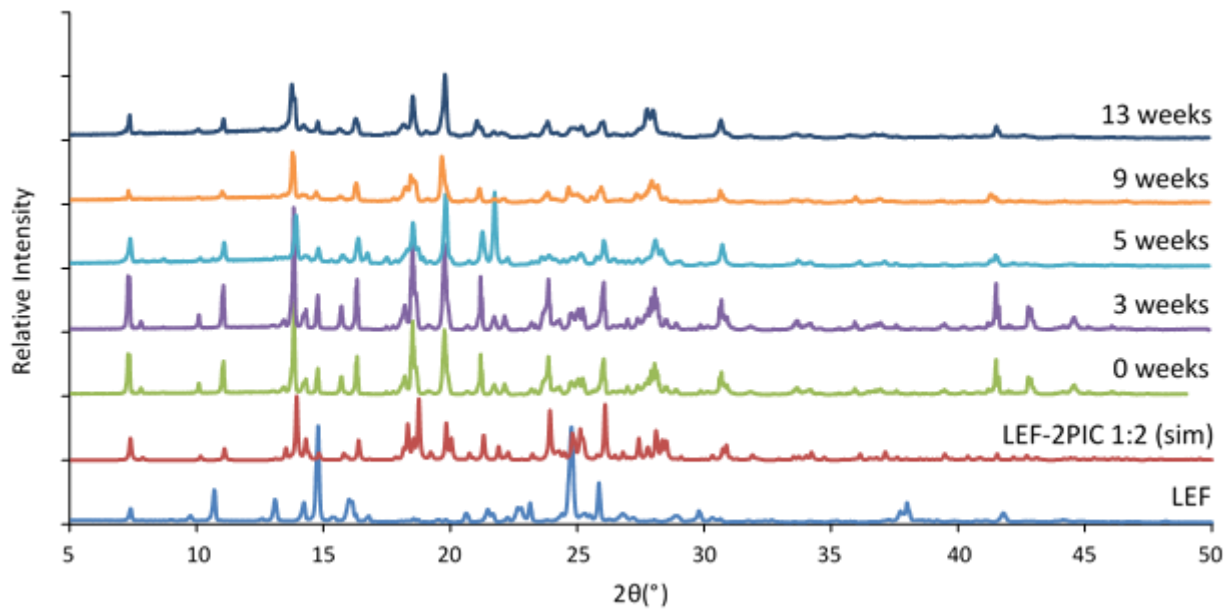

Figure B.24 XRPD patterns of LEF-2PIC obtained under accelerated storage conditions, with reference to LEF and the simulated pattern of LEF-2PIC
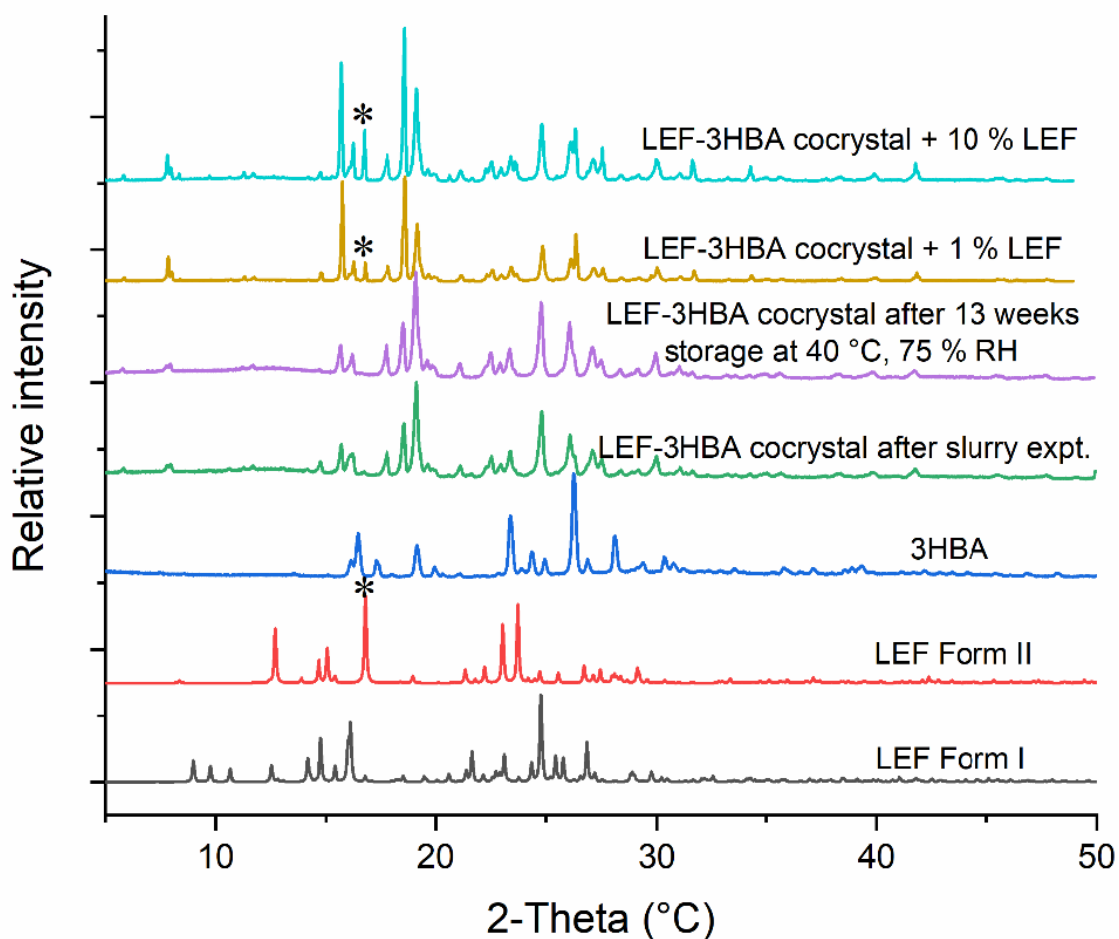
Figure B.25 XRPD patterns of LEF-2PIC 1:2 obtained under accelerated storage conditions, with reference to LEF and the simulated pattern of LEF-2PIC 1:2

Figure B.26 Comparison of XRPD pattern of LEF-3HBA after slurry and storage (at 40 °C/75 % RH) stability experiment with cocrystal powder samples that contain varying amounts of the bulk LEF

The peak at 2θ =16.77° (indicated with a '*') is characteristic of LEF

The absence of LEF characteristic peaks in the powder obtained from stability experiments suggests that the cocrystal is stable in these conditions

B.9 Intrinsic Dissolution Rate
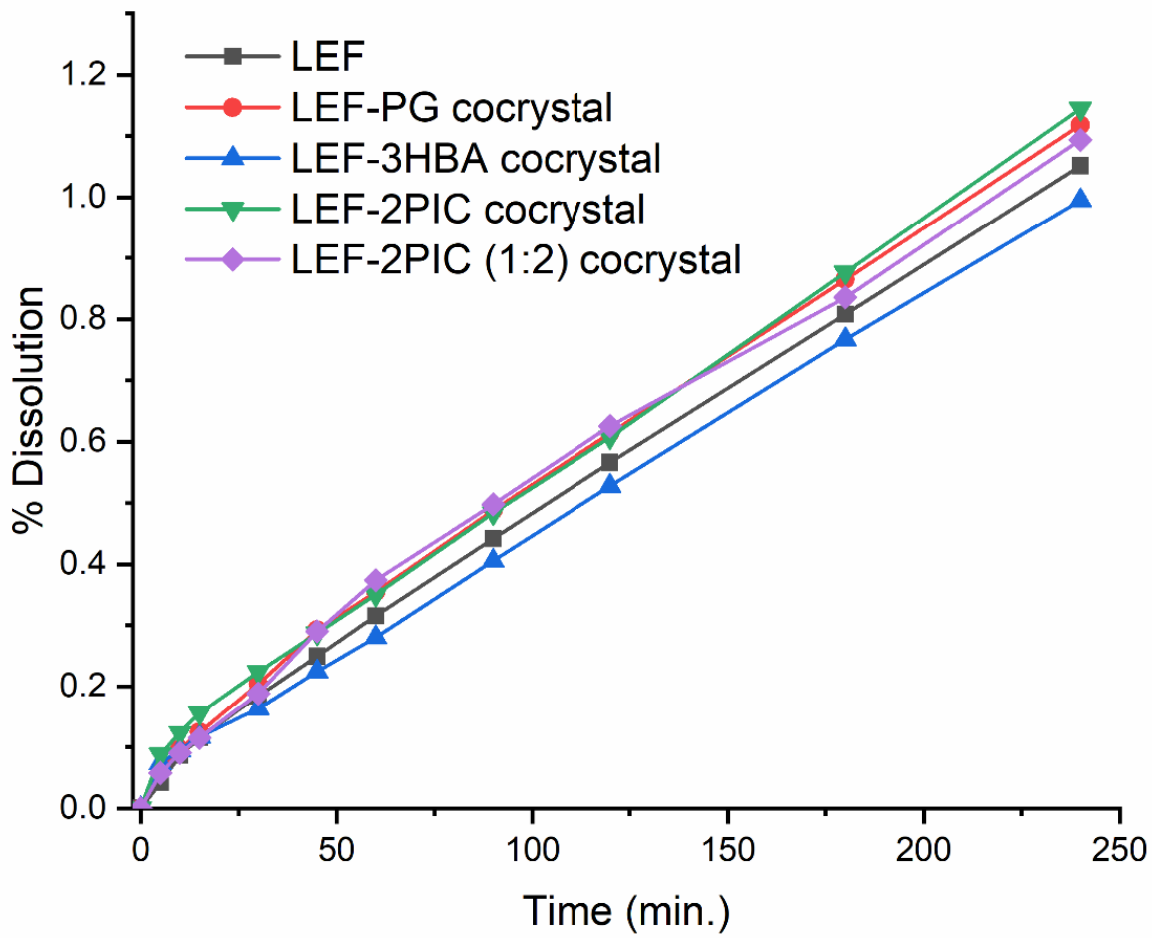
Figure B.27 Comparison of the IDR profile of LEF and cocrystals

Appendix C LEF Formulation Experimental

C.1   Simulation Models and Methods

Figure C.1 represents the planar view of the crystal structure of the LEF and the cocrystals, along with the molecular structure of lactose and the phosphate ion (HPO_4^{2-}). A 3D simulation model containing a LEF-2PIC cocrystal and four molecules of lactose in water is also shown in Figure B.1. The Optimized Potentials for Liquid Simulations all-atom (OPLS-AA) force field is used to describe the LEF, 3HBA, 2PIC, lactose and calcium ion.[97] The parameter files were generated using the MKTOP[98] tool and charges on the atoms were adopted from OPLS-AA force field. The bonded and non-bonded parameters for the HPO_4^{2-} ion were taken from OPLS-AA except the charges, which were adopted from the literature. The water was modelled by the simple point charge (SPC).[99] The Lennard-Jones (LJ) and Coulombic potentials were used to describe the non-bonded interactions as

$$U_{\text{non-bonded}} = \sum 4\varepsilon_{ij} \left[\left(\frac{\sigma_{ij}}{r_{ij}} \right)^{12} - \left(\frac{\sigma_{ij}}{r_{ij}} \right)^{6} \right] + \sum \frac{q_i q_j}{4\pi\varepsilon_0 r_{ij}} \tag{1}$$

where r_{ij} is the distance between atoms i and j, q_i is the atomic charge of atom i, ε_{ij} and σ_{ij} are the well depth and collision diameter, and ε_0 (8.8542×10^{-12} $C^2N^{-1}m^{-2}$) is the permittivity of vacuum. The stretching, bending and torsional potentials were used to represent the bonded interactions as

$$U_{\text{stretching}} = \sum \frac{1}{2} k_r \left(r_{ij} - r_{ij}^0 \right)^2 \tag{2}$$

$$U_{\text{bending}} = \sum \frac{1}{2} k_\theta \left(\theta_{ijk} - \theta_{ijk}^0 \right)^2 \tag{3}$$

$$U_{\text{torsional}} = \sum_{n=0}^{5} C_n [\cos(\phi_{ijkl} - \phi_{ijkl}^0)]^n \tag{4}$$

where k_r, k_θ and C_n are the force constants; r_{ij}, θ_{ijk} and ϕ_{ijkl} are bond lengths, bond angles and torsional angles, respectively; r_{ij}^o, θ_{ijk}^0 and θ_{ijkl}^0 are the equilibrium values.
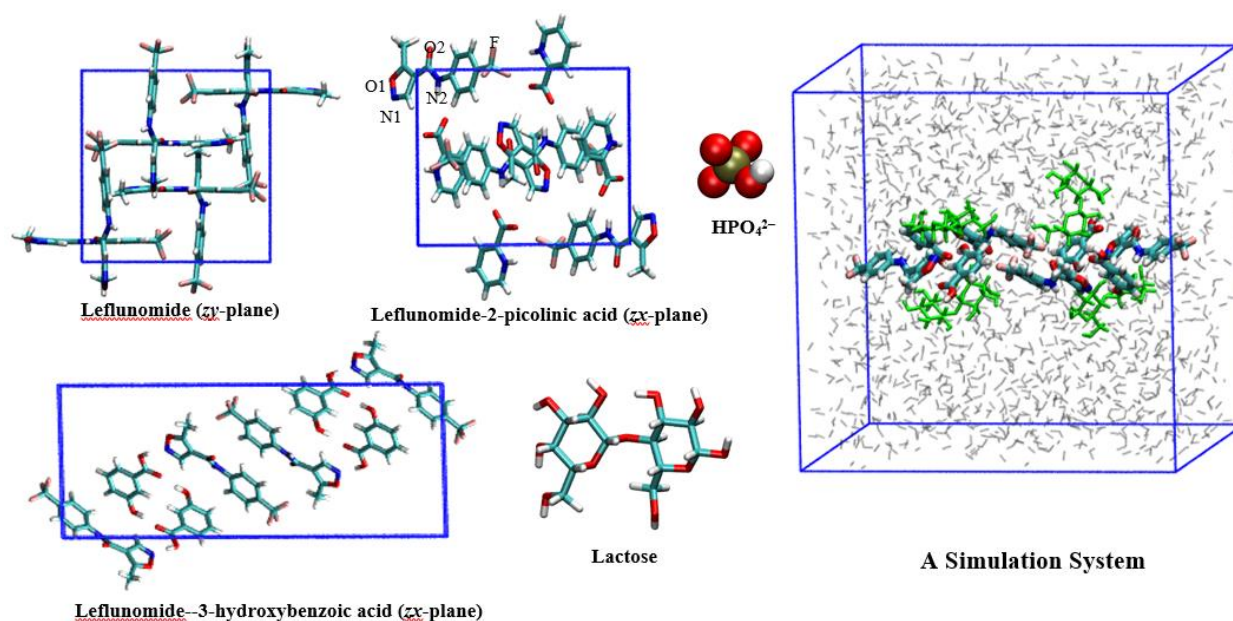
Figure C.1 Planar view of the molecular structures of LEF and the cocrystals, molecular structures of lactose and HPO_4^{2-}, and a model to represent simulation system

Colour code: P, gold; F, light orange; O, red; N, blue; C, cyan; H, white, grey, water in the simulation system

Four sets of simulations were performed. In the first set, the crystal structures of LEF and cocrystals were kept in the centre of a large simulation box of dimensions ~5 nm × 5 nm × 5 nm and solvated with water in the absence of excipients. The solvated systems were simulated at room temperature using an isothermal and isochoric (NVT: during the simulations, number of molecules, volume and temperature of the system remains constant) MD scheme. In the second set of simulations, the crystal structure of LEF/cocrystals was kept in a simulation box of the same dimensions and four excipient molecules were randomly distributed within. This system was simulated at room temperature using the NVT MD scheme. The second set of simulations allow the excipients to interact with most favourable sites of LEF/cocrystal. Finally, in the third set of simulations, the output from second set was solvated with water and simulated again in the NVT MD scheme at room temperature. During the first 3 sets of simulations, the position of the atoms of LEF/cocrystals were restrained by applying a force constant of 10000 kJ mol^{-1} nm^{-2}. Finally, in order to evaluate dissolution behaviour, in the fourth set of simulations position restraints were removed. As such, all atoms in the system were allowed to move during the simulation. Prior to the above simulations, crystal structures of the parent LEF crystal and LEF-3HBA and LEF-2PIC were extended to 4 × 4 × 4, 4 × 8 × 2, and 4 × 4 × 4 unit cells and isobaric-isothermal MD simulations were performed at 1 bar. The calculated densities of LEF and cocrystals, derived from the OPLS-AA model, are 1.49, 1.42 and 1.43 g cc^{-1} respectively, which are close to the experimental values of 1.47, 1.48, and 1.45 g cc^{-1}.

Initially, using the steepest descent method, all four systems were subjected to energy minimisation. The initial velocities of the atoms were generated by the Maxwell–Boltzmann distribution equation, followed by MD simulations. The velocity-rescaling scheme was adopted to control the temperature with a relaxation time of 0.1 ps. The equations of motion were integrated by the leap-frog algorithm and periodic boundary conditions were applied in all directions. A cut-off of 14 Å was used to calculate the LJ interactions, while the particle-mesh Ewald summation method was used to evaluate the Coulombic interactions with grid spacing of 1.2 Å. A time step of 1 fs was used, and the trajectories were saved every 5 ps. The duration for the first 3 sets of simulations was 5 ns (last 3 ns trajectories were used for analysis) and for the fourth set it was 2.5 ns. The GROMACS v5.0.6[100] package was used to perform all the MD simulations.

C.2   Experimental

LEF was purchased from Biotain Pharma Co., Ltd., China. The coformers were purchased from Sigma-Aldrich, Singapore, and used as received. The excipients, lactose (α-lactose monohydrate, ≥99%) and DCP (98%) were purchased from Sigma Aldrich, Singapore and were used as received.

C.2.1   Tablet Preparation

The excipients used in formulations were aligned with those used in the marketed LEF (ARAVA) such that each 100 mg of the tablet contains 20 mg of LEF (or a cocrystal that contains an equivalent amount of LEF, e.g. 30.2 mg of LEF-33HBA), 74.5 mg of lactose monohydrate/DCP – adjusted for cocrystal mass (e.g. 64.3 mg in the LEF-3HBA formulation), 5.0 mg of corn starch, and 0.5 mg of magnesium stearate (as a lubricant). The tablet samples for dissolution experiments were prepared by direct compression. Prior to tablet pressing, a formulation mixture of ca. 5 g each were thoroughly mixed using a laboratory powder mixing machine (Alphie powder mixer, Hexagon product development, Vadodara, Gujarat, India). For the tableting process, each mixed powder was then placed in a tablet press (Minipress II, Karnawati Engineering, India) and pressed at varying load to form 200 mg tablets. Hardness testing of the tablets was conducted using DT-YD-3 hardness tester (Guangzhou Raysky Scientific, China) and tablets of similar hardness were used in dissolution experiments.

C.2.2   Dissolution Rate

The dissolution experiments on all samples (neat LEF, cocrystals, and their formulations) were conducted using an Agilent 708-DS dissolution sampling apparatus. As recommended by the US

Food and Drug Administration, all the dissolution experiments were conducted in water as the dissolution medium (900 mL), with a rotation speed of 100 rpm at 37 °C. All the tablets were found to disintegrate instantly within a minute. 2 mL aliquots of sample from the vessel were withdrawn and filtering through a 45 µm syringe tip filter for analysis by HPLC. This was conducted at times of 5, 10, 15, 30, 45, 60, 90, 120, 180, 240, 300 and 360 min. Total dissolution volume was maintained at 900 mL by replacing the samples with an equivalent amount of fresh dissolution medium. The dissolution experiments were run in triplicate (n=3).

C.2.3   Fourier Transform Infrared Spectroscopy

A Frontier FT-IR/NIR Spectrometer (PIKE Technologies I, PerkinElmer) with a MIR TGS detector and a combined scan direction was used to collect transmission spectra of neat samples (without KBR). The samples were scanned over a range of 4000–650 cm^{-1} at a scan speed of 0.2 $cm^{-1}s^{-1}$ with a spectral resolution of 4 cm^{-1}.
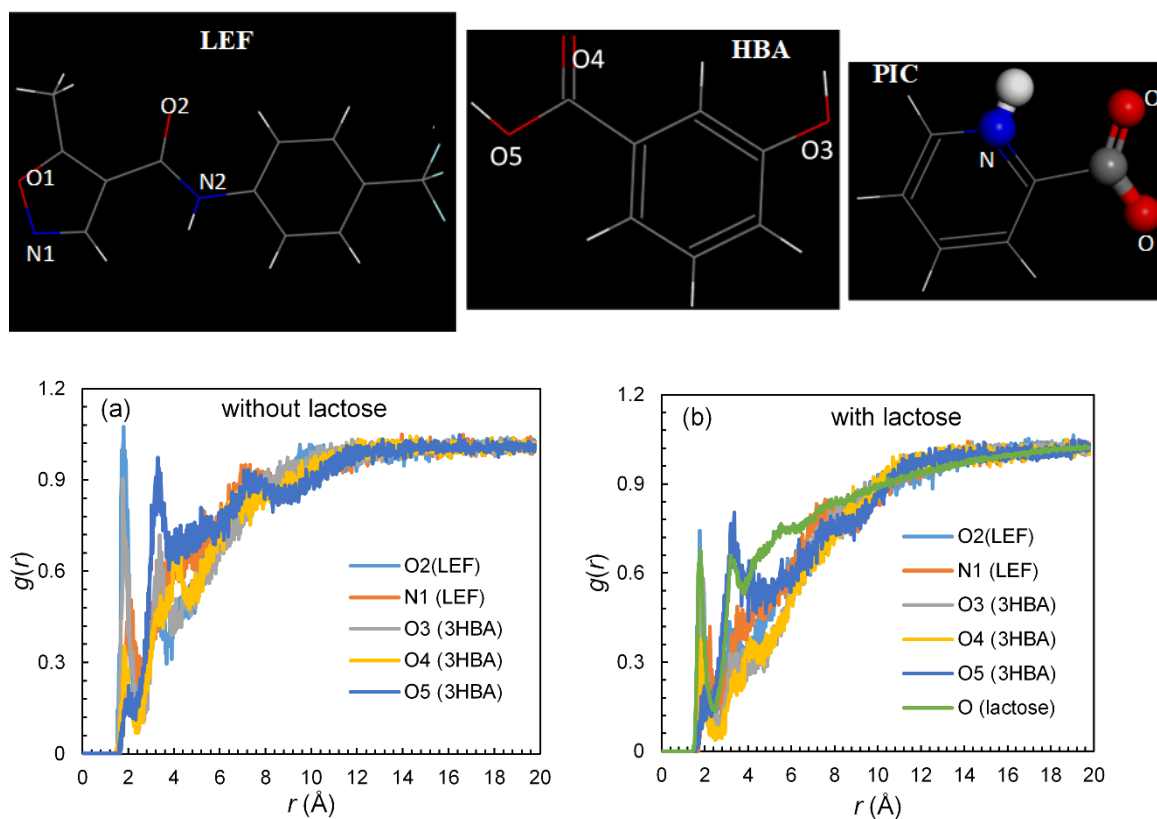
Appendix D   LEF Formulation

D.1   Hardness Evaluation of Tablets
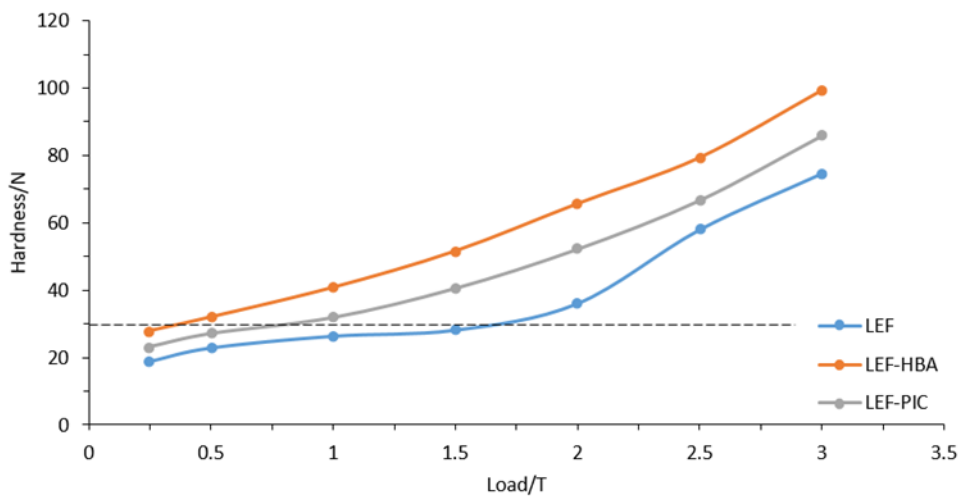
Figure D.1 Hardness values of LEF and cocrystal formulation tablets when pressed at various loads

A ~30 N value of hardness (dashed line) was targeted for dissolution experiments

D.2   Radial Distribution Function

Figure D.2 Radial distribution functions $g(r)$ of the H atom of water around (a) the atoms of LEF-3HBA and (b) the atoms of LEF-3HBA as well as the O atom of lactose

The top figures indicate the atom notations
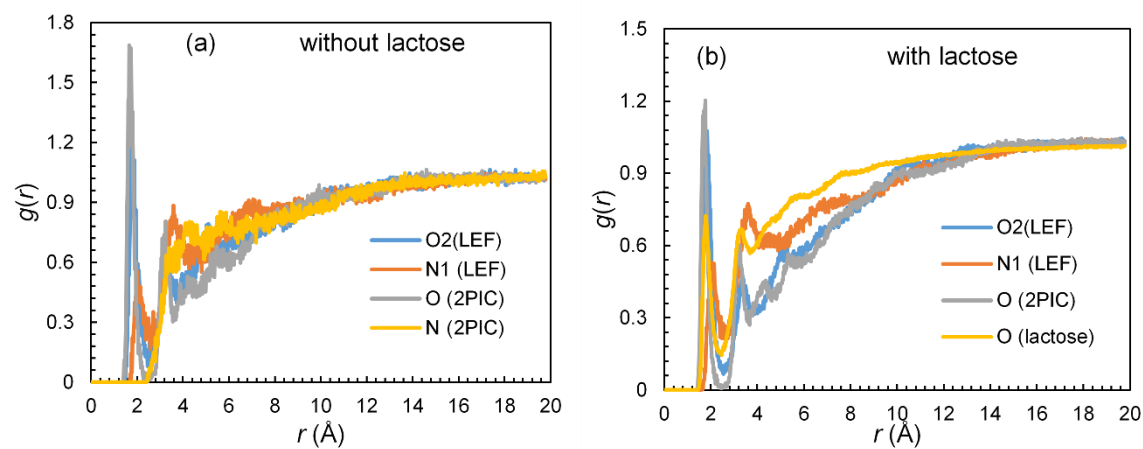
Figure D.3 Radial distribution functions $g(r)$ of the H atom of water around (a) the atoms of LEF-2PIC and (b) the atoms of LEF-2PIC as well as the O atom of lactose
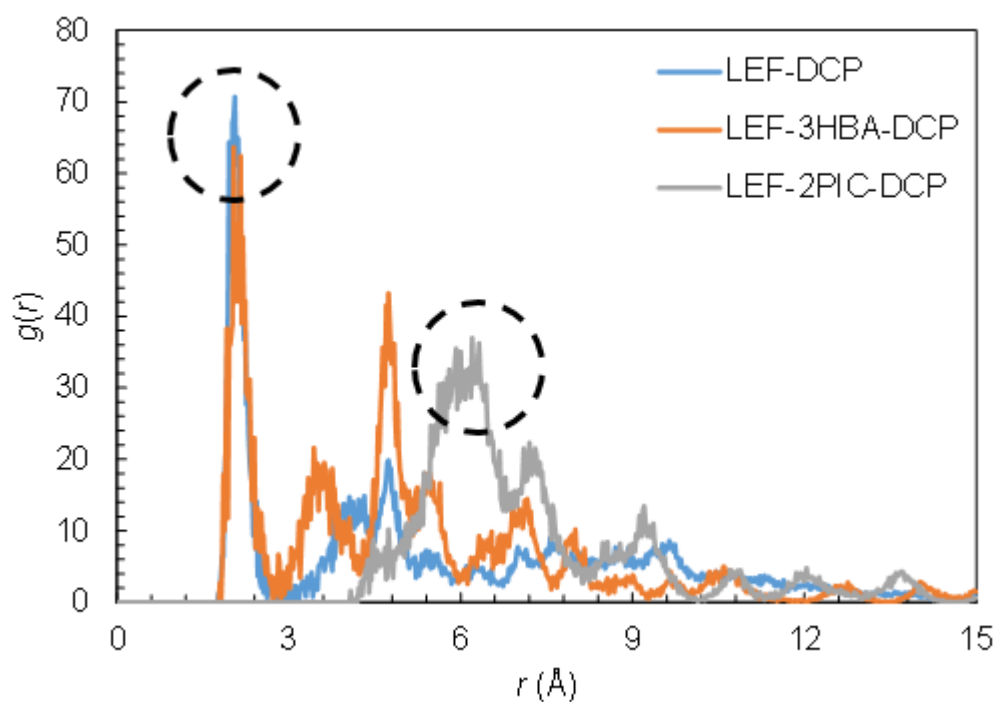
Figure D.4 The radial distribution function ($g(r)$) of the H atom of N–H in LEF around the O atoms of DCP for LEF-DCP, LEF-3HBA-DCP, and LEF-2PIC-DCP systems in the absence of water

D.3   Scanning Electron Microscopy
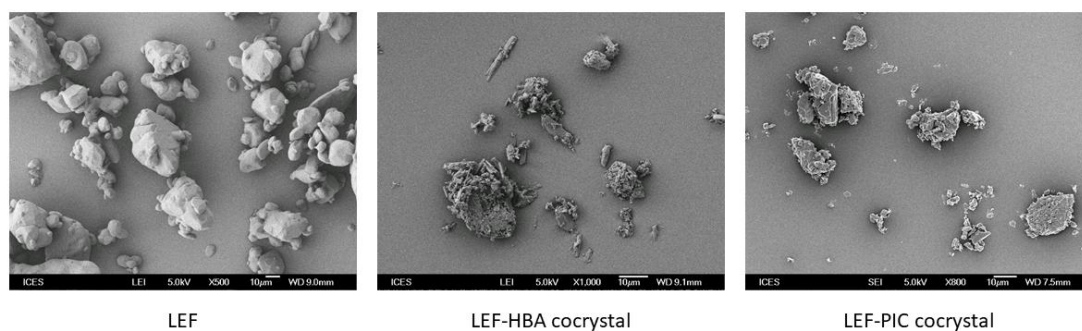
Figure D.5 SEM images of LEF and cocrystal powders used for preparation of formulations studied in this work

D.4   Fourier Transform Infrared Spectroscopy
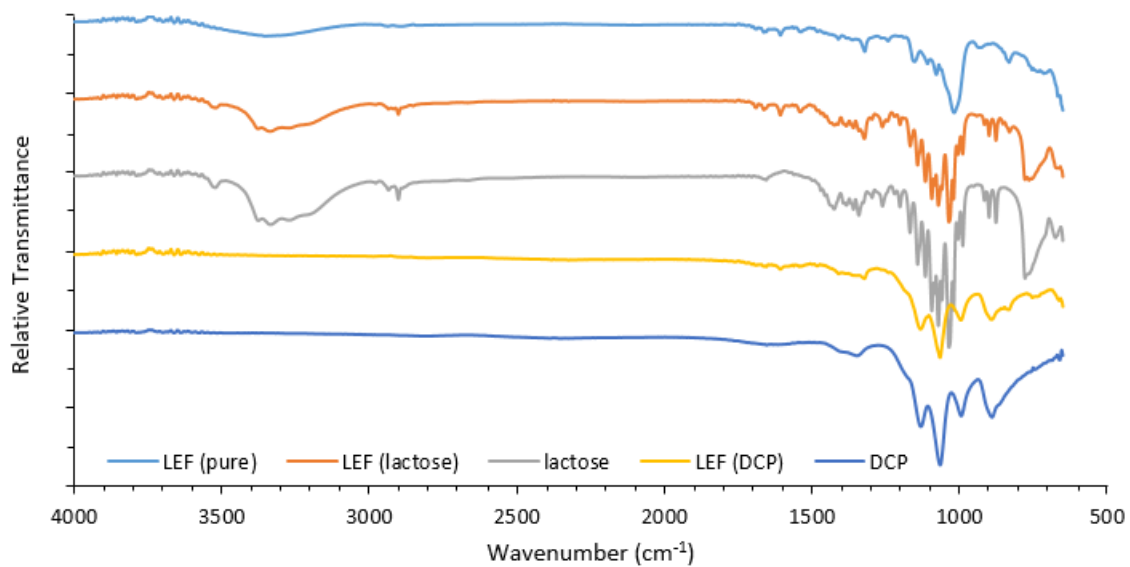
Figure D.6 Overlay of FT-IR spectra of the three LEF samples used: pure, lactose complex, and DCP complex
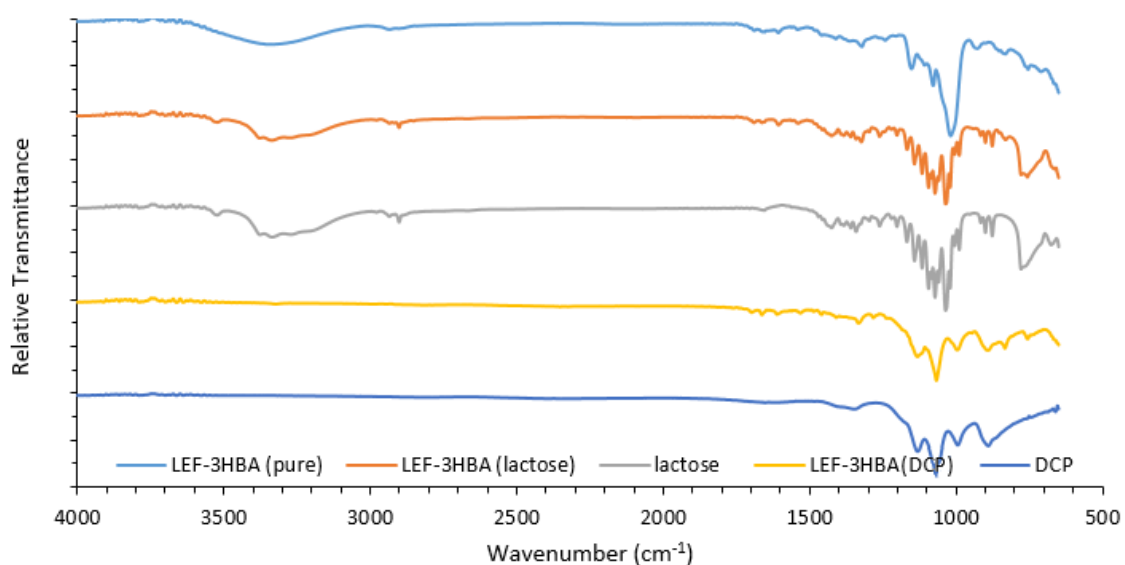
Figure D.7 Overlay of FT-IR spectra of the three LEF-3HBA samples used: pure, lactose complex, and DCP complex

Figure D.8 Overlay of FT-IR spectra of the three LEF-2PIC samples used: pure, lactose complex, and DCP complex

Table D.1 Assignments of the vibrational modes of LEF, LEF-3HBA, LEF-2PIC and their respective formulations with lactose and DCP

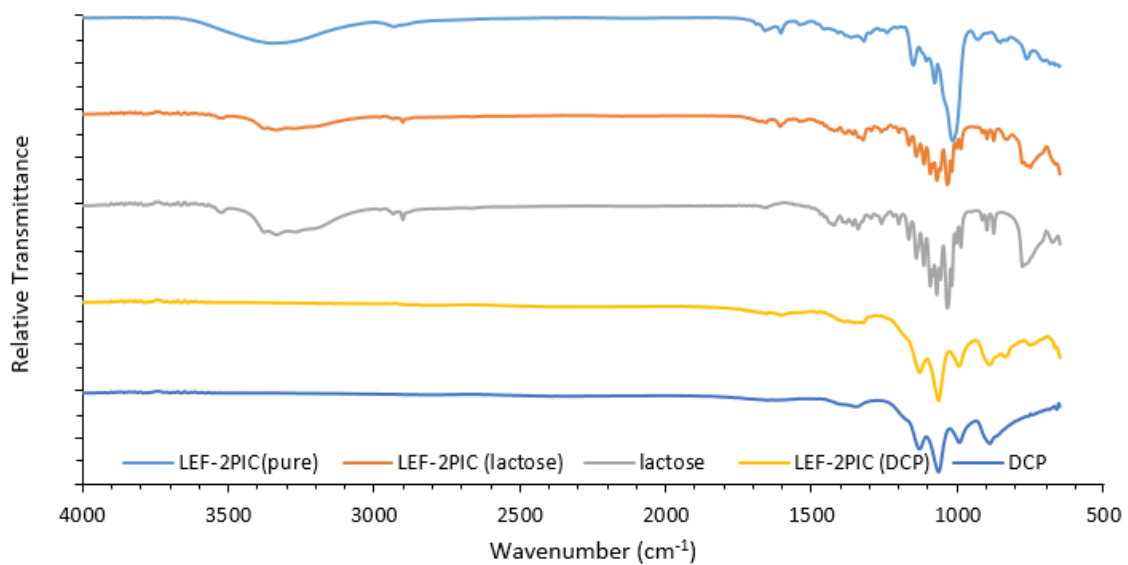| Assignment	Wavenumber/cm^{-1}								
	LEF pure	LEF-lactose	LEF-DCP	LEF-3HBA-pure	LEF-3HBA-lactose	LEF-3HBA-DCP	LEF-2PIC-pure	LEF-2PIC-lactose	LEF-2PIC-DCP
νNH	3354	3335		3344	3335		3354	3335	
νCH(ar)	2932	2902		2935	2935		2932	2935	
νCH(ar)					2902			2902	
νC=O	1689	1690		1689	1689	1699			1683
νC–N	1662	1663	1654	1654	1663	1663	1661	1654	1654
νC=C	1608	1607	1608	1607	1606	1612	1607	1609	1601
βNH	1538	1538	1544	1543	1538	1532	1539	1538	1549
βOH(carboxyl)				1410	1426	1409	1410	1423	1383
δCOH		1384			1384			1385	
βOH, νCF				1321	1324	1333	1321	1325	1327
νC–OH				1242	1221	1282			
νCF	1321	1323	1322						
βOH		1262						1262	
νC–O	1153	1167	1132	1152	1167	1132	1152	1168	1131
νC–O		1142			1142			1142	
νP=O			1132			1132			1131
βCH	1108	1116		1079	1072		1108	1116	

νC–O		1094						1094	
ρCH3	1079	1072					1079	1072	
νP–O			1066			1067			1066
νCF	1018	1036	1066			1067	1017	1036	1066
νₛP–O			996			996			995
γCH(ar)	832		833	832	878	892	854	831	839
δCCO		778			778			778	
δCCC(ar)	714	764	754						
δCCC(ar)				754	757	756	764	751	754
δOPO			754			756			754

ν = stretching, νₛ = symmetric stretching, νₐ = asymmetric stretching, δ = scissoring, β = in-plane bending, ρ = rocking, γ = out-of-plane bending

Assignments: black = LEF, green = coformer, red = excipient

References

1 E. Grothe, E., Meekes, H., Vlieg, E., ter Horst, J. H. & de Gelder, R. *Cryst. Growth Des*. 2016 **16**, 3237-3243

2 Aitipamula, S., Banerjee, R., Bansal, A. K., Biradha, K., Cheney, M. L., Choudhury, A. R., Desiraju, G. R., Dikundwar, A. G., Dubey, R., Duggirala, N., Ghogale, P. P., Ghosh, S., Goswami, P. K., Goud, N. R., Jetti, R. R. K. R., Karpinski, P., Kaushik, P., Kumar, D., Kumar, V., Moulton, B., Mukherjee, A., Mukherjee, G., Myerson, A. S., Puri, V., Ramanan, A., Rajamannar, T., Reddy, C. M., Rodriguez-Hornedo, N., Rogers, R. D., Row, T. N. G., Sanphui, P., Shan, N., Shete, G., Singh, A., Sun, C. C., Swift, J. A., Thaimattam, R., Thakur, T. S., Kumar Thaper, R., Thomas, S. P., Tothadi, S., Vangala, V. R., Variankaval, N., Vishweshwar, P., Weyna, D. R. & Zaworotko, M. J. *Cryst. Growth Des*. 2012, **12**, 2147-2152

3 Duggirala, N. K., Perry, M. L., Almarsson, Ö.; Zaworotko, M. J. *Chem. Commun*. 2016, **52**, 640-655

4 Cherukuvada, S. & Row, T. N. G. *Cryst. Growth Des.* 2014, **14**, 4187-4198

5 Almarsson, Ö. Zaworotko, M. J. *Chem. Commun.* 2004, **17**, 1889-1896

6 Healy, A. M., Worku, Z. A., Kumar, D. & Madi, A. M. *Advanced Drug Delivery Reviews* 2017, **117**, 25-46

7 Aakeroy, C. B.; Salmon, D. J. CrystEngComm 2005, **7**, 439-448

8 Cruz-Cabeza, A. J. *CrystEngComm* 2012, **14**, 6362-6365

9 Delori, A., Galek, P. T. A., Pidcock, E., Patni, M. & Jones, W. *CrystEngComm* 2013, **15**, 2916-2928

10 Delori, A. & Jones, W. *CrystEngComm* 2011, **13**, 6315-6318

11 Childs, S. L., Stahly, G. P. & Park, A. *Mol. Pharmaceutics* 2007, **4**, 323-338

12 Mapp, L. K., Coles, S. J. & Aitipamula, S. *CrystEngComm* 2017, **19**, 2925-2935

13 Blagden, N., Matas, M., Gavan, P. T. & York, P. *Adv. Drug Deliv. Rev*. 2007, **59**, 617-30

14 Salole, E. G. & Al-Sarraj, F. A. *Drug Dev. Ind. Pharm*. 1985, **11**, 855-864

15 Bhugra, C.; Pikal, M. J. *J Pharm Sci.* 2008, **97**, 1329–1349

16 Pajula, K.; Lehto, V.-P.; Ketolainen, J.; Korhonen, O. *Mol. Pharm.* 2012, **9**, 2844-2855

17 Amidon G. L.; Lennernäs, H.; Shah V. P.; Crison J. R. *Pharm. Res.* 1995, **12**, 413-420

18 Gupta, U.; Agashe, H. B.; Asthana, A.; Jain, N. K. *Biomacromolecules* 2006, **7**, 649-658

19 Thayer, A. M. *Chem. Eng. News* 2010, **88**, 13-18

20 Reverchon, E.; Della Porta, G.; Spada, A.; Antonacci, A. *J Pharm. Pharmacol.* 2004, **56**, 1379-1387

21 Alam, M. M.; Mallik, S.; Ahmad, S.; Ibrahim, M.; Raza, A. K.; Hasan, A. *Pharmagene* 2013, **3**, 66-72

22 Vishweshwar, P.; McMahon, J. A.; Bis, J. A.; Zaworotko, M. J. *J. Pharm. Sci.* 2006, **95**, 499–516

23 Almarsson, Ö. Zaworotko, M. J. *Chem. Commun.* 2004, **17**, 1889-1896

24 Thakuria, R.; Delori, A.; Jones, W.; Lipert, M. P.; Roy, L.; Rodríguez-Hornedo, N. *Int. J. Pharm.* 2013, **453**, 101-125

25 Blagden, N.; De Matas, M. *Advanced Drug Delivery Reviews* 2007, **59**, 617-630

26 Morissette, S. L.; Almarsson Ö.; Peterson, M. L.; Remenar, J. F.; Read, M. J.; Lemmoa, A. V.; Ellis, S.; Cima, M. J.; Gardner, C. R. *Advanced Drug Delivery Reviews* 2004, **56**, 275-300

27 Groom, C. R.; Bruno, I. J.; Lightfoot, M. P..; Ward, S. C. *Acta Crystallographica Section B* 2016, **72**, 171-179

28 Zhou, L.; Dodd, S.; Capacci-Daniel, C.; Garad, S.; Panicucci, R.; Sethuraman, V. *Eur. J. Pharm. Sci.* 2016, **88**, 191-201

29 Mapp, L. K., Coles, S. J., Aitipamula, S. *Cryst. Growth Des.* 2017, **17**, 163-174

30 Desiraju, G. R. *Crystal Engineering: The Design of Organic Solids*, Elsevier: Amsterdam, 1989

31 Galek, P.; Pidcock, E.; Wood, P.; Bruno, I.; Groom, C. *CrystEngComm* 2012, **14**, 2391-2403

32 Delori, A.; Galek, P. T. A.; Pidcock, E.; Jones, W. *Chem.-Eur. J.* 2012, **18**, 6835-6846

33 Karki, S.; Friščić, T.; Fábián, L.; Jones, W. *CrystEngComm* 2010, **12**, 4038-4041

34 Takata, N.; Takano, R.; Uekusa, H.; Hayashi, Y.; Terada, K. *Cryst. Growth Des.* 2010, **10**, 2116-2122

35 Aitipamula, S.; Vangala, V. R.; Chow, P. S.; Tan, R. B. H. *Cryst. Growth Des.* 2012, **12**, 5858-5863

36 Childs, S. L.; Kandi, P.; Lingireddy, S. R. *Mol. Pharmaceutics* 2013, **10**, 3112-3127

37 Panakanti, R.; Narang, A. S. *Pharm. Res.* 2012, **29**, 2639-2659

38 Wong, J.; Yuen, K. *Drug Development and Industrial Pharmacy* 2003, **29**, 1035-1044

39 Kaukonen, A. M.; Lennernas, H.; Mannermaa, J. P. *J Pharm Pharmacol.* 1998, **50**, 611-619

40 Dhanaraju, M. D.; Kumaran, K. S.; Baskaran, T.; Moorthy M.S. *Drug Development and Industrial Pharmacy* 1998, **24**, 583-587

41 Kuentz, M.; Holm, R.; Elder, D. P. *Eur. J. Pharm. Sci.* 2016, **87**, 136-163

42 Bergström, C. A. S.; Charman, W. N.; Porter, C, J. H. *Advanced Drug Delivery Reviews* 2016, **101**, 6-21

43 Morissette, S. L.; Almarsson Ö.; Peterson, M. L.; Remenar, J. F.; Read, M. J.; Lemmoa, A. V.; Ellis, S.; Cima, M. J.; Gardner, C. R. *Advanced Drug Delivery Reviews* 2004, **56**, 275-300

44 Li, C.; Wang, J. X.; Le, Y.; Chen, J. F. *Mol. Pharm.* 2013, **10**, 2362-2369

45 Childs, S. L.; Kandi, P.; Lingireddy, S. R. *Mol. Pharmaceutics* 2013, **10**, 3112-3127

46 Alhalaweh, A.; Ali, H. R. H.; Velaga, S. P. *Cryst. Growth Des*. 2014, **14**, 643-648

47 Koranne, S.; Sahoo, A.; Krzyzaniak, J. F.; Luthra, S.; Arora, K. K.; Suryanarayanan, R. *Mol. Pharmaceutics* 2018, **15**, 3297-3307

48 Thakuria, R.; Delori, A.; Jones, W.; Lipert, M. P.; Roy, L.; Rodríguez-Hornedo, N. *Int. J. Pharm.* 2013, **453**, 101-125

49 Duggirala, N. K.; Vyas, A.; Krzyzaniak, J. F.; Arora, K. K.; Suryanarayanan, R. *Mol. Pharmaceutics* 2017, **14**, 3879-3887

50 Ogienko, A. G.; Myz, S. A.; Ogienko, A. A.; Nefedov, A. A.; Stoporev, A. S.; Mel'gunov, M. S.; Yunoshev, A. S.; Shakhtshneider, T. P.; Boldyrev, V. V.; Boldyreva, E. V. *Cryst. Growth Des.* 2018, **18**, 7401-7409

51 Avdeef, A. *Eur. J. Pharm. Sci.* 2017, *110*, 2-18

52 Avdeef, A. *Pharm. Res*. 2018, **35**, 40

53 Avdeef, A.; Fuguet, E.; Llinàs, A.; Ràfols, C.; Bosch, E.; Völgyi, G.; Verbj , T.; Boldyreva, E.; Takács Novák, K. *Admet and Dmpk* 2016, **4**, 117-178

54 Ganesan, A.; Coote, M. L.; Barakat, K. *Drug Discovery Today* 2017, **22**, 249-269

55 Katiyar, R. S.; Jha, P. K., *WIREs Computational Molecular Science* 2018, **8**, e1358

56 Jha, P. K.; Larson, R. G. *Molecular Pharmaceutics* 2014, **11**, 1676-1686

57 Li, C.; Wang, J.-X.; Le, Y.; Chen, J.-F. *Molecular Pharmaceutics* 2013, **10**, 2362-2369

58 Tomba, E.; Barolo, M.; García-Muñoz, S. *Chemical Engineering Research and Design*, 2014, **92**, 534-544

59 Huynh, L.; Grant, J.; Leroux, J-C.; Delmas, P.; Allen, C. *Pharmaceutical Research* 2008, **25**, 147-157

60 Yu, A. B. *Engineering Computations*, 2003, 21, 205-214

61 Zhu, H. P.; Zhou, Z. Y.; Yang, R. Y.; Yu, A. B. *Chemical Engineering Science* 2007, **62**, 3378-3396

62 El-Mahdy El-Sayyad, N. M. *et al. Bulletin of Faculty of Pharmacy* 2017, **55**, 53-62

63 Rozman, B. *Clin. Pharmacokinet.* 2002, **41**, 421-430

64 Vega, D.; Petragalli, A.; Fernández, D.; Ellena, J. A. *J. Pharm. Sci.* 2006, **95**, 1075-1083

65 Bruno, I.; Cole, J.; Lommerse, J. M.; Rowland, R. S.; Taylor, R.; Verdonk, M. *J. Comput. Aided Mol. Des*. 1997, **11**, 525-537

66 Macrae, C. F.; Bruno, I. J.; Chisholm, J. A.; Edgington, P. R.; McCabe, P.; Pidcock, E.; Rodriguez-Monge, L.; Taylor, R.; van de Streek, J.; Wood, P. A. *J. Appl. Cryst*. 2008, **41**, 466-470

67 Spek, A. L. *J. Appl. Cryst.* 2003, **36**, 7-11

68 Stanton, M. K.; Bak, A. *Cryst. Growth Des.* 2008, **8**, 3856-3862

69 Schultheiss, N.; Newman, A. *Cryst. Growth. Des*. 2009, **9**, 2950-2967

70 Santra, R.; Ghosh, N.; Biradha, K. *New J. Chem.* 2008, **32**, 1673-1676

71 Padmapreetha, J.; Arulkumaran, K. S. G. *J. Pharm. Sci.* 2016, **8**, 586-593

72 Glomme, A.; Marz, J.; Dressman, J. B. *J. Pharm. Sci*. 2005, **94**, 1-16

73 Fagerberg, J. H.; Tsinman, O.; Sun, N.; Tsinman, K.; Avdeef, A. *Mol. Pharmaceutics,* 2010, **7**, 1419-1430

74 Babu, N. J.; Nangia, A. *Cryst. Growth Des.* 2011, **11**, 2662-2679

75 Nordström, F. L.; Rasmuson, Å. C. *Eur. J. Pharm. Sci.* 2006, **28**, 377-384

76 Good, D. J.; Rodríguez-Hornedo, N. R. *Cryst. Growth Des.* 2009, **9**, 2252-2264

77 Maginn, E. J. *AIChE Journal* 2009, **55**, 1304-1310

78 Gupta, J.; Nunes, C.; Vyas, S.; Jonnalagadda, S. *The Journal of Physical Chemistry B* 2011, **115**, 2014-2023

79 Maus, M.; Wagner, K. G.; Kornherr, A.; Zifferer, G. *Molecular Simulation* 2008, **34**, 1197-1207

80 Yani, Y.; Kanaujia, P.; Chow, P. S.; Tan, R. B. H. *Industrial & Engineering Chemistry Research* 2017, **56**, 12698-12707

81 Gao, Y.; Olsen, K. W. *Mol. Pharm.* 2013, **10**, 905-917

82 Gao, Y.; Olsen, K. W. *Molecular Pharmaceutics* 2014, **11**, 3056-3067

83 Hebbink, G. A.; Dickhoff, B. H. J., *Chapter 5 - Application of lactose in the pharmaceutical industry. In Lactose*, Paques, M.; Lindner, C., Eds. Academic Press: 2019; pp 175-229

84 Rowe, R. C.; Sheskey, P. J.; Owen, S. C.; American Pharmacists, A., *Handbook of Pharmaceutical Excipients*. Pharmaceutical Press: 2006

85 Doldán, C.; Souto, C.; Concheiro, A.; Martínez-Pacheco, R.; Gómez-Amoza, J. L. *Int. J. Pharm.* 1995**, *124*, 69-74

86 Matziari, M.; Dellis, D.; Dive, V.; Yiotakis, A.; Samios, J. *The Journal of Physical Chemistry B* 2010**, 114**, 421-428

87 Luzar, A.; Chandler, D., Hydrogen-bond kinetic in liquid water. *Nature* 1996**, 379**, 55-57

88 van der Merwe, J.; Steenekamp, J.; Steyn, D.; Hamman, J. *Pharmaceutics* 2020, **12**, 393

89 Liltorp, K.; Larsen, T. G.; Willumsen, B.; Holm, R. *J. Pharm. Biomed. Anal.* 2011**, 55**, 424-428

90 Duggirala, N. K.; LaCasse, S. M.; Zaworotko, M. J.; Krzyzaniak, J. F.; Arora, K. K. *Cryst. Growth Des.* 2020, **20**, 617-626

91 Takahashi, T.; Yamamoto, R. *J. Pharm. Soc. Jpn.* 1998, **89**, 925-932

92 Pharmacology review of leflunomide
www.accessdata.fda.gov/drugsatfda_docs/nda/98/20905_ARAVA_PHARMR_P1.pdf

93 Mill, D.; Dawson, J.; Johnson, J. L. *Therapeutic Advances in Drug Safety* 2018, **9**, 227-235

94 Spackman, M. A. *Cryst. Growth Des.* 2015, **15**, 5624–5628

95 Gaussian 16, Revision C.01, Frisch, M. J.; Trucks, G. W.; Schlegel, H. B.; Scuseria, G. E.; Robb, M. A.; Cheeseman, J. R.; Scalmani, G.; Barone, V.; Petersson, G. A.; Nakatsuji, H.; Li, X.; Caricato, M.; Marenich, A. V.; Bloino, J.; Janesko, B. G.; Gomperts, R.; Mennucci, B.; Hratchian, H. P.; Ortiz, J. V.; Izmaylov, A. F.; Sonnenberg, J. L.; Williams-Young, D.; Ding, F.; Lipparini, F.; Egidi, F.; Goings, J.; Peng, B.; Petrone, A.; Henderson, T.; Ranasinghe, D.; Zakrzewski, V. G.; Gao, J.; Rega, N.; Zheng, G.; Liang, W.; Hada, M.; Ehara, M.; Toyota, K.; Fukuda, R.; Hasegawa, J.; Ishida, M.; Nakajima, T.; Honda, Y.; Kitao, O.; Nakai, H.; Vreven, T.; Throssell, K.; Montgomery, J. A., Jr.; Peralta, J. E.; Ogliaro, F.; Bearpark, M. J.; Heyd, J. J.; Brothers, E. N.; Kudin, K. N.; Staroverov, V. N.; Keith, T. A.; Kobayashi, R.; Normand, J.; Raghavachari, K.; Rendell, A. P.; Burant, J. C.; Iyengar, S. S.; Tomasi, J.; Cossi, M.; Millam, J. M.; Klene, M.; Adamo, C.; Cammi, R.; Ochterski, J. W.; Martin, R. L.; Morokuma, K.; Farkas, O.; Foresman, J. B.; Fox, D. J. *Gaussian, Inc.* Wallingford CT, 2016

96 Mackenzie, C. F., Spackman, P. R., Jayatilaka, D., & Spackman, M. A. *IUCrJ*, *4* (Pt 5), 2017, 575-587

97 Jorgensen, W. L.; Maxwell, D. S.; Tirado-Rives, J. *J. Am. Chem. Soc.* 1996, **118**, 11225-11236

98 Ribeiro, A. A.; Horta, B. A.; Alencastro, R. B. d. *Journal of the Brazilian Chemical Society* 2008, **19**, 1433-1435

99 Berendsen, H. J.; Postma, J. P.; van Gunsteren, W. F.; Hermans, J. *Intermolecular forces*, Springer: 1981; pp 331-342

100 Hess, B.; Kutzner, C.; van der Spoel, D.; Lindahl, E. *J. Chem. Theory Comput.* 2008, **4**, 435-447